VOLUME 87, NO. EM5
OCTOBER 1961
PART I

JOURNAL of the

Engineering Mechanics Division

PROCEEDINGS OF THE
AMERICAN SOCIETY
OF CIVIL ENGINEERS

BASIC REQUIREMENTS FOR MANUSCRIPTS

Original papers and discussions of current papers should be submitted to the Manager of Technical Publications, ASCE. Authors should indicate the technical division to which the paper is referred. The final date on which a discussion should reach the Society is given as a footnote with each paper. Those who are planning to submit material will expedite the review and publication procedures by complying with the following basic requirements:

1. Titles must have a length not exceeding 50 characters and spaces.

2. A summary of approximately 10 words must accompany the paper, a 300-word synopsis must precede it, and a set of conclusions must end it.

3. The manuscript (an original ribbon copy and two duplicate copies) should be double-spaced on one side of 8½-inch by 11-inch paper. Three copies of all illustrations, tables, etc., must be included.

4. The author's full name, Society membership grade, and footnote reference stating present employment must appear on the first page of the paper.

5. Mathematics are recomposed from the copy that is submitted. Because of this, it is necessary that letters be drawn carefully, and that special symbols be properly identified. The letter symbols used should be defined where they first appear, in the illustrations or in the text, and arranged alphabetically in an Appendix.

6. Tables should be typed (an original ribbon copy and two duplicate copies) on one side of 8½-inch by 11-inch paper. Specific illustrations and explanation must be made in the text for each table.

7. Illustrations must be drawn in black ink on one side of 8½-inch by 11-inch paper. Because illustrations will be reproduced with a width of between 3-inches and 4½ inches, the lettering must be large enough to be legible at this width. Photographs should be submitted as glossy prints. Explanations and descriptions must be made within the text for each illustration.

8. The desirable average length of a paper is about 12,000 words and the absolute maximum is 18,000 words. As an approximation, each full page of typed text, table, or illustration is the equivalent of 300 words.

9. Technical papers intended for publication must be written in the third person.

10. The author should distinguish between a list of "Reading References" and a "Bibliography," which would encompass the subject of his paper.

Reprints from this Journal may be made on condition that the full title, name of author, name of publication, page reference, and date of publication by the Society are given. The Society is not responsible for any statement made or opinion expressed in its publications.

This Journal is published bi-monthly by the American Society of Civil Engineers. Publication office is at 2300 South State Street, Ann Arbor, Michigan. Editorial and General Offices are at United Engineering Center, 345 East 47th Street, New York 17, N. Y. $4.00 of a member's dues are applied as a subscription to this Journal. Second-class postage paid at Ann Arbor, Michigan.

The index for 1960 was published as ASCE Publication 1961-15 (list price $2.00); indexes for previous years are also available.

Vol. 87, No. EM 5

Journal of the
ENGINEERING MECHANICS DIVISION
Proceedings of the American Society of Civil Engineers

ENGINEERING MECHANICS DIVISION
EXECUTIVE COMMITTEE
Egor P. Popov, Chairman; Bruce G. Johnston, Vice Chairman;
John W. Clark; Merit P. White; Donald L. Dean, Secretary
Elmer K. Timby, Board Contact Member

COMMITTEE ON PUBLICATIONS
Bruce G. Johnston, Chairman; Hans H. Bleich; Jack E. Cermak;
Donald L. Dean; John E. Goldberg; William J. Hall; John D. Haltiwanger;
Herbert S. Suer; Joseph F. Throop

CONTENTS

October, 1961

Papers

Page

Effect of Structure and Foundation Interaction
by Daniel L. Lycan and Nathan M. Newmark 1

Elastic Rayleigh Wave Effects Due to Nuclear Blasts
by Melvin L. Baron and Charles Lecht 33

Interfacial Mixing in Stratified Flow
by Enzo Oscar Macagno and Hunter Rouse 55

(over)

Copyright 1961 by the American Society of Civil Engineers.

Note.—Part 2 of this Journal is the 1961-40 Newsletter of the Engineering Mechanics Division.

The three preceding issues of this Journal are dated April 1961, June 1961, and August 1961.

DISCUSSION

Page

Dynamic Response of Beams Traversed by Two-Axle Loads, by Robert K. Wen. (October, 1960. Prior discussion: April, 1961. Discussion closed.)
by Robert K. Wen (closure) 85

Bearing Capacity of Floating Ice Sheets, by G. G. Meyerhof. (October, 1960. Prior discussion: May, 1961. Discussion closed.)
by G. Y. Sebastyan and F. Penner 87

Elasto-Plastic Analysis by Numerical Procedures, by Annabel L. Tong. (December, 1960. Prior discussion: May, 1961. Discussion closed.)
by Annabel L. Tong (closure) 97

Response of Multi-Story Structures to Earthquake, by Glen V. Berg. (April, 1961. Prior discussion: None. Discussion closed.)
by Richard G. Troy. 99

Commentary on Plastic Design in Steel, Joint WRC-ASCE Committee on Plasticity Related to Design. (Prior discussion: January, 1960. April, 1960. October, 1960. Discussion closed.)
by Joint-WRC-ASCE Committee on Plasticity Related to Design (closure) 103

Journal of the
ENGINEERING MECHANICS DIVISION
Proceedings of the American Society of Civil Engineers

EFFECT OF STRUCTURE AND FOUNDATION INTERACTION

By Daniel L. Lycan,[1] M. ASCE, and Nathan M. Newmark,[2] F. ASCE

SYNOPSIS

In the design of structures subjected to shock-type loadings, such as earthquakes or ground shock from nuclear blasts, the shock is described by a record of the foundation motion generally obtained from a structure that has been subjected to a similar type of shock. This information is often presented in the form of response spectra. When this information is used to design or analyze a structure, the assumption is made that the spectrum obtained from the foundation motion of a particular structure is an accurate representation of the effects of the shock. This implicitly assumes that the dynamic response of the structure does not affect the recorded foundation motion.

Analytical models for particular types of structures are developed and analyzed in this paper toward the purpose of studying the type and the magnitude of the errors that may occur when the record of the foundation motion of a specific structure is used to determine the response of another dissimilar structure. The effect of various assumed structural and foundational parameters on these errors is examined.

INTRODUCTION

In many engineering problems it is necessary to estimate the required strength of a structure or its behavior when it is subjected to a variety of

Note.—Discussion open until March 1, 1962. To extend the closing date one month, a written request must be filed with the Executive Secretary, ASCE. This paper is part of the Engineering Mechanics Division, Proceedings of the American Society of Civil Engineers, Vol. 87, No. EM 5, October, 1961.

[1] Capt., Corps of Engrs., U.S. Army Engr. Waterways Experiment Sta., Vicksburg, Miss.

[2] Head, Dept. of Civ. Engrg., Univ. of Illinois, Urbana, Ill.

shocks. Such problems arise in shock-mounting sensitive equipment, in the resistance of a structure to earthquake shock and, more recently, in the resistance of a structure to ground shock from an atomic explosion. Also, the problem has become important in the shock isolation of missile systems and underground protective structures. The specification of the type and intensities of shocks a structure must resist is of great importance in these problems. If the specification or description of the shock motion is inaccurate, the structure may be overdesigned or underdesigned. Such an error may result in the failure of the structure, or it may result in a structure that is made many times stronger and more costly than is necessary.

In the design of structures subjected to shock, the shock is generally described by a record of the foundation motion of another structure that has been subjected to a similar shock. Thus, the assumption is made that the foundation motion of a particular structure is an accurate representation of the shock. This implies that the motion of the structure does not affect the foundation motion, which is incorrect; however, this effect has usually been considered negligible. The object of this paper is to study the errors that may occur when the record of the foundation motion of a particular structure is used to determine the response of other dissimilar structures, and to analyze the effect of several structural and foundational parameters on these errors.

It is not intended to use specific types of shocks or specific structures in this study, but rather to use a broad approach in order to obtain information that will lead to a general understanding of the errors that may result. Because most of the work in this problem area has been concerned with aseismic design, the examination presented herein will refer to a building founded on ground. However, the generalizations used permit this study to apply to other types of vibrating systems on other types of foundations.

Notation.—The letter symbols adopted for use in this paper are defined where they first appear, in the illustrations or in the text, and are arranged alphabetically, for convenience of reference, in Appendix I.

STRUCTURAL RESPONSE

Development of Problem.—In the determination of the response of structures to a dynamic load it is convenient to use the so-called response spectrum concept. This concept was described in connection with engineering seismology by M. A. Biot in 1943 (3), and extensive work has been done since that time by G. W. Housner, M. ASCE, (12), (14), (15). A response spectrum may be defined as a plot of the maximum value of displacement, velocity, or acceleration of a single-degree-of-freedom system as a function of the frequency of the system. These maximum values are obtained for a given type of input. In the study of the response of buildings to earthquakes, the spectrum is obtained, briefly, as follows: A record is obtained during an earthquake of the motion of the base of a building by means of an accelerometer or displacement meter installed in the basement of the building. Using a shaking table or, more usually, an electrical analog computer or a digital computer, this motion record is used as an input of the base motion for a large number of fixed-base, single-degree-of-freedom, spring-mass systems, each with a

[3] Numerals in parentheses refer to corresponding items in the Bibliography, Appendix II.

different frequency. The maximum response of each spring-mass system is obtained and plotted as a function of the frequency. Shock spectra are obtained in this manner for a large number of recorded earthquakes and an envelope of these spectra is used as a design spectrum.

For a multi-degree-of-freedom system the response for each mode can be obtained from the spectrum, and by combining the modal responses, the total response of the system can be approximated. The response obtained by assuming that the maximum response in each mode occurs at the same time gives an upper bound to the actual maximum response.

The development of a general response spectrum from the motion recorded in the basement of a building implies the assumption that the recorded motion is an accurate description of the ground motion. In other words, the assumption is made that the vibrating structure does not affect the input foundation motion. The question of this effect of structure-foundation interaction has been raised by several investigators (4),(8),(13),(20),(47), but it has only been since 1958 that studies of this effect have been made (29),(30),(31).

There is evidence that an analysis using the response spectrum concept may give results that are overconservative. T. P. Tung and Newmark (46), using the same method of analysis as was used for the fixed-base systems in this study, computed values of dynamic shear in a ten-story building that were considerably greater than the design values. Calculated values considerably higher than design values have also been reported by other authors (1),(4),(11), (33),(45). There are many factors that may contribute to the great variation between computed shears and actual observed shears. An excellent discussion of some of these factors is given by John A. Blume, F. ASCE (4).

Generally, the discrepancies between observed and computed values of response are attributed to an inadequate recognition of the structural properties of building materials or of the manner in which buildings are fabricated (4),(11), however, G. J. O'Hara has presented evidence (30),(31) that a part of these discrepancies may be related to the method in which the shock intensity is described by the shock spectrum. The results of experimental work (30) indicate that there is an error in using the envelope of the individual spectra to determine the design spectrum. The analyses performed in this study indicate that even using an individual spectrum may lead to errors.

General Assumptions.—The response of a multistory building to dynamic loading is complex because the distribution of mass, stiffness of each story, height of each story, and type and quality of construction will determine the vibration characteristics of the structure. The structure has an infinite number of degrees of freedom and a complete solution to the problem is not practical. However, by making certain assumptions, a complicated structure can be simplified to an equivalent dynamic system with a finite number of degrees of freedom. The simplification of a structure for the purpose of making a dynamic analysis requires a great deal of judgment in order that the results of the analysis will closely approximate the response of the actual structure.

In a flexible structure, such as a rigid frame building, lateral forces are transmitted mainly through bending of the columns, whereas in a stiff structure, such as a shear wall structure, lateral forces are transferred through both bending and shearing action of the shear walls. For many types of structures, it is usually assumed that the building will deflect as a shear-beam, that is, the floors are assumed to move parallel to each other with the relative deflection in any story being dependent only on the shear in that story. These

structures are called shear-beam buildings. The mass of each floor and a portion of the mass of the columns attached to each floor are assumed to be concentrated at each floor level. Thus, a structure with an infinite number of degrees of freedom is reduced to a system which has as many degrees of freedom as it has concentrated masses. The shear-beam building shown in Fig. 1(a) can, therefore, be represented by a spring-mass system as shown in Figs. 1(b) and 1(c). The masses represent the lumped mass of each floor and its associated columns, the springs represent the resistance of each story to shear forces, and the dashpots represent a damping effect caused by frictional forces in the vibrating building. A four-story, shear-beam building was used in most of the analytical studies described in this paper. The column shears were assumed to be proportional to the relative horizontal displacements between stories and the spring constants, k, were assumed to remain constant regardless of the amount of deflection, that is, the structure was assumed to deflect in a linearly elastic manner. Damping was of a viscous type, and was taken either proportional to the absolute velocity of each story or to the relative velocity between adjacent stories.

Governing Differential Equations.—In this study two different types of foundation conditions are assumed. In one case a four-degree-of-freedom, spring-mass system is assumed to be attached to a movable or "free" base mass which is subjected to an applied, time-dependent force, P(t). This system, without damping, is shown in Fig. 2(a). A set of simultaneous, second-order, differential equations is then obtained by writing the equation of motion for each of the masses. The general form of the equations, which depends on the type of damping considered, is,

$$m_o\ddot{x}_o + c_o\dot{x}_o - k_1(x_1 - x_o) = P(t) \quad \ldots\ldots\ldots\ldots (1a)$$

and

$$m_i\ddot{x}_i + c_i\dot{x}_i + k_i(x_i - x_{i-1}) - k_{i+1}(x_{i+1} - x_i) = 0 \quad (i = 1, 2, 3, 4) \ldots (1b)$$

for absolute damping and

$$m_o\ddot{x}_o + c_o\dot{x}_o - c_1(\dot{x}_1 - \dot{x}_o) - k_1(x_1 - x_o) = P(t) \quad \ldots\ldots\ldots (2a)$$

and

$$m_i\ddot{x}_i + c_i(\dot{x}_i - \dot{x}_{i-1}) - c_{i+1}(\dot{x}_{i+1} - \dot{x}_i) + k_i(x_i - x_{i-1}) - k_{i+1}(x_{i+1} - x_i)$$

$$= 0 \quad (i = 1, 2, 3, 4) \quad \ldots\ldots\ldots\ldots\ldots\ldots\ldots\ldots\ldots\ldots (2b)$$

for relative damping.

In the other case, the spring-mass system is assumed to be attached to a rigid or "fixed" base and the base undergoes a time-dependent displacement, $x_o(t)$. This system, undamped, is shown in Fig. 2(b). The equation of motion for each mass is obtained as before and the resulting set of simultaneous differential equations is the same except for the deletion of the equation for the base mass. In both cases only displacements and forces parallel to the long axes of the spring-mass systems are considered. This means that in the actual structure only the horizontal component of the displacements are being considered.

Numerical Method of Solution.—An exact solution of the simultaneous differential equations for a multi-degree-of-freedom system is usually impractical, and numerical methods are used. An exact solution of the equations implies the determination of the displacement and velocity as a function of time. A numerical solution consists in obtaining numerical values of dis-

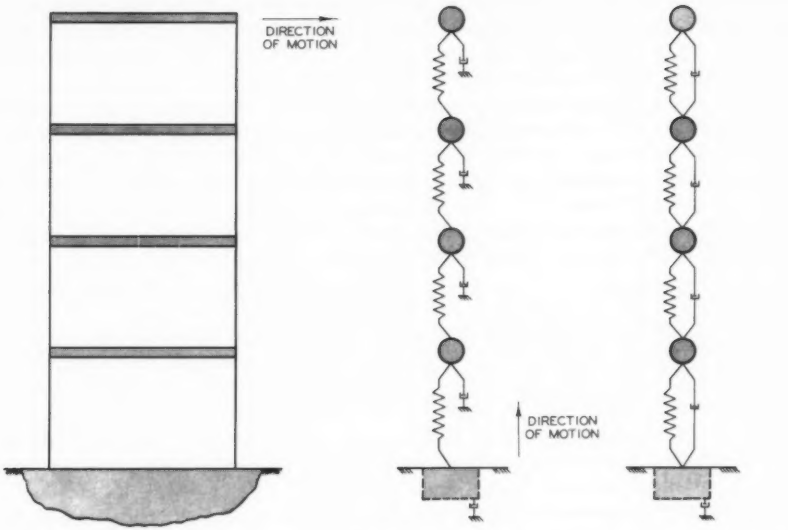

FIG. 1.–SPRING-MASS MODELS

a. APPLIED FORCE INPUT FOR FREE-BASE SYSTEMS

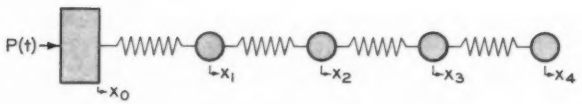

b. BASE DISTURBANCE FOR FIXED-BASE SYSTEMS

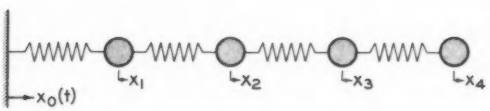

FIG. 2.–METHOD USED TO COMPARE RESPONSE

placement and velocity at discrete times. In addition, numerical-integration methods are particularly well suited to digital-computer operations. There are many different procedures available for the numerical integration of the differential equations. The method used in this study for obtaining the response of the spring-mass systems is a successive approximation method of integration (24),(27) with an assumed linear variation of acceleration in each time interval (a value of $\beta = 1/6$). The time intervals used in the numerical calculations were chosen so that the value of h/T_{min} was within the stability and convergence limits (27). Calculations were made on the ILLIAC at the University of Illinois, Urbana, Ill. and on the IBM 650 computer at the Waterways Experiment Station, Vicksburg, Miss.

Natural Frequencies.—One of the principal parameters defining the dynamic response of a multi-degree-of-freedom system is the set of natural frequencies. When a system freely moves with simple harmonic motion, this motion is called a natural or normal mode of vibration, and the frequency of this motion is the natural frequency. For a multi-degree-of-freedom system, the number of modes and frequencies is equal to the number of degrees of freedom of the system. For moderately damped systems, the damped and undamped natural frequencies differ only slightly, and it is customary to compute the undamped natural modes and frequencies.

For the four-degree-of-freedom systems studied, the equations of motion for each mass were written in the same manner as before except that for free vibration there is no external disturbing function. The eigenvalues and the corresponding natural frequencies were determined by setting the determinant of the coefficients of this set of equations equal to zero.

For a free system the lowest frequency corresponds to rigid body motion of the system; that is, it degenerates to zero. Therefore, although there are five natural frequencies for the five-mass free systems, only the four nonzero values are of interest and the lowest nonzero value is referred to as the first natural frequency.

METHOD OF ANALYSIS

Procedure.—The objective of this study is to determine if the shock spectra computed from the recorded base motion of a structure can be used to predict accurately the response of another dissimilar structure. A four-story shear building is used in order to introduce higher modes, yet not require extensive time for computing the response. It is assumed that a certain mass of soil acts with the base of the building when the structure is subjected to a ground shock. Therefore, two spring-mass models are used to represent the structure. One is a "free-base" system representing the structure and the surrounding soil, and the other is a "fixed-base" system representing the type of system generally used in dynamic analyses.

The procedure used to compare the accuracy of the spectrum method of predicting response is shown diagrammatically in Fig. 2, and is as follows:

1. A dynamic load is applied to the base mass of a series of free-base, spring-mass systems. The parameters of the spring-mass systems are chosen so that a range of frequencies is obtained.
2. The response of each free-base system to the dynamic load is computed.

3. A record of the base displacement, as a function of time, of the base mass of one of the free-base, spring-mass systems subjected to the dynamic load is obtained.

4. The record of the base displacement obtained in step 3 is used as an input base displacement for a series of fixed-base, spring-mass systems. The fixed-base systems have the same properties as the free-base systems used in step 1, with the exception of the base mass.

5. The response of each fixed-base system to the base displacement is computed.

6. The responses computed in 2 and 5 are plotted as a function of the frequency of the systems and the results are compared.

The primary purpose of a dynamic analysis is to determine the maximum stresses in the structure. It is, therefore, important to determine the maximum relative displacement between stories because the stresses are proportional to this quantity. Thus, the term "response" as used hereafter will indicate the absolute value of the maximum relative displacement, or introducing the notation y,

$$y_i = \left| (x_i - x_{i-1}) \right| \quad (i = 1, 2, 3, 4) \quad \ldots\ldots\ldots\ldots \quad (3)$$

Spring-Mass Systems.—Fig. 3 illustrates the various spring-mass systems studied. Each system is identified by a two-part code designation. The alphabetic character in the designation indicates a specific value for each mass in the spring-mass system and a particular distribution of spring stiffnesses. The numeric characters indicate specific values for the spring stiffnesses. The spring stiffnesses are varied for each spring-mass system within a particular alphabetic group in order to obtain a range of frequencies. The code designation is used as a subscript to designate that a quantity refers to a certain system. Thus, $x_{i(A1)}$ indicates the absolute displacement of the i^{th} mass of system A1.

The mass and spring stiffness ratios are maintained constant during a particular study so that the mode shapes of each system are the same. In the A, B, and C systems the story mass and spring stiffness ratios are all equal to unity, whereas in the D systems, the upper two stories have a value of story mass and spring stiffness equal to one-half of those in the lower two stories. A small number of calculations were made for the E systems that had two equal masses.

Three different values are assumed for the magnitude of the base mass. It is equal to the sum of the story masses in the A, D, and E systems; to one of the story masses in the B systems; and to ten times one of the story masses in the C systems. The magnitude of the mass of soil that acts with the foundation of a structure will depend on a variety of factors such as the type of foundation, that is pile, footing or raft; the geologic characteristics of the site; the presence of water; the physical properties of the soil; the amount of restraint of the soil mass; the type of failure planes within the soil; and the type of motion that the structure undergoes. It is impossible to define accurately this mass of soil (17),(19),(42),(44) and the values chosen herein are used merely to obtain a variety of conditions.

Another problem in determining a suitable model for the soil mass acting with the foundation of a building is the character of the resistance of the soil. In considering foundation motion, investigators have used many methods to

define soil stiffness. Various types of stiffness constants with a large range of values have been presented (3),(10),(17),(35),(38). Also studies have been made on the propagation of stress waves in soils and various modeling schemes have been used. R. D. Smith, A.M. ASCE, (37) used a Maxwell model, a Voigt model and a modified Voigt model, and also developed a more complex model. R. L. Schiffman, M. ASCE, (36) describes the use of Bingham models and Burgers models. In addition to the complexity of these types of models, the problem of modeling is complicated by the lack of knowledge about the behavior of soils under dynamic loads. Because of the advent of nuclear weapons and the associated requirement for underground protective structures to resist blast-type loadings, there has been an increase in research on determining the dynamic properties of soils (19),(36),(41),(49). At the present time (1961) the exact properties of soil which are pertinent to its dynamic response are uncertain.

Because of the many uncertainties in soil properties and the lack of information about the changes in these properties under dynamic loadings, and be-

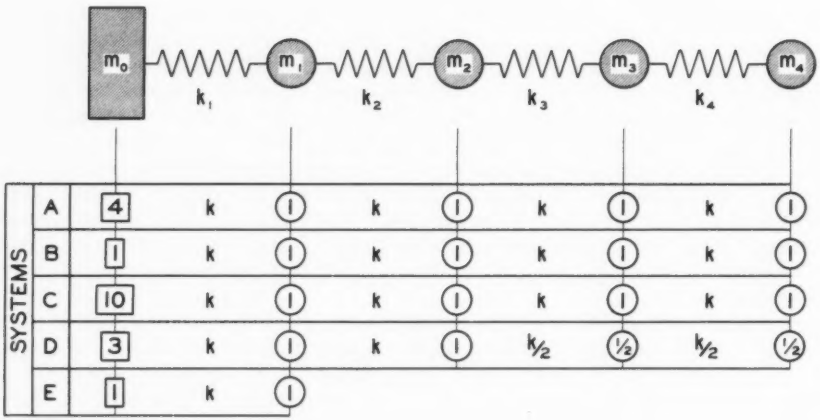

FIG. 3.–DESCRIPTION OF SPRING-MASS SYSTEMS

cause it is not the purpose of this study to investigate these effects per se, the resistance of the soil to deformation is represented by a single dashpot. H. Kawasumi and K. Kanai indicate (18) that studies on actual buildings show that the vibration energy of a building dissipates into the ground in a manner "exactly similar to that of usual viscous damping."

Although the problem of nonelastic deformation of structures is important (11),(40), it is not considered in this study. The structure is assumed to remain linearly elastic, which considerably simplifies the numerical calculations. However, the application of the integration method used can be applied to nonlinear behavior (27).

The assumed values of the masses in each alphabetic spring-mass system and the spring stiffness distribution are shown in Fig. 3. The values of the fixed-base natural frequencies, f_j, and the free-base natural frequencies, $\bar{f}_j$,

were computed for all the systems. The subscripts of the f and f notations refer to the first (that is, lowest) frequency, second frequency, and so on.

Damping Conditions.—Damping in buildings may be due partly to external friction between structural members at connections, partly to internal friction in the material, and partly to damping from air or other adjacent buildings. It is not known just what type of damping is most representative of structural damping (28). For mathematical simplicity, it is usually assumed that the damping is a viscous damping which is taken either proportional to the absolute velocity of each mass, or to the relative velocity of each mass with respect to adjacent masses, or both. P. E. Stevens (39) uses a model based on interfloor dashpots; Tung and Newmark (46) use absolute viscous damping, whereas R. G. Merritt and G. W. Housner (22) recommend a combination of both types. In this study both types were considered separately.

It is customary to define the damping of a system (c) as a proportion (r) of the coefficient of critical damping (c_{cr}). For a linear, spring-mass-dashpot, single-degree-of-freedom system, with a circular natural frequency of $p = \sqrt{k/m}$, this proportion is

$$r = \frac{c}{c_{cr}} = \frac{c}{2\,m\,p} \quad \ldots\ldots\ldots\ldots\ldots\ldots (4)$$

For ease of identification herein, the notation β_o is used to designate the proportion of damping applied to the base mass, m_o, which is proportional to the absolute velocity of m_o; μ_i is used to designate the proportion of damping applied to the i^{th} mass, m_i, which is proportional to the absolute velocity of m_i; and η_i is used to designate the proportion of damping which is proportional to the relative velocity between masses m_i and m_{i-1}. Damping of the base mass is considered proportional to the circular natural frequency of the first free-base mode, $\bar{p}_1$, and damping of the story masses is considered proportional to the circular natural frequency of the first fixed-base mode, p_1. Thus,

$$\beta_o = \frac{c_o}{2\,m_o\,\bar{p}_1} \quad \ldots\ldots\ldots\ldots\ldots\ldots (5a)$$

and

$$\mu_i = \frac{c_i}{2\,m_i\,p_1} \quad (i = 1, 2, 3, 4) \quad \ldots\ldots\ldots\ldots (5b)$$

for systems with absolute damping, and

$$\beta_o = \frac{c_o}{2\,m_o\,\bar{p}_1} \quad \ldots\ldots\ldots\ldots\ldots\ldots (6a)$$

and

$$\eta_i = \frac{c_i}{2\,m_i\,p_1} \quad (i = 1, 2, 3, 4) \quad \ldots\ldots\ldots\ldots (6b)$$

for systems with relative damping.

The amount of damping that can be expected in structures is not easily determined. Merit P. White, F. ASCE, (48) as a result of tests on a reinforced-concrete storage building, indicates a value of absolute damping of approximately 7% of critical. Results of tests on a four-story concrete building also show (14) damping in the order of 0.07. Values of damping in other real buildings have been found (22) to range from 0.07 to 0.40 of critical damping. In this study values of damping of 10% and 20% were used for the base mass, and values of 2% and 10% were used for the story masses. A higher value of damp-

ing was used for the base mass considering the fact that the entire dissipation of energy into the soil is represented by a single dashpot. Calculations of response were made using all possible combinations of the values of damping. The values of damping previously indicated were used for both absolute and relative damping.

Applied Force Functions.—Four time-dependent force functions were arbitrarily selected for the force applied to the base mass. Two of these force functions, P_3 and P_4, are shown diagrammatically in Fig. 4. The first force function, P_1, was a single-cycle sine pulse with a period equal to 10 in terms of the time parameter, t, used. The second force function, P_2, was a single-cycle sine pulse with a period of 4. These two forces were selected in order to compare the effect of the period of the force on the response of the systems.

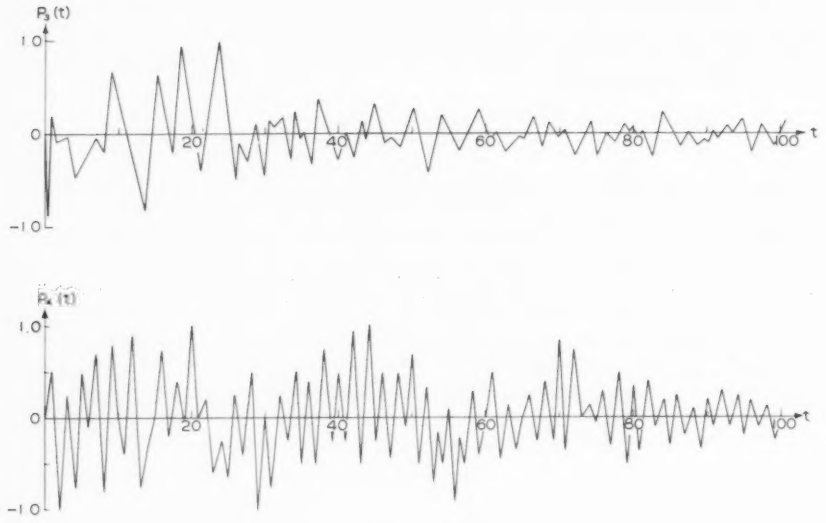

FIG. 4.—APPLIED FORCE FUNCTIONS. P_3 AND P_4

After the initial studies with the simple sine pulses, random force functions, P_3 and P_4, were developed. Force P_3 was obtained by making the force and time scales proportional to the accelerogram of the S 82° E component of the Vernon, California, earthquake of October 2, 1933. The portion of the accelerogram that was used represents an actual time of 5 sec. Because, in this study, this value of time is made equal to 100 in terms of the time parameter t, a unit value of t equals 0.05 second. If this time proportionality is applied to the spring-mass systems studied, their fixed-base periods range from 0.13 sec to 3.0 sec. Therefore, this particular time scale makes the spring-mass system periods compatible with the range of periods for which spectra have been obtained (approximately 0.2 sec to 3.0 seconds) (9).

Force P_4 was selected arbitrarily to represent a forcing function as nearly random as possible, based on studies of a number of earthquake accelerograms.

Dimensions.—The maximum value of each applied force function is expressed in terms of a dimensionless quantity multiplied by a force, F. Other quantities are expressed as nondimensional numerical quantities multiplied by factors related to k_1 and m_1. The dimensional relations for the various multiplying factors used are as follows:

acceleration,	$\ddot{x}$: $\frac{F}{m}$	(LT^{-2})
velocity,	$\dot{x}$: $F\sqrt{\frac{1}{m_1 k_1}}$	(LT^{-1})
displacement,	x: $\frac{F}{k_1}$	(L)
time,	t: $\sqrt{\frac{m_1}{k_1}}$	(T)
frequency,	f: $\sqrt{\frac{k_1}{m_1}}$	(T^{-1})

RESULTS

Shock Response Spectra.—As mentioned previously, a response spectrum is a plot of the response of a system to a specified shock as a function of the frequency of the system. The response can be represented by the maximum value of acceleration, velocity, or displacement. An example of the shock response spectra used in this study is shown in Fig. 7. Frequency, f, is plotted on the abscissa; pseudovelocity, v, on the ordinate; relative displacement, y, on the scale sloping upward to the left; and acceleration, a, on the scale sloping upward to the right.

For an undamped, linearly elastic, single-degree-of-freedom system initially at rest and subjected to a base motion, the spectrum values of response (that is, the absolute value of the maximum quantity) can be simply related (16). These relations also apply to the spectrum values for the separate modes of a multi-degree-of-freedom system. However, when the total response of the system is calculated by the simultaneous solution of the governing differential equations of motion, these relations are no longer applicable. In this study, the maximum value of the total relative displacement was computed for a particular spring under certain conditions of damping and applied forces, and the absolute magnitude was plotted as the spectrum value of relative displacement, y. Therefore, this value is the only one with a direct physical significance. The spectrum values of pseudovelocity and of acceleration are computed from the same formal relations applicable to a single-degree-of-freedom system. The terms "v" and "a" are called "spectrum value of pseudovelocity" and "spectrum value of pseudoacceleration," respectively.

Amplification Factor.—Because the objective of this study is to compare the response of a free-base system subjected to a force applied to the base mass with the response of the same system considered to be a fixed-base system subjected to a base motion assumed to represent the effects of the actual disturbing force, it is helpful to compare these responses in terms of a ratio

called the amplification factor, AF. This amplification factor is defined as the ratio of the "erroneous" spectrum value of displacement of the fixed-base system to the "true" spectrum value of displacement for the free-base system. A separate amplification factor is computed for each spring and it is

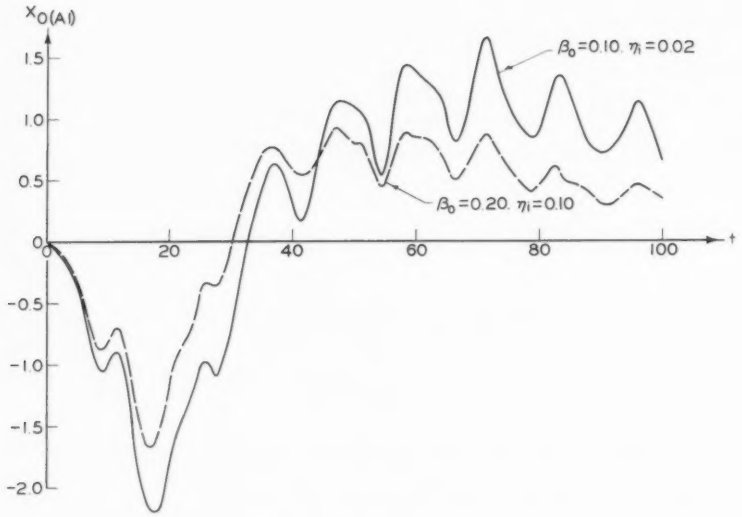

FIG. 5.–BASE DISPLACEMENT OF SYSTEM A1, APPLIED FORCE P_3

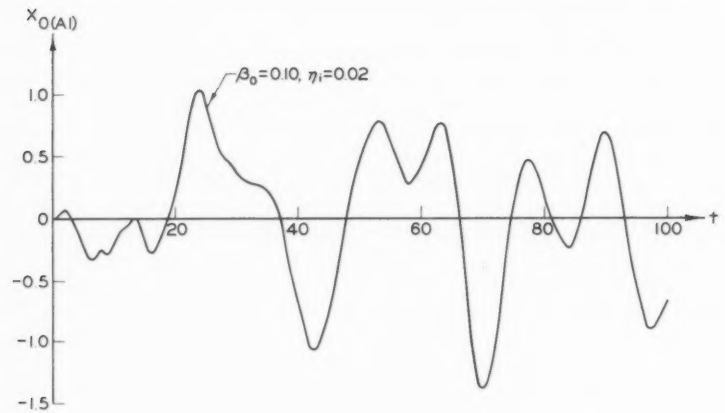

FIG. 6.–BASE DISPLACEMENT OF SYSTEM A1, APPLIED FORCE P_4

given a subscript to indicate the particular spring in question. Thus,

$$AF_i = \frac{\text{fixed-base } y_i}{\text{free-base } y_i} \quad (i = 1, 2, 3, 4) \ldots\ldots\ldots\ldots (7)$$

General Form of Results.—Thirty-four different problem groups were analyzed in order to study the effects of the various parameters. Within each problem group, an average of twenty spring-mass systems were analyzed as both fixed-base systems and free-base systems. Thus, the response was calculated for over 1,300 separate problems. Both absolute and relative damping were included, and the amount of damping was varied for each series of problems analyzed in a particular group. Response spectra were plotted for each spring of each system for every set of assumed conditions.

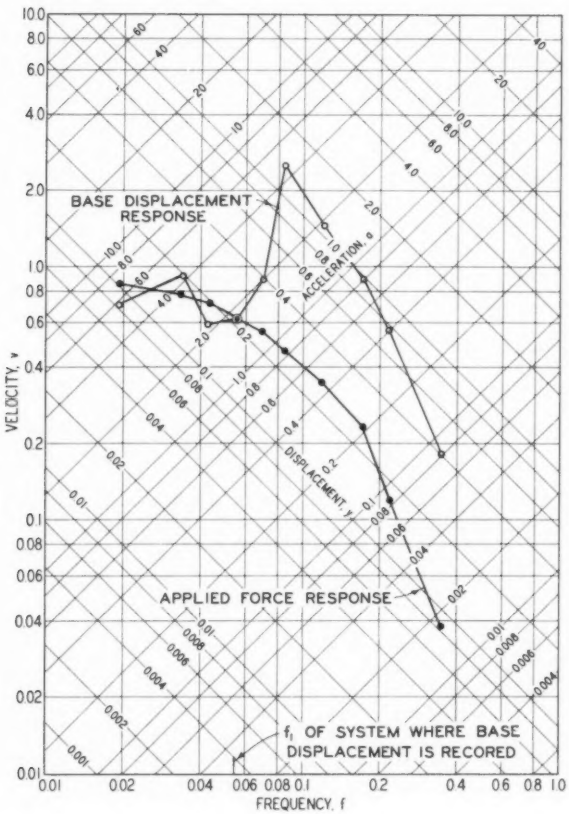

FIG. 7.—GENERAL FORM OF RESPONSE SPECTRA

Figs. 5 and 6 show the base displacement record that was obtained on one of the free-base systems for subsequent use as the base motion input of the fixed-base systems. These records are typical of the others used for this particular forcing function.

Figs. 8, 9, and 10 represent typical response spectra that were obtained. Fig. 8 is the spectra for the first spring of the B systems with the amount of damping as indicated and subjected to applied force, P_1. Fig. 9 is the spectra for the second spring of the same systems under the same conditions.

Fig. 7 indicates the general form of the response spectra. The solid circles indicate the response of the various free-base systems to the particular force function under study. The open circles indicate the response of the various fixed-base systems to a base motion that was recorded during the application of the applied force to a particular spring-mass system. The response of each system is plotted as a function of the first fixed-base natural frequency of the system, f_1. The value of f_1 for the free-base system on which the record of the base motion was obtained is indicated on the frequency scale. The free-

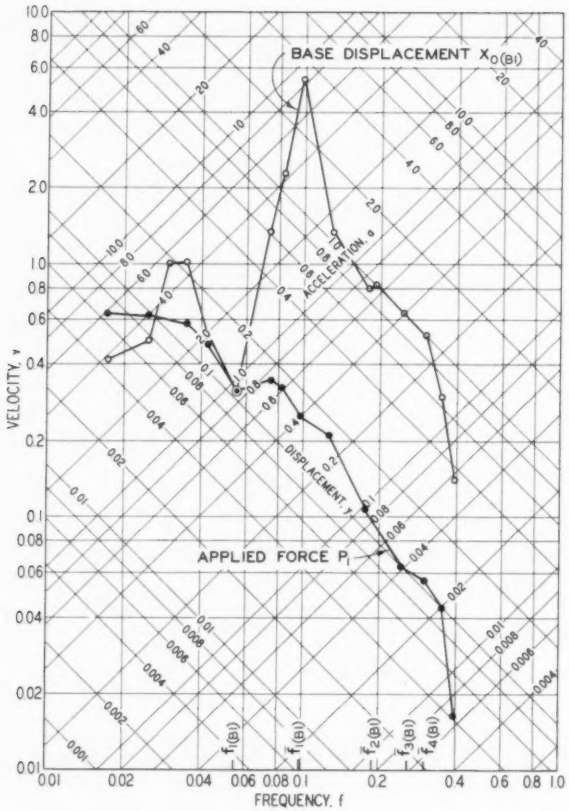

FIG. 8.—RESPONSE SPECTRA $y_1 : v_1 : a_1$ FOR "B" SYSTEMS, APPLIED FORCE P_1, DAMPING—$\beta_0 = 0.10, \eta_1 = 0.02$

base frequencies, $\bar{f}_j$, of each particular system plotted are of interest and in subsequent spectra these four values are also indicated on the frequency scale.

The free-base response and the fixed-base response are identical, except coincidentally, only for the particular system on which the base motion record was obtained. For all systems with a natural frequency higher than this system, the fixed-base response is larger than the "true" free-base response.

For all systems with a natural frequency lower than this system, there is a random distribution of values, although in general the fixed-base response is smaller than the "true" free-base response. The value of the amplification factor varies depending on the parameters of a specific problem; however, usually the fixed-base response in the higher frequency range, that is, frequencies higher than the frequency of the system on which the base motion was recorded, is much more in error than is the fixed-base response in the lower frequency range.

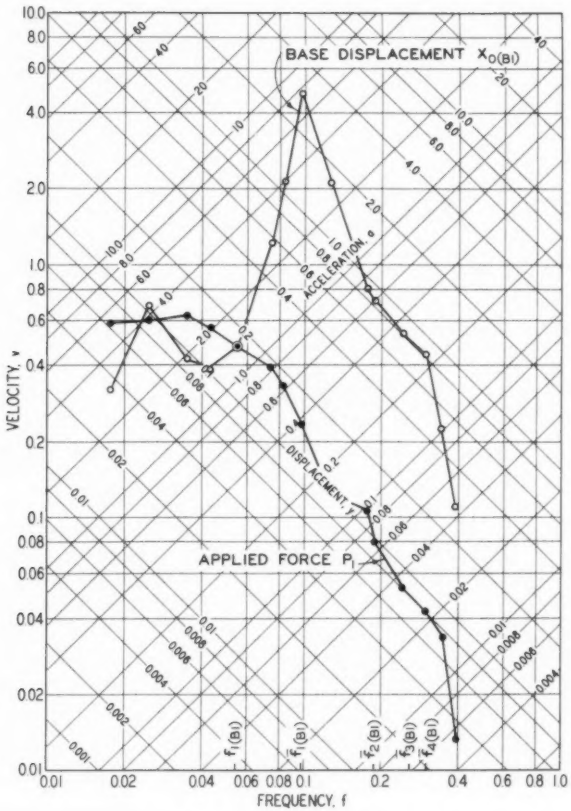

FIG. 9.–RESPONSE SPECTRA $y_2 : v_2 : a_2$ FOR "B" SYSTEMS, APPLIED FORCE P_1, DAMPING – $\beta_0 = 0.10, \eta_1 = 0.02$

The AF was computed for all the systems studied and some of these values are shown as a function of frequency in Figs. 11 through 15. The difference in the value of the AF in the lower frequency range and in the higher frequency range can be readily observed from these figures. The AF tends to reach a peak value at each of the free-base frequencies of the system on which the base motion was recorded. However, the important observation that can be

made from these figures is that the AF remains large throughout the entire range of higher frequencies.

A summary of all the amplication factors computed for the first spring, AF_i, is presented in Table 1. The range of values and the mean value are listed separately for the higher frequency range and the lower frequency range. Because there appears to be a transition range between the first fixed-base

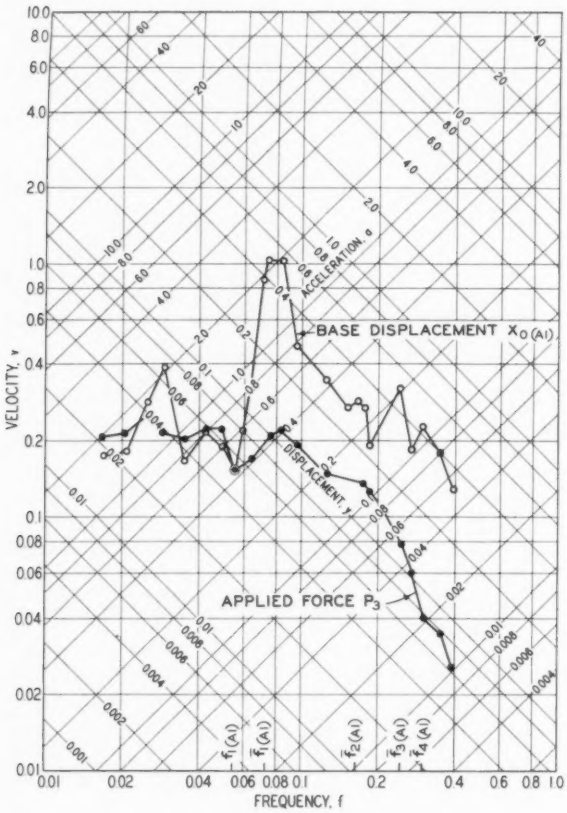

FIG. 10.–RESPONSE SPECTRA $y_1 : v_1 : a_1$ FOR "A" SYSTEMS, APPLIED FORCE P_3, DAMPING – $\beta_0 = 0.10$, $\eta_1 = 0.02$

frequency of the system on which the base motion was recorded and the first free-base frequency of that system, the values of AF in this range have not been included when computing the averages. The lower frequency range includes all frequencies smaller than the first fixed-base frequency and the higher frequency range includes the first free-base frequency and all larger values. The mean value may be slightly biased in the higher range, because

TABLE 1.—AMPLIFICATION FACTOR, AF_1

Systems	Applied Force	Damping Conditions	$f \geq \bar{f}_{1(A1)}, \bar{f}_{1(B1)}$, etc.			$f < f_{1(A1)}, f_{1(B1)}$, etc.		
			High AF_1	Low AF_1	Avg. AF_1	High AF_1	Low AF_1	Avg. AF_1
A	P_1	$\beta_o = 0.10, \mu_i = 0.02$	4.48	2.20	3.24	1.29	0.65	0.89
		$\beta_o = 0.10, \mu_i = 0.10$	3.15	1.84	2.52	1.17	0.61	0.85
		$\beta_o = 0.20, \mu_i = 0.02$	3.54	3.06	3.31	1.15	0.50	0.81
		$\beta_o = 0.20, \mu_i = 0.10$	2.92	1.60	2.37	0.94	0.57	0.79
		$\beta_o = 0.10, \eta_i = 0.02$	5.12	3.58	4.21	1.62	0.83	1.06
		$\beta_o = 0.20, \eta_i = 0.10$	5.10	2.72	3.56	1.42	0.70	1.03
	P_2	$\beta_o = 0.10, \mu_i = 0.02$	3.65	1.74	2.50	1.29	0.76	0.90
		$\beta_o = 0.20, \mu_i = 0.10$	3.95	1.16	2.19	0.96	0.75	0.86
		$\beta_o = 0.10, \eta_i = 0.02$	4.00	1.89	2.91	1.34	0.74	0.95
		$\beta_o = 0.20, \eta_i = 0.10$	3.61	1.81	2.60	0.95	0.75	0.86
	P_3	$\beta_o = 0.10, \eta_i = 0.02$	6.01	1.89	3.57	1.72	0.85	1.04
		$\beta_o = 0.20, \eta_i = 0.10$	6.30	1.80	3.92	1.31	0.71	0.94
	P_4	$\beta_o = 0.10, \eta_i = 0.02$	6.20	2.83	4.37	1.48	0.53	0.98
B	P_1	$\beta_o = 0.10, \mu_i = 0.02$	15.36	6.00	9.05	2.44	0.62	1.11
		$\beta_o = 0.20, \mu_i = 0.10$	7.75	4.88	5.83	1.40	0.40	0.64
		$\beta_o = 0.10, \eta_i = 0.02$	20.65	6.53	10.82	2.59	0.65	1.37
		$\beta_o = 0.20, \eta_i = 0.10$	13.50	5.19	7.66	1.76	0.49	1.05
C	P_1	$\beta_o = 0.10, \mu_i = 0.02$	3.43	1.47	2.02	1.28	0.66	0.87
		$\beta_o = 0.20, \mu_i = 0.10$	3.21	1.13	2.09	1.07	0.61	0.77
		$\beta_o = 0.10, \eta_i = 0.02$	2.74	1.60	2.00	1.49	0.65	0.94
		$\beta_o = 0.20, \eta_i = 0.10$	2.58	1.83	2.23	1.04	0.61	0.83
D	P_1	$\beta_o = 0.10, \eta_i = 0.02$	6.10	2.00	3.51	0.98	0.63	0.79
		$\beta_o = 0.20, \eta_i = 0.10$	4.46	2.23	3.25	0.89	0.60	0.76
	P_3	$\beta_o = 0.10, \eta_i = 0.02$	6.78	1.91	4.09	1.08	0.70	0.87
		$\beta_o = 0.20, \eta_i = 0.10$	8.03	2.03	3.58	0.93	0.69	0.84
E	P_3	$\beta_o = 0.10, \mu_i = 0.02$	5.39	2.57	3.80	0.96	0.24	0.65
		$\beta_o = 0.20, \mu_i = 0.10$	3.48	1.83	2.83	0.73	0.26	0.56
		$\beta_o = 0.10, \eta_i = 0.02$	5.58	2.48	3.80	1.01	0.23	0.67
		$\beta_o = 0.20, \eta_i = 0.10$	4.04	1.73	2.70	0.79	0.33	0.63
	P_4	$\beta_o = 0.10, \eta_i = 0.02$	6.49	2.16	4.25	1.24	0.26	0.89
		$\beta_o = 0.20, \eta_i = 0.10$	4.39	1.93	3.22	1.01	0.26	0.71

more systems were studied in the area in which the amplification factor appears to be largest.

ANALYSIS OF RESULTS

The response spectra give the magnitude of the effects of the various parameters; however, the amplification factor, that is the ratio of the responses, gives a qualitative representation of the effects. Whereas only values of AF_1 are presented in this paper, the figures indicate the trends that were observed in the other amplification factors.

Effect of Damping.—Viscous damping proportional to absolute velocity and proportional to relative velocity was studied. Figs. 11 and 12 indicate the typical results obtained. These figures are for the A systems subjected to applied force function P_1.

Fig. 11, which shows the AF for absolute damping, indicates that increased damping substantially reduces the AF in the region of the first free-base frequency, $\bar{f}_{1(A1)}$. This would be expected because the damping was taken proportional to the first natural frequency. As the frequency increases above $\bar{f}_{1(A1)}$ the difference in AF between the two extreme cases of damping becomes less. In the region of frequencies below the first fixed-base frequency, $f_{1(A1)}$, there is only a slight difference in AF. Except for the region around $\bar{f}_{1(A1)}$, the general shape of the amplification curves is similar.

For the conditions shown in Fig. 11, the average values of AF for the higher frequency range were: $AF_1 = 3.24, 2.37$; $AF_2 = 3.16, 2.31$; $AF_3 = 3.21, 2.26$; and $AF_4 = 3.15, 2.24$, where the first value listed is for the smaller amount of damping and the second is for the larger amount of damping. In the lower frequency range the values were: $AF_1 = 0.89, 0.79$; $AF_2 = 0.93, 0.84$; $AF_3 = 1.03, 0.83$; and $AF_4 = 1.01, 0.81$. This ratio of difference in values is generally true in the other problems in which the systems and the applied force function were varied. Thus, doubling the amount of damping on the base mass and increasing by five the amount of damping on the other masses decreases the AF by about 40% in the higher frequency range and by about 15% in the lower frequency range. The only major deviation from this pattern was found in the C systems which have a large base mass. In the C systems the AF appears to be insensitive to increased amounts of damping.

Fig. 12, which shows the AF for relative damping, indicates that increased amounts of relative damping have less effect on the AF than did increased amounts of absolute damping. The larger amount of relative damping decreases the AF by about 15% in the higher frequency range and by 5% to 10% in the lower frequency range. Again, the AF for the C systems appears to be insensitive to the amount of damping.

A comparison can also be made between the AF for absolute damping in a system versus the AF for relative damping in the same system. Using the conditions given in Figs. 11 and 12 and comparing values for the smaller amount of damping $(\beta_0 = 0.10,\ \mu_i = \eta_i = 0.02)$ gives average values in the higher frequency range of $AF_1 = 3.24, 4.21$; $AF_2 = 3.16, 4.15$; $AF_3 = 3.21, 4.21$; and $AF_4 = 3.15, 4.05$, where the first value is for absolute damping and the second is for relative damping. Thus, if the same percentage of damping is used, relative damping will give slightly higher values of AF than absolute damping would give.

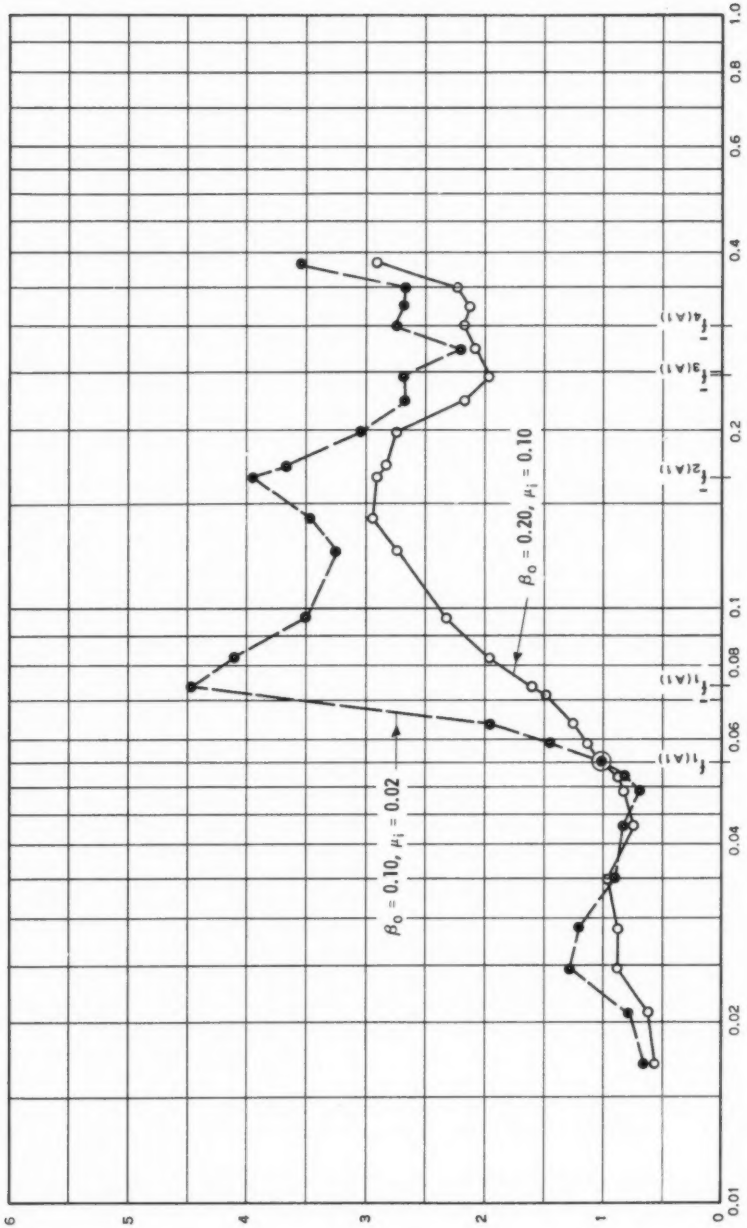

FIG. 11.–AMPLIFICATION FACTOR FOR "A" SYSTEMS, APPLIED FORCE P_1, ABSOLUTE DAMPING

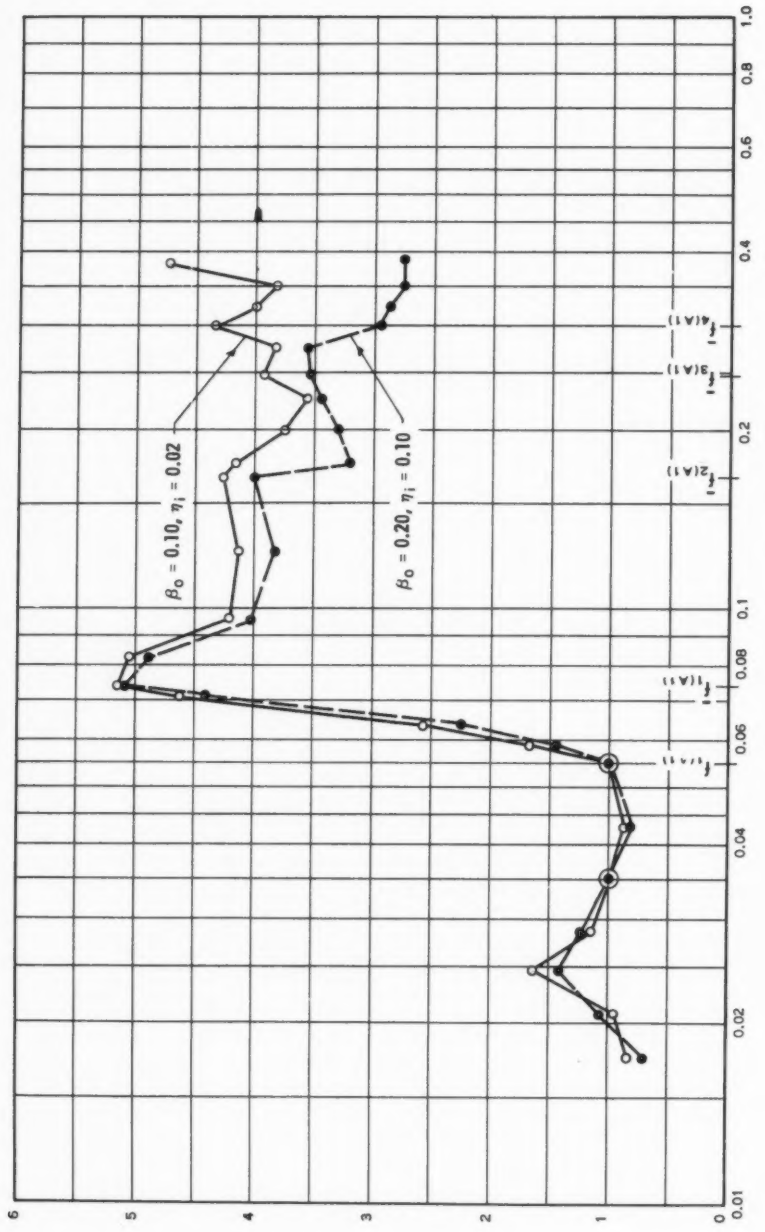

FIG. 12.–AMPLIFICATION FACTOR FOR "A" SYSTEMS, APPLIED FORCE P_1, RELATIVE DAMPING

Effect of Applied Force Function.—A comparison of AF for the various force functions applied to the A systems with relative damping ($\beta_0 = 0.10$, $\eta_1 = 0.02$) is shown in Fig. 13. All the amplification curves show the same general tendency to peak at the four free-base natural frequencies of the system on which the base motion was recorded (that is, $\bar{f}_{j(A1)}$); however, the AF values at these peaks and the shape of the curves between peaks vary considerably. Considering the higher frequency range (that is, $\geq \bar{f}_{1(A1)}$) and listing the AF for P_1, P_2, P_3, and P_4 in that order, the average values are: $AF_1 = 4.21$, 2.91, 3.57, 4.37; $AF_2 = 4.15$, 2.94, 3.28, 4.24; $AF_3 = 4.21$, 2.54, 2.98, 3.95; and $AF_4 = 4.05$, 2.33, 2.70, 3.76. The AF values in the lower frequency range (that is $< f_{1(A1)}$) are more closely related and follow approximately the same distribution regardless of the applied force function.

Applied force P_1 reaches a maximum amplification effect at the first free-base frequency, $\bar{f}_{1(A1)}$, and then produces an almost constant AF over the entire range of higher frequencies. Applied force P_2 reaches a maximum effect at the second free-base frequency, $\bar{f}_{2(A1)}$, while P_3 produces a large amplification at both the first and fourth free-base frequencies ($\bar{f}_{1(A1)}$ and $\bar{f}_{4(A1)}$). Applied force P_4 produces large effects at both the first and second free-base frequencies ($\bar{f}_{1(A1)}$ and $\bar{f}_{2(A1)}$). Also, the peaks are much more pronounced for applied forces P_3 and P_4.

Effect of Magnitude of Base Mass.—The effect of the magnitude of the base mass is presented in Fig. 14 which shows the amplification curves for force P_1 applied to the A, B, and C systems with relative damping ($\beta_0 = 0.20$, $\eta_1 = 0.10$). The A systems have a base mass equal to the sum of the story masses, the B systems have a base mass equal to one of the story masses, and the C systems have a base mass equal to ten times one of the story masses. As would be expected, the amplification is several times greater for the systems with a small base mass than for the systems with a large base mass.

The amplification curve for the B system shows more of a tendency to peak at certain free-base frequencies of the system on which the base displacement was recorded ($\bar{f}_{1(B1)}$ and $\bar{f}_{3(B1)}$) than do the other curves. In the higher frequency range, considering AF_1, AF_2, AF_3, and AF_4 compositely, the AF for the B systems varies from 13.50 to 5.10 with an average of about 7.6. The values of AF for the A and C systems in the higher frequency range are more uniformly distributed with an average of about 3.5 and 2.2, respectively. Again, the AF values were more closely related in the lower frequency range with a composite average for the A, B, and C systems of approximately 1.0, 0.8, and 0.8, respectively.

This limited study indicates that an approximate relation exists between the average amplification to be expected in the higher frequency range and the magnitude of the base mass. This relation indicates that the amplification factor varies roughly as the square root of the inverse ratio of the magnitude of the base masses. Thus,

$$\frac{\text{AF of systems with } m_0 = y}{\text{AF of systems with } m_0 = x} = \sim \left[\frac{x}{y}\right]^{1/2} \quad \ldots\ldots\ldots \quad (8)$$

This relation is crude because the amplification is far from uniform, but it does serve to give some insight into the effect of the base mass upon the errors that can be expected. A similar relation is derived relating the maxi-

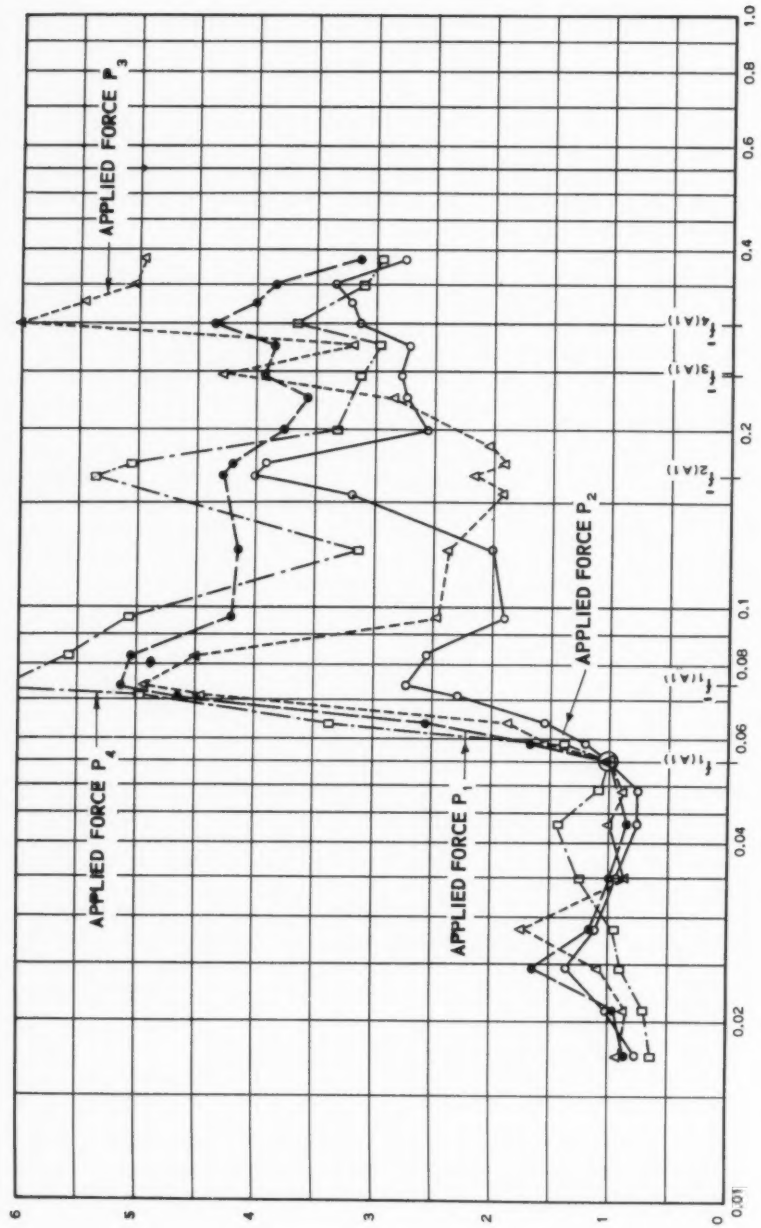

FIG. 13.—AMPLIFICATION FACTOR FOR "A" SYSTEMS, APPLIED FORCES, DAMPING - $\beta_0 = 0.10$, $\eta_1 = 0.02$

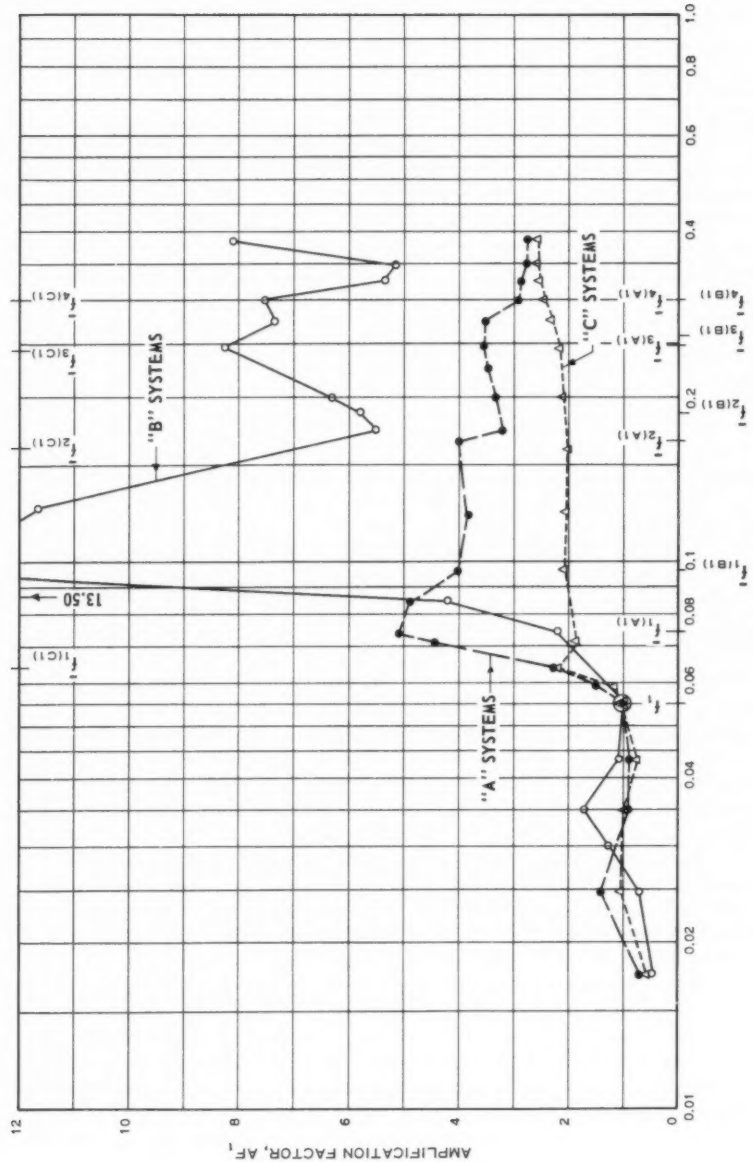

FIG. 14.–AMPLIFICATION FACTOR FOR "A", "B" & "C" SYSTEMS, APPLIED FORCE P_1, DAMPING – $\beta_0 = 0.20$, $\eta_1 = 0.10$

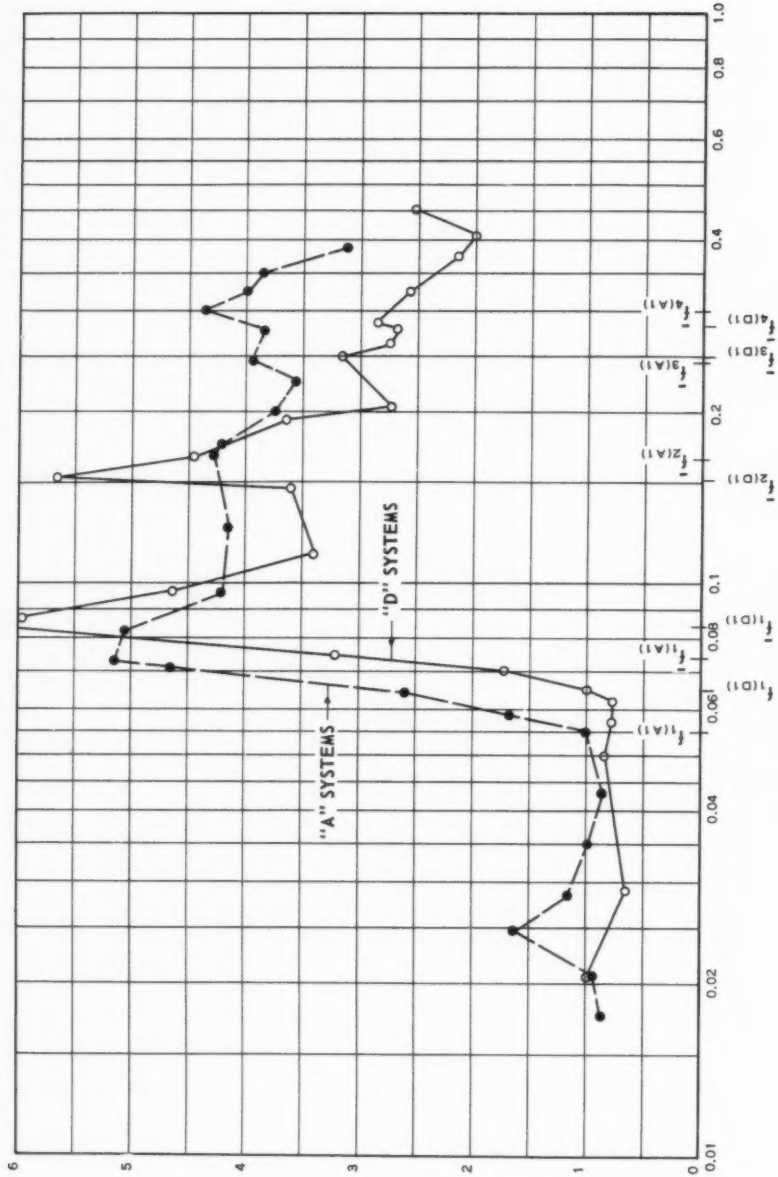

FIG. 15.–AMPLIFICATION FACTOR FOR "A" & "D" SYSTEMS, APPLIED FORCE P_1, DAMPING – $\beta_0 = 0.10$, $\eta_1 = 0.02$

mum values of AF obtained in this study as follows:

$$\frac{AF_{max} \text{ of system with } m_o = y}{AF_{max} \text{ of system with } m_o = x} = \sim \left[\frac{x}{y}\right]^{0.7} \quad \ldots\ldots\ldots (9)$$

Effect of Mass and Spring Stiffness Distribution.—In all of the problems previously examined, the spring-mass systems studied had a uniform distribution of mass and spring stiffness. Fig. 15 shows the amplification curves for A and D systems with relative damping ($\beta_o = 0.10$, $\eta_i = 0.02$) subjected to applied force P_1. The A systems have equal masses and equal spring stiffnesses whereas the D systems have the upper two-story masses and spring stiffnesses equal to one-half of the lower story values. The tendency to peak at the free-base natural frequencies of the system on which the base motion was recorded is again evident and is more pronounced in the D systems. The average values of AF in the higher frequency range for the A and D systems were: AF_1 = 4.21, 3.51; AF_2 = 4.15, 3.40; AF_3 = 4.21, 3.33; and AF_4 = 4.05, 3.21, respectively. The amplification factor in the lower frequency range varied approximately in the same manner as other problems that have been described.

The base mass in both the A and D systems is equal to the sum of the story masses, but because the upper two-story masses are smaller in the D systems, the base mass of the D systems is smaller than the base mass of the A systems. Therefore, the free-base natural frequencies of the D systems are larger than those of the A systems. A comparison of the amplification curve of the D systems subjected to applied force P_1 (Fig. 15) and the amplification curve of the A systems subjected to applied force P_2 (Fig. 13) shows a remarkable similarity in shape and in tendency to reach a maximum value at the second free-base natural frequency ($\bar{f}_{2(D1)}$ and $\bar{f}_{2(A1)}$). Thus, as was mentioned before, there appears to be evidence of a relation between the frequency of the applied force function and the free-base frequencies of the system.

Applying the relation derived previously for the effect of the magnitude of the base mass on the average amplification in the higher frequency range, it was found that in this case the relation was not valid. As a matter of fact, the square root of the ratio of base masses is more applicable than the square root of the inverse ratio. No explanation can presently be given for this discrepancy. However, if the maximum values of AF are used, it was found that the 0.7 power of the inverse base-mass ratio is still applicable.

It is interesting to compare these values of AF in the higher frequency range for the moderate-sized base-mass systems A and D with the values reported by Tung and Newmark (46). From the analysis of a ten-story building, they found values of story shears from about 1.2 to 4 times larger than the design shears computed by the procedure recommended by the Joint Committee on Lateral Forces (1). Depending on what system the base motion record was obtained for subsequent use as an input disturbance, the AF values for the A and D systems averaged from about 2 to 4. It is only a coincidence that these values fall in the same range; however, the effect of structure and foundation interaction may explain the reason for part of the discrepancy between the results of analyses and the behavior of buildings subjected to earthquakes.

CONCLUSIONS

The purpose of this investigation was to study the errors that may occur when the foundation motion of particular structure is used to determine the

response of other dissimilar structures. It is common practice in dynamic design problems to use a response spectrum concept to describe or to specify the shock that the designed structure must withstand; however, in developing this spectrum the base motion of a structure that has been subjected to a similar shock is used by assuming that this base motion is an accurate description of the shock. That is to say, the assumption is made that the motion of a structure does not affect the foundation motion. If the errors in this assumption are large, then a design based on this concept will be inaccurate. The designed structure may be greatly overdesigned or it may be quite incapable of withstanding the anticipated shock.

In this study various multi-degree-of-freedom, spring-mass models were developed to represent dynamically actual structures. For all of the model systems studied, it was found that the lowest fixed-base natural frequency of the model on which the base motion record was obtained was an important parameter. When the base motion recorded on this model was applied as a base disturbance to any fixed-base model with a higher natural frequency, the response of the fixed-base model always exceeded the "true" free-base response of that model. When the base motion was applied to models with a lower natural frequency, the fixed-base response, although variable, was generally about equal to the "true" free-base response of that model.

The magnitude of the responses was found to vary widely, depending on the model parameters used. In the higher frequency range, the fixed-base response was as much as 20 times the free-base response. In the lower frequency range, the fixed-base responses for the systems studied varied from a maximum of 2.59 to a minimum of 0.25 times the free-base responses.

Although there was a large range in the amount of variance, it is important to note that higher frequency systems always had a larger fixed-base response and lower frequency systems usually had a smaller fixed-base response when compared to the true free-base response. Because the free-base and fixed-base responses only coincide for the exact system on which the base motion was recorded, it is evident that errors will be developed in actual use. The actual dynamic properties and the behavior of a structure subjected to shock can only be estimated. Thus, when a base motion record of an actual structure is used as an input disturbance for a model of the same structure, the calculated response will be in error unless the model exactly depicts the real structure. If the model has a higher frequency than the actual structure, the model analysis will predict responses that are larger than the actual responses. If the model has a lower frequency than the real structure, the model analysis may predict smaller responses.

Considering the model parameters used in this study, the difference in actual and computed response is much less in the range of frequencies smaller than the natural fixed-base frequency of the system on which the base disturbance was measured. Thus, it would seem that base motion records obtained on relatively high frequency structures, such as stiff, short buildings or on equipment with a high fundamental frequency, would provide more reliable data. Although this study primarily concerns buildings subjected to ground

motion, the generalization of the parameters makes it applicable to other shock transmission problems.

ACKNOWLEDGMENT

This paper is based on a dissertation prepared by Lycan[1] and submitted to the Graduate College of the University of Illinois, Urbana, Ill. in partial fulfillment of the requirements for the degree of Doctor of Philosophy in Civil Engineering. The investigation was conducted under the direction of Newmark.[2] Appreciation is expressed to all the personnel of the United States Army Engineer Waterways Experiment Station who assisted in preparing the manuscript and especially to the Director, Edmund H. Lang, F. ASCE, Corps of Engineers, for his continual interest and encouragement, and for having made this assistance available.

APPENDIX I.—NOTATIONS

The symbols used in the paper are presented here for ease of reference and for the use of discussers:

A = alphabetic designation of a series of MDF spring-mass systems;

AF = amplification factor designating the ratio of spectrum value of displacement of fixed-base system to spectrum value of displacement of free-base system;

a = spectrum value of pseudoacceleration;

B = alphabetic designation of a series of MDF spring-mass systems;

C = alphabetic designation of a series of MDF spring-mass systems;

c = coefficient of viscous damping;

c_{cr} = coefficient of critical damping;

D = alphabetic designation of a series of MDF spring-mass systems;

E = alphabetic designation of a series of MDF spring-mass systems;

F = dimension of force;

f = undamped natural frequency (fixed-base system);

$\bar{f}$ = undamped natural frequency (free-base system);

h = time interval in β-integration method;

Subscript i = i^{th} mass;

Subscript j = j^{th} natural frequency;

k = spring stiffness;

L = dimension of length;

MDF = multi-degree-of-freedom system;

m = mass;

P = applied force function;

p = undamped natural circular frequency (fixed-base system);

$\bar{p}$ = undamped natural circular frequency (free-base system);

r = proportion of critical viscous damping;

T = dimension of time;

T_{min} = shortest natural period of vibration;

t = time;

u = relative displacement of mass;

$\dot{u}$ = relative velocity of mass;

v = spectrum value of pseudovelocity;

x = absolute displacement of mass;

$\dot{x}$ = absolute velocity of mass;

$\ddot{x}$ = absolute acceleration of mass;

y = spectrum value of relative displacement;

β = parameter in numerical integration method;

β_o = proportion of critical viscous damping applied to base mass (proportional to absolute velocity);

η = proportion of critical viscous damping applied to story mass (proportional to relative velocity); and

μ = proportion of critical viscous damping applied to story mass (proportional to absolute velocity).

APPENDIX II.—BIBLIOGRAPHY ON STRUCTURE AND FOUNDATION INTERACTION

---

1. "Lateral Forces of Earthquake and Wind," by A. W. Anderson, J. A. Blume, et al., Transactions, ASCE, Vol. 117, 1952, p. 716.

2. "Methods for Calculating the Earthquake Response of 'Shear' Buildings," by R. S. Ayre, Proceedings, World Conf. on Earthquake Engrg., Earthquake Engrg. Research Inst. and Univ. of California, Berkeley, Calif., June, 1956, Paper No. 13.

3. "Analytical and Experimental Methods in Engineering Seismology," by M. A. Biot, Transactions, ASCE, Vol. 108, 1943, p. 366.

4. "Structural Dynamics in Earthquake-Resistant Design," by J. A. Blume, Transactions, ASCE, Vol. 126, 1960.

5. "Stresses in the Linings of Shield-Driven Tunnels," by A. Bull, Transactions, ASCE, Vol. 111, 1946, p. 443.

6. "Earthquake Forces in a Tall Building," by R. W. Clough, Civil Engineering, Vol. 26, January, 1956, p. 22.

7. "The Theory of Vibrations for Engineers," by E. B. Cole, The MacMillan Co., New York, 3rd edition, 1957.

8. "Effects of Ground on Destructiveness of Large Earthquakes," by C. M. Duke, Proceedings, ASCE, Vol. 84, No. SM3, August, 1958.

9. "Aseismic Design of Elastic Structures Founded on Firm Ground," by L. E. Goodman, E. Rosenblueth, and N. M. Newmark, Tech. Report to the Office of Naval Research, Contract N6 onr-71, Task Order VI, Project NR-064-183, Civ. Engrg. Studies, Univ. of Illinois, Urbana, Ill., Structural Research Series No. 26.

10. "Dynamic Testing of Pavements," by W. Heukelom and C. R. Foster, Proceedings, ASCE, Vol. 86, No. SM1, February, 1960, p. 1.

11. "Behavior of Structures During Earthquakes," by G. W. Housner, Proceedings, ASCE, Vol. 85, No. EM4, October, 1959, p. 109.

12. "Spectrum Intensities of Strong Motion Earthquakes," by G. W. Housner, Proceedings, Symposium on Earthquake and Blast Effects on Structures, Earthquake Engrg. Research Inst. and Univ. of California, Los Angeles, Calif., June, 1952, p. 20.

13. "Interaction of Building and Ground During an Earthquake," by G. W. Housner, Bulletin, Seismological Soc. of Amer., Vol. 47, No. 3, July, 1957, p. 179.

14. "Spectrum Analysis of Strong-Motion Earthquakes," by G. Housner, R. R. Martel, and J. L. Alford, Bulletin, Seismological Soc. of Amer., Vol. 43, No. 2, April, 1953, p. 97.

15. "The Analysis of Strong-Motion Earthquake Records with the Electric Analog Computer," by G. W. Housner and G. D. McCann, Bulletin, Seismological Soc. of Amer., Vol. 39, No. 1, January, 1949, p. 47.

16. "Response Spectrum Techniques in Engineering Seismology," by D. E. Hudson, Proceedings, World Conf. on Earthquake Engrg., Earthquake Engrg. Inst., and Univ. of California, Berkeley, Calif., June, 1956, Paper No. 4.

17. "Engineering Vibrations," by L. S. Jacobson and R. S. Ayre, McGraw-Hill Book Co., Inc., New York, 1958.

18. "Small Amplitude Vibrations of Actual Buildings," by H. Kawasumi and K. Kanai, Proceedings, World Conf. on Earthquake Engrg., Earthquake Engrg. Research Inst. and Univ. of California, Berkeley, Calif., June, 1956, Paper No. 7.

19. "Studies of Investigations into the Dynamic Bearing Properties of Cohesionless Soils," by T. D. Landale, thesis presented to M.I.T., in Cam-

bridge, Mass., in September, 1954, in partial fulfilment of the requirements for the degree of Master of Science.

20. "Effect of Foundation on Earthquake Motion," by R. R. Martel, Civil Engineering, Vol. 10, January, 1940, p. 7.

21. "Development of Procedures for Rapid Computation of Dynamic Structural Response," by J. W. Melin, Final Report for the Period July 1, 1955, to June 30, 1956, Contract No. AF 33 (600)-24994 for Physical Vulnerability Div., Directorate of Intelligence, U. S. Air Force, Civ. Engrg. Studies, Univ. of Illinois, Urbana, Ill., Structural Research Series No. 126.

22. "Effect of Foundation Compliance on Earthquake Stresses in Multistory Buildings," by R. G. Merritt and G. W. Housner, Bulletin, Seismological Soc. of Amer., Vol. 44, No. 4, October, 1954, p. 551.

23. "Electrical Analog for Earthquake Shear Stresses in Multi-Story Building," by M. J. Murphy, G. N. Bycroft, and L. W. Harrison, Proceedings, World Conf. on Earthquake Engrg., Earthquake Engrg. Research Inst. and Univ. of California, Berkeley, Calif., June, 1956, Paper No. 9.

24. "Analysis and Design of Structures to Resist Atomic Blast," by N. M. Newmark, Bulletin, Virginia Polytechnic Inst., Engrg. Experiment Sta. Series No. 106, Vol. XLIX, No. 3-Part 2, January, 1956, p. 49.

25. "Computation of Dynamic Structural Response in the Range Approaching Failure," by N. M. Newmark, Proceedings, Symposium on Earthquake and Blast Effects on Structures, Earthquake Engrg. Research Inst. and Univ. of California, Los Angeles, Calif., June, 1952, p. 114.

26. "The Effect of Dynamic Loads on Offshore Structures," by N. M. Newmark, Tech. Report to Office of Naval Research, Contract Nonr 1834(03), Project NR-064-183, Civ. Engrg. Studies, Univ. of Illinois, Urbana, Ill., Structural Research Series No. 155.

27. "A Method of Computation for Structural Dynamics," by N. M. Newmark, Proceedings, ASCE, Vol. 85, No. EM3, July, 1959, p. 67.

28. "Structural Design for Dynamic Loads," by C. H. Norris, R. J. Hansen, et al., McGraw-Hill Book Co., Inc., New York, 1959.

29. "Impedance and Shock Spectra," by G. J. O'Hara, Journal, Acoustical Soc. of Amer., Vol. 31, No. 10, October, 1959, p. 1300.

30. "Effect upon Shock Spectra of the Dynamic Reaction of Structures," by G. J. O'Hara, U. S. Naval Research Lab., Washington, D. C., NRL Report 5236, December, 1958.

31. "Shock Spectra and Design Shock Spectra," by G. J. O'Hara, U. S. Naval Research Lab., Washington, D. C., NRL Report 5386, November, 1959.

32. "Impact Wave Propagation in Columns of Sand," by B. R. Parkin, Rand Corp., Santa Monica, Calif., RM-2486, November, 1959.

33. "Earthquake Design Criteria for Stack-Like Structures," by J. E. Rinne, Proceedings, ASCE, Vol. 84, No. ST4, July, 1958.

34. "Dynamics of Framed Structures," by G. L. Rogers, John Wiley and Sons, Inc., New York, 1959.

35. "Earthquake Stresses in Shear Buildings," by M. G. Salvadori, Transactions, ASCE, Vol. 119, 1954, p. 171.

36. "The Use of Visco-Elastic Stress-Strain Laws in Soil Testing," by R. L. Schiffman, Dept. of Civ. Engrg., R.P.I., Troy, N. Y., June, 1959.

37. "Numerical Integration of One-Dimensional Stress Wave," by R. D. Smith and N. M. Newmark, Tech. Report of a Research Project Sponsored by the Office of Naval Research, Navy Dept., Contract Nonr 1834 (03), Project NR-064-183, Civ. Engrg. Studies, Univ. of Illinois, Urbana, Ill., Structural Research Series No. 162, August, 1958.

38. "Stresses in Pressure Pipelines and Protective Casing Pipe," by M. G. Spangler, Proceedings, ASCE, Vol. 82, No. ST5, September, 1956.

39. "Vibrations in Multiple-Story Structures from Earthquakes," by P. E. Stevens, Bulletin, Seismological Soc. of Amer., Vol. 39, No. 4, October, 1949, p. 261.

40. "Studies on the Nonlinear Vibrations of Structures Subjected to Destructive Earthquakes," by R. Tanabashi, Proceedings, World Conf. on Earthquake Engrg., Engrg. Research Inst. and Univ. of California, Berkeley, Calif., June, 1956, Paper No. 6.

41. "The Behavior of Soils Under Dynamic Loadings, 3. Final Report on Laboratory Studies," by D. W. Taylor, R. V. Whitman, et al., Report to Office of the Chf. Engr., Contract DA-49-129-eng-227, Dept. of Civ. and San. Engrg., M.I.T., Cambridge, Mass., August, 1954.

42. "Theoretical Soil Mechanics," by K. Terzaghi, John Wiley and Sons, Inc., New York, 5th edition, 1948.

43. "Vibration Problems in Engineering," by S. Timoshenko, D. Van Nostrand Co., Inc., Princeton, N. J., 3rd edition, 1956.

44. "Soil Mechanics, Foundations, and Earth Structures," by G. P. Tschebotarioff, McGraw-Hill Book Co., Inc., New York, 1951.

45. "Aseismic Design of Structures by Rigidity Criterion," by E. Y. W. Tsui, Proceedings, ASCE, Vol. 85, No. ST2, February, 1959, p. 81.

46. "Numerical Analysis of Earthquake Response of a Tall Building," by T. P. Tung and N. M. Newmark, Bulletin, Seismological Soc. of Amer., Vol. 45, No. 4, October, 1955, p. 269.

47. "Vibrations of Structures," by F. P. Ulrich and D. S. Carter, Proceedings, Symposium on Earthquake and Blast Effects on Structures, Earthquake Engrg. Research Inst. and Univ. of California, Los Angeles, Calif., June, 1952, p. 130.

48. "Friction in Buildings: Its Magnitude and Its Importance in Limiting Earthquake Stresses," by M. P. White, Bulletin, Seismological Soc. of Amer., Vol. 31, No. 2, April, 1941, p. 93.

49. "The Behaviour of Soils Under Transient Loadings," by R. V. Whitman, Proceedings, 4th Internatl. Conf. on Soil Mechanics and Foundation Engrg., Vol. 1, London, England, August, 1957, p. 207.

2961 October, 1961 EM 5

Journal of the
ENGINEERING MECHANICS DIVISION
Proceedings of the American Society of Civil Engineers

ELASTIC RAYLEIGH WAVE EFFECTS DUE TO NUCLEAR BLASTS

By Melvin L. Baron,[1] M. ASCE and Charles Lecht[2]

SYNOPSIS

A nuclear burst on the surface of a semi-infinite elastic half-space produces a time decaying pressure pulse that acts over a circular surface area of increasing radius. This paper presents results for the stresses and displacements due to Rayleigh waves that are produced by such a transient normal surface pressure distribution.

Expressions for the Rayleigh wave displacements and stresses produced by a concentrated load on the surface of the medium are used as influence functions to construct, by means of suitable integrations in space and time, the corresponding quantities produced by the transient normal pressure distributions from a nuclear burst. A numerical example is presented in which the Rayleigh stresses at various depths and locations are given. The results were obtained using an electronic computer, and the numerical procedure is described.

A discussion of the numerical results and of the applicability of the theory to actual situations is presented. It is noted that the Rayleigh stresses predicted by the elastic theory are an upper bound to the stresses in a real me-

Note.–Discussion open until March 1, 1962. To extend the closing date one month, a written request must be filed with the Executive Secretary, ASCE. This paper is part of the Engineering Mechanics Division, Proceedings of the American Society of Civil Engineers, Vol. 87, No. EM 5, October, 1961.

[1] Assoc., Paul Weidlinger, Consulting Engineer, New York; and Adjunct Assoc. Prof. of Civ. Engr., Columbia Univ.

[2] Chf., Programming Div., U. S. Army Ordnance Industrial Data Agency, Snowville, Va.; on leave of absence from the Mitre Corp.

dium. Their use for practical design purposes, such as in the design of underground facilities, is outlined.

INTRODUCTION

At large distances from a disturbance on the surface of an elastic half-space (Fig. 1), the major effects near the surface are produced by Rayleigh Surface Waves. (These results have been shown theoretically by Rayleigh and are well confirmed by seismological measurements.) This paper presents results for the stresses and displacements due to Rayleigh Waves which are produced by transient normal pressure distributions on the surface of the medium. Specifically, a time decaying pressure pulse acting over a circular area of increasing radius R is considered.

The geometry of the problem is shown in Fig. 1 in which the coordinates r and z locate the distance and depth of the field point at which the stresses, or displacements, or both, are to be obtained and R is the radius of the disc of pressure at any time t. Expressions for the displacements and stresses due

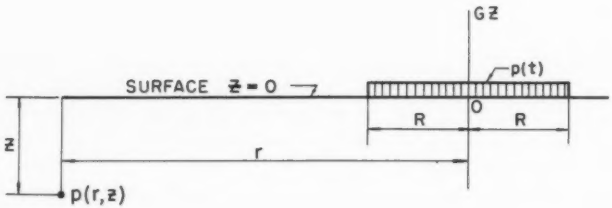

FIG. 1

to Rayleigh Waves produced by a concentrated load with a step pressure distribution in time, applied at the point O on the surface of the elastic half-space have been obtained by C. C. Chao, H. H. Bleich, F. ASCE, and J. L. Sackman.[3] The corresponding stresses and displacements produced by the transient normal pressure which varies both in space and time are constructed by suitable integrations in space and time of the corresponding concentrated load quantities. The results are valid at points in the medium for which the ratios $\frac{z}{r}$ and $\frac{R}{r}$ are small, that is for points located at a shallow depth and at a sufficiently large distance from the radius R of the applied pressure disc.

Numerical results are presented for normal pressure loadings produced by thermonuclear explosions; specifically the Rayleigh effects from a 20 MT surface burst are evaluated.

---

3 "Surface Waves in an Elastic Half-Space," by C.C. Chao, H.H. Bleich and J.L. Sackman, Report P-2066, Rand Corp., August, 1960.

Notation.—The letter symbols adopted for use in this paper are defined where they first appear, in the illustrations or in the text, and are arranged alphabetically, for convenience of reference, in the Appendix.

MATHEMATICAL FORMULATION

Expressions for the stresses and displacements due to Rayleigh Waves produced by transient normal pressure distributions on the surface of a homogeneous and isotropic linearly elastic half-space are derived in this section. These results are obtained by integrations in space and time of the corresponding stresses and displacements due to Rayleigh Wave effects from a concentrated, suddenly applied force on the surface of the half-space.

The complete solution for stresses and displacements produced by a suddenly-applied concentrated load with a step distribution in time has been treated by C. L. Pekeris and H. Lifson.[4,5] The portion of these quantities which are due to Rayleigh effects were extracted from these results by Chao, Bleich and Sackman,[3] as the contribution of certain poles in the inversion integrals of the Pekeris solution (the branch integrals appearing in the complete solution can be ignored). (The fact that surface effects can be obtained by the transform approach as the contribution of certain poles in the complete solution was noted by A. Sommerfeld[6] and Pekeris.[5]) This procedure is based on reasoning due to Sommerfeld that in the vicinity of the Rayleigh wave front, the pole is the leading term, exceeding all other contributions in magnitude.

The expressions for the Rayleigh stresses at points located by the coordinates r, z (Fig. (1)) at a time t (measured from the instant of surface pressure application at the origin O), due to a concentrated suddenly applied load P on an elastic half-space with Lamé constants $\lambda = \mu \left(\nu = \frac{1}{4}\right)$ (The Pekeris solution is given for an elastic material in which the Lamé constants are equal, $\lambda = \mu$. This relation holds for a medium with a Poisson's ratio $\nu = \frac{1}{4}$.) are[3]

$$\sigma_{ij}(r,z,t) = \frac{3P}{16\sqrt{6\gamma}\,\pi\, r^{\frac{1}{2}} z^{\frac{3}{2}}}\, \sigma_{ij}^{*}\left[\frac{c_s t}{z} - \frac{\gamma r}{z}\right] \quad \ldots (1)$$

in which (The notation R_e and I_m stand for the real and imaginary portions of the function respectively.)

$$\sigma_{rr}^{*} = \left(1-2\gamma^2\right) \mathrm{Re}\left[\left(2\gamma^2 + \frac{1}{3}\right) Z_1^{-\frac{3}{2}} + \left(1-2\gamma^2\right) Z^{-\frac{3}{2}}\right] \quad \ldots . (2a)$$

---

4 "The Seismic Surface Pulse," by C.L. Pekeris, Proceedings, Natl. Academy of Science, 1955, Vol. 41.7, p. 469.

5 "Motion of the Surface of a Uniformly Elastic Half-Space Produced by a Buried Pulse," by C.L. Pekeris and H. Lifson, Journal of the Acoustical Society of America, November, 1957, Vol. 29, No. 11, p. 1233.

6 "Uber die Ausbreitung der Wellen in der drahtlosen Telegraphie," by A. Sommerfeld, Annalen der Physik 4, Folge, Vol. 28, 1909, p. 667.

$$\sigma_{rz}^{*} = (-2\gamma)\left(\gamma^2 - \frac{1}{3}\right)^{\frac{1}{2}} \mathrm{I_m}\left[Z_1^{-\frac{3}{2}} - Z_2^{-\frac{3}{2}}\right] \quad \ldots\ldots\ldots (2b)$$

$$\sigma_{zz}^{*} = \left(2\gamma^2 - 1\right)^2 \mathrm{Re}\left[Z_1^{-\frac{3}{2}} - Z_2^{-\frac{3}{2}}\right] \quad \ldots\ldots\ldots (2c)$$

$$\sigma_{\theta\theta}^{*} = \frac{1 - 2\gamma^2}{3} \mathrm{Re}\left[Z_1^{-\frac{3}{2}}\right] \quad \ldots\ldots\ldots (2d)$$

$$Z_1 = \frac{c_s t - \gamma r}{z} + i\left(\gamma^2 - \frac{1}{3}\right)^{\frac{1}{2}} \quad \ldots\ldots\ldots (2e)$$

and

$$Z_2 = \frac{c_s t - \gamma r}{z} + i\left(\gamma^2 - 1\right)^{\frac{1}{2}} \quad \ldots\ldots\ldots (2f)$$

and $c_s = \sqrt{\frac{\mu}{\rho}}$ is the velocity of shear waves in the elastic medium, $\gamma = \frac{1}{2}\sqrt{3 + \sqrt{3}}$, μ denotes the shear modulus and ρ refers to the mass density of the elastic medium.

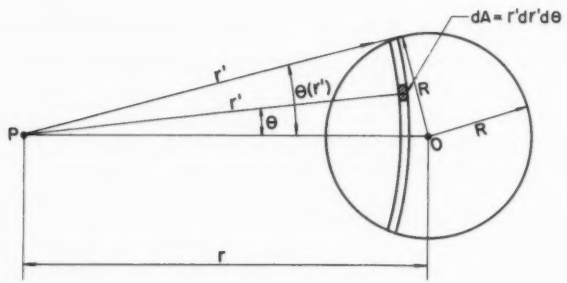

FIG. 2

A first step in the evaluation of the Rayleigh stresses due to a normal surface pressure distribution p (r,t) is the evaluation of the corresponding stresses $\bar{\sigma}_{ij}$ that are produced by a surface pressure which is constant in magnitude, pU(t), and uniformly distributed over a circle of radius $\overline{R}$. From Fig. 2, the

stresses $\bar{\sigma}_{ij}$ are obtained from the integral

$$\bar{\sigma}_{ij}(r,z,t) = \frac{3\sqrt{\gamma}\, p}{8\sqrt{6}\,\pi\, z^{\frac{3}{2}}} \int_{r-\bar{R}}^{r+\bar{R}} r'^{\frac{1}{2}} \int_{0}^{\theta(r')} \sigma_{ij}^{*}\left[\frac{c_s t - \gamma r'}{z}\right] d\theta\, dr' \ldots (3)$$

(In the stress coefficient $\sigma_{ij}^{*}\left[\frac{c_s t - \gamma r'}{z}\right]$ as used in Eq. 3 and in the subsequent equations, the quantity in the brackets gives the real part of arguments of the quantities Z_1 and Z_2 (Eqs. 2e and 2f) which appear in the equations for $\sigma_{ij}^{*}(r,z,t)$.) Assuming that $\frac{\bar{R}}{r} << 1$, that is, that the results will be valid at points in the medium which are located at sufficiently large distances from the radius $\bar{R}$ of the pressure disc, the relation

$$\theta_o = 2 \sin^{-1}\left[\frac{1}{2}\sqrt{\frac{\bar{R}^2 - (r' - r)^2}{r\, r'}}\right] = \sqrt{\frac{\bar{R}^2 - (r' - r)^2}{r\, r'}} \ldots\ldots (4)$$

is substituted into Eq. 3 and, upon integration,

$$\bar{\sigma}_{ij}(r,z,t) = \frac{3\sqrt{\gamma}\, p}{8\sqrt{6}\,\pi\, z^{\frac{3}{2}}\, r^{\frac{1}{2}}} \int_{-\bar{R}}^{\bar{R}} \sqrt{\bar{R}^2 - y^2}\; \sigma_{ij}^{*}\left[\frac{c_s t - \gamma r - \gamma y}{z}\right] dy \ldots (5)$$

The stresses $\bar{\bar{\sigma}}_{ij}$ produced by a normal time-varying surface pressure distribution p (t), distributed over the circular disc of radius $\bar{R}$ is obtained from the Duhamel integral

$$\bar{\bar{\sigma}}_{ij}(r,z,t) = \int_{0}^{t} p(t-\tau)\, \frac{d\bar{\sigma}_{ij}(r,z,\tau)}{d\tau}\, d\tau \ldots\ldots\ldots (6)$$

in which $\bar{\sigma}_{ij}$, the Rayleigh stresses produced by a normal pressure with a step function distribution in time, is obtained from Eq. 5. Substituting Eq. 5 into Eq. 6, and simplifying,

$$\bar{\bar{\sigma}}_{ij}(r,z,t) = \frac{-9\, c_s}{16\sqrt{6\gamma}\,\pi\, z^{\frac{5}{2}}\, r^{\frac{1}{2}}} \int_{0}^{t}\int_{-\bar{R}}^{\bar{R}} p(\tau)\sqrt{\bar{R}^2 - y^2}\; \dot{\sigma}_{ij}^{*}\left[\frac{c_s t - c_s \tau - \gamma r - \gamma y}{z}\right] dy\, d\tau \ldots (7)$$

in which the $\dot{\sigma}_{ij}^{*} = -\frac{2z}{3c_s}\frac{d}{dt}\sigma_{ij}^{*}(z,r,t)$ are as follows:

$$\dot{\sigma}_{rr}^{*} = \left(1-2\gamma^2\right) \mathrm{Re}\left[\left(2\gamma^2+\frac{1}{3}\right) Z_1^{-\frac{5}{2}} + \left(1-2\gamma^2\right) Z_2^{-\frac{5}{2}}\right] \quad \ldots\ldots (8)$$

$$\dot{\sigma}_{zz}^{*} = \left(2\gamma^2-1\right)^2 \mathrm{Re}\left[Z_1^{-\frac{5}{2}} - Z_2^{-\frac{5}{2}}\right] \quad \ldots\ldots\ldots (9)$$

$$\dot{\sigma}_{\theta\theta}^{*} = \left(\frac{1-2\gamma^2}{3}\right) \mathrm{Re}\left[Z_1^{-\frac{5}{2}}\right] \quad \ldots\ldots\ldots (10)$$

and

$$\dot{\sigma}_{rz}^{*} = (-2\gamma)\left(\gamma^2-\frac{1}{3}\right)^{\frac{1}{2}} \mathrm{I_m}\left[Z_1^{-\frac{5}{2}} - Z_2^{-\frac{5}{2}}\right] \ldots\ldots\ldots (11)$$

Finally, the pressure $p(t)$ is allowed to expand radially in time according to the relation $\overline{R} = R(t)$. The Rayleigh stresses σ_{ij} are obtained by substituting $R(t)$ into Eq. 6:

$$\sigma_{ij}(r,z,t) = \frac{-9c_s}{16\sqrt{6\gamma}\,\pi\, r^{\frac{1}{2}} z^{\frac{5}{2}}} \int_0^t \int_{-R(\tau)}^{R(\tau)} p(\tau)\left[R^2(\tau)-y^2\right]^{\frac{1}{2}} \dot{\sigma}_{ij}^{*}\left[\frac{c_s t - c_s\tau - \gamma r - \gamma y}{z}\right] dy\, d\tau \ldots (12)$$

It should be noted that the expressions for the influence coefficients σ_{ij}^{*}, Eqs. 2 are not valid at the surface $z = 0$ and hence, the integration procedure of Eq. 12 cannot be used to evaluate the stresses $\sigma_{ij}(r,z,t)$ at the surface $z = 0$. The determination of the responses from transient distributed loads for $z = 0$ requires a separate approach starting from the transform expressions for the loads, or an equivalent procedure of going to the limit $z \to 0$. The reasons for this are explained in the section "Conclusions." Expressions for the stresses which are valid at the surface $z = 0$ are not presented in this paper.

The radial and longitudinal displacement components u_r and u_z, produced by Rayleigh effects from the time decaying pressure acting over a circular area of increasing radius R, are obtained in a similar manner. The displacements u_r^* and u_z^* due to a concentrated surface load with a step distribution in time are,[3]

$$u_z^{*} = \frac{3P\left(\gamma^2-\frac{1}{3}\right)^{\frac{1}{2}}}{8\sqrt{6\gamma}\,\pi\,\mu\, r^{\frac{1}{2}} z^{\frac{1}{2}}} \mathrm{I_m}\left[\left(1-2\gamma^2\right) Z_1^{-\frac{1}{2}} + 2\gamma^2 Z_2^{-\frac{1}{2}}\right] \ldots\ldots (13)$$

and

$$u_r^* = \frac{3\,P\,\gamma}{8\sqrt{6\,\gamma}\,\pi\,\mu\,r^{\frac{1}{2}}\,z^{\frac{1}{2}}}\,\mathrm{Re}\left[\left(1-2\,\gamma^2\right)\,Z_1^{-\frac{1}{2}} + 2\left(\gamma^2-1\right)^{\frac{1}{2}}\left(\gamma^2-\frac{1}{3}\right)^{\frac{1}{2}}\,Z_2^{-\frac{1}{2}}\right] \quad . . \quad (14)$$

in which Z_1 and Z_2 are defined by Eqs. 2e and 2f. Proceeding through the successive space and time integrations (as in the case for the stresses), the corresponding Rayleigh displacements u_z and u_r due to the normal pressure $p(t)$, which is uniformly distributed over a circular disc of increasing radius $R(t)$, are given by the relations

$$u_z = \frac{-3\,c_s}{8\sqrt{6\,\gamma}\,\pi\,\mu\,r^{\frac{1}{2}}\,z^{\frac{3}{2}}}\int_0^t\int_{-R(\tau)}^{R(\tau)} p(\tau)\left[R(\tau)-y^2\right]^{\frac{1}{2}}\,\dot{u}_z^*\left[\frac{c_s\,t - c_s\,\tau - \gamma\,r - \gamma\,y}{z}\right]\,dy\,d\tau \quad . . \quad (15)$$

and

$$u_r = \frac{-3\,c_s}{8\sqrt{6\gamma}\,\pi\,\mu\,r^{\frac{1}{2}}\,z^{\frac{3}{2}}}\int_0^t\int_{-R(\tau)}^{R(\tau)} p(\tau)\left[R(\tau)-y^2\right]^{\frac{1}{2}}\,\dot{u}_r^*\left[\frac{c_s\,t - c_s\,\tau - \gamma\,r - \gamma\,y}{z}\right]\,dy\,d\tau \quad . . \quad (16)$$

in which the $\dot{u}_j^* = -\frac{z}{2\,c_s}\,\frac{d}{dt}\,u_j^*$ are as follows:

$$\dot{u}_z^* = \left(\gamma^2-\frac{1}{3}\right)^{\frac{1}{2}}\,I_m\left[\left(1-2\,\gamma^2\right)\,Z_1^{-\frac{3}{2}} + 2\,\gamma^2\,Z_2^{-\frac{3}{2}}\right] \quad . . . . . \quad (17)$$

and

$$\dot{u}_r^* = \gamma\,\mathrm{Re}\left[\left(1-2\,\gamma^2\right)\,Z_1^{-\frac{3}{2}} + 2\left(\gamma^2-1\right)^{\frac{1}{2}}\left(\gamma^2-\frac{1}{3}\right)^{\frac{1}{2}}\,Z_2^{-\frac{3}{2}}\right] \quad . . . . \quad (18)$$

The evaluation of the double integrals for the stresses, Eq. 12, and the displacements, Eqs. 16 and 17, for a given set of pressure and range inputs, $p(t)$ and $R(t)$, is performed numerically, using finite difference integration formulas for both the space and time integrations.

NUMERICAL PROCEDURE

The evaluation of the Rayleigh stresses and displacements at a particular field point (r,z) and time, t, from Eqs. 12, 16 and 17 respectively can be performed numerically for a given set of pressure-time, $p(t)$ and range-time, $R(t)$, input functions. The numerical integration of the double integrals in these equations represents a major computational effort for cases of practical in-

terest such as a normal surface pressure produced by a nuclear explosion. The variable upper and lower limits on the integration in the variable y add materially to the numerical complexity of a problem. The numerical work required the use of a large capacity electronic computer; an I. B. M. 704 with a 32K word memory was used to obtain the results which will be presented in the following section.

The present section describes in some detail the numerical procedures which were used in the analyses. The evaluation of the Rayleigh stresses σ_{ij} will be illustrated. For convenience, the stresses σ_{ij} are written in the form:

$$\sigma_{ij}(r,z,t) = \frac{-9\,c_s}{16\sqrt{6\gamma}\,\pi\, r^{\frac{1}{2}} z^{\frac{5}{2}}} \int_0^t p(\tau)\, I_1(r,z,\tau)\, d\tau \quad \ldots\ldots\ldots \quad (19)$$

in which

$$I_1(r,z,\tau) = \int_{-R(\tau)}^{R(\tau)} \left[R^2(\tau) - y^2\right]^{\frac{1}{2}} \dot{\sigma}_{ij}^{*}\left[Z_1, Z_2\right] dy \quad \ldots\ldots\ldots \quad (20)$$

and $Z_1(r,z,y,\tau)$ and $Z_2(r,z,y,\tau)$ are defined as:

$$Z_1 = \frac{c_s t - c_s \tau - \gamma r - \gamma y}{z} + i\left(\gamma^2 - \frac{1}{3}\right)^{\frac{1}{2}} \quad \ldots\ldots\ldots \quad (21a)$$

and

$$Z_2 = \frac{c_s t - c_s \tau - \gamma r - \gamma y}{z} + i\left(\gamma^2 - 1\right)^{\frac{1}{2}} \quad \ldots\ldots\ldots \quad (21b)$$

The integrals in Eqs. 19 and 20 are integrated successively using Simpson's Rule.[7] The integration interval $h_1 = \Delta\tau$ is chosen for Eq. 19, thus yielding the pivotal values $\tau = \tau_i$ at which the inner integrals $I_1(r,z,\tau_i)$ are to be evaluated. For each value of τ_i, Eq. 20 is integrated between the limits of $R(\tau_i)$ and $-R(\tau_i)$, using a spacing $h_2 = \Delta y = \frac{2\,R(\tau_i)}{m}$ in which m is chosen so that the integration is performed over an even number of subintervals. Each value of $I_1(r,z,\tau_i)$ is multiplied by the pressure $p(\tau_i)$ to form the integrand for the integration in time of Eq. 19. This integral in turn is evaluated by Simpson's Rule with $h_1 = \Delta\tau$, thus yielding the stress σ_{ij} at the point defined by the coordinates r, z, and at the time t. The procedure is repeated for each combination of the input parameters r, z, and t.

A critical consideration from the viewpoint of both accuracy and machine economy is the determination of optimum values for the integration intervals h_1 and h_2. The computer program contains a large number of options which allow the printout of key intermediate results such as the inner integrals

---

7 "Numerical Methods in Engineering," by M.G. Salvadori and M.L. Baron, Prentice Hall, Inc., Englewood Cliffs, N.J., 1953.

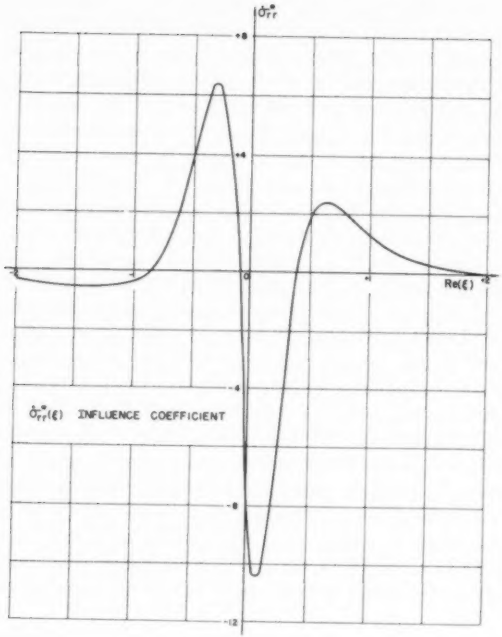
$\dot{\sigma}^*_{rr}$
+8
+4
0
-4
-8
-12
-2
-1
+1
+2
Re(ξ)
$\dot{\sigma}^*_{rr}(\xi)$ INFLUENCE COEFFICIENT

FIG. 3

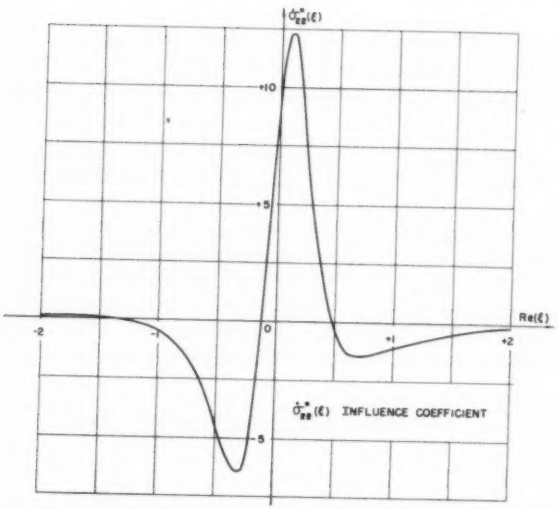
$\dot{\sigma}^*_{\theta\theta}(\xi)$
+10
+5
0
-5
-2
-1
+1
+2
Re(ξ)
$\dot{\sigma}^*_{\theta\theta}(\xi)$ INFLUENCE COEFFICIENT

FIG. 4

$I_1(r,z,\tau_i)$, thus permitting a series of preliminary sensitivity investigations to be made and optimal values of h_1 and h_2 to be selected. These investigations are particularly necessary in determining h_2, due to the nature of the functions $\dot{\sigma}_{ij}^*$ which appear in the integral I_1. Figs. 3 through 6 show the $\dot{\sigma}_{ij}^*$ as a function of the non-dimensional real part of the argument of Z_1 and Z_2. The extremely oscillatory character of these influence functions necessitate the use of an extremely fine grid spacing h_2; in some cases as many as 400 to 500 pivotal points were required. It should also be noted that the $\dot{\sigma}_{ij}^*$ may be neglected in each case beyond a value of ± 2 for the real part of the argument of Z_1 and Z_2. Consequently, a cutoff was incorporated into the program which set the $\dot{\sigma}_{ij}^*$ equal to zero for Re (Z_1 and Z_2) greater than 2 and less than -2; this resulted in a significant saving of computation time.

The input functions p(t) and R(t) which describe the transient normal surface pressure are chosen for typical nuclear explosions. Figs. 7 and 8 show curves for a 20 MT burst, used in the computation of the numerical results in the following section. (The pressures produced by the blast have been considered to be uniformly distributed over a circle of radius R(t). This neglects a small spike of pressure, located near R(t), which at early times contains only a small portion of the total load on the medium and which consequently may be neglected in the present study.[8]) In each case, a series of sensitivity runs defined a cutoff time t_c with a corresponding pressure $p_c(t_c)$ and range $R(t_c)$ beyond which the pressure p(t) could be taken as zero with a negligible loss of accuracy. The significance of this cutoff is that major Rayleigh effects are produced at points in the medium by the relatively high intensity pressures on the surface at early times.

The magnitude of the numerical computations required that the τ integration in Eq. 19 be made in two steps. For the 20 MT burst the integration was made from $\tau = 0$ to $\tau = 0.100$ ms in steps of $h_1 = 0.025$ ms and from $\tau = 0.100$ ms to $\tau = 6.100$ ms in steps of $h_2 = 0.200$ ms. A pressure cutoff of $t_c = 6.1$ ms was used.

Upon completion of the sensitivity investigations which lead to the determination of h_1, h_2 and t_c, the program was run without intermediate printouts. The computer program was prepared using the FORTRAN language.

NUMERICAL EXAMPLE AND CONCLUSIONS - APPLICATION TO NUCLEAR EXPLOSIONS

The Rayleigh stresses σ_{rr}, $\sigma_{\theta\theta}$, σ_{rz} and σ_{zz} which are produced in a semi-infinite elastic medium by the surface pressure from 20 MT nuclear burst are evaluated at the location r = 2000 ft, 3200 ft, and 5,000 ft from Ground Zero for various values of the depth z. These values of r correspond to the 10,000 psi, 2000 psi, and 700 psi surface pressure contours for the 20 MT explosion. The elastic constants for the medium were chosen as follows:

$$c_s = \sqrt{\frac{\mu}{\rho}} = \text{velocity of shear waves} = 10{,}000 \text{ fps.}$$

8 "Cratering From a Megaton Surface Burst," by H.L. Brode and R.L. Bjork, RM-2600, Rand Corp., June, 1960; and "Theoretical Studies on Ground Shock Phenomena," by M.L. Baron, H.H. Bleich, and P. Weidlinger, Paper SR-19, Mitre Corp., October, 1960.

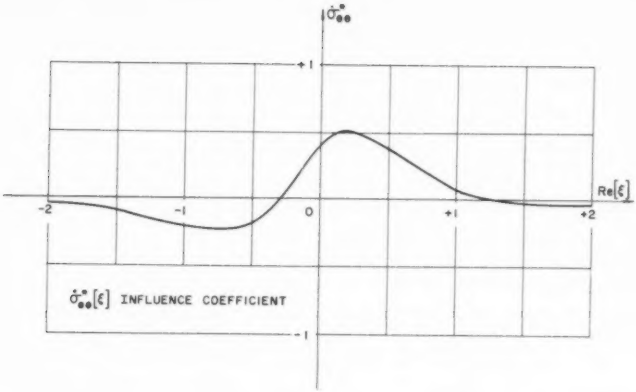
$\dot{\sigma}^{\circ}_{\theta\theta}$
+1
-2
-1
0
+1
+2
Re[ξ]
$\dot{\sigma}^{\circ}_{\theta\theta}[\xi]$ INFLUENCE COEFFICIENT
-1

FIG. 5

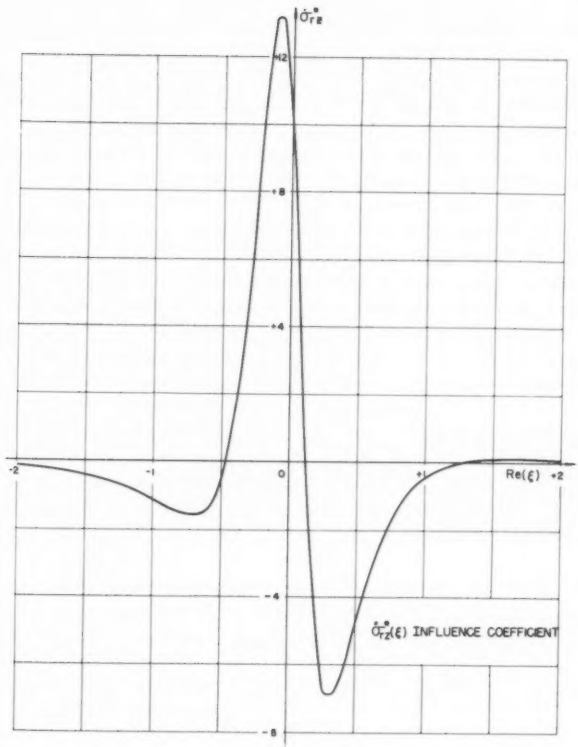
$\dot{\sigma}^{\circ}_{rz}$
+12
+8
+4
-2
-1
0
+1
Re(ξ) +2
-4
$\dot{\sigma}^{\circ}_{rz}(\xi)$ INFLUENCE COEFFICIENT
-8

FIG. 6

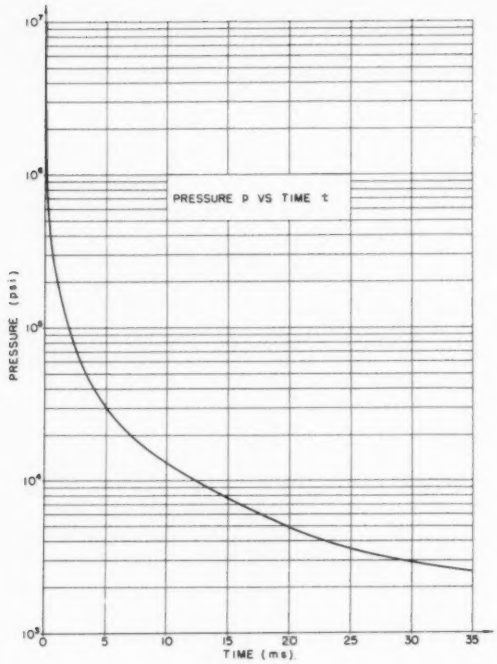
PRESSURE P VS TIME t
PRESSURE (psi)
TIME (ms)
0
5
10
15
20
25
30
35

FIG. 7

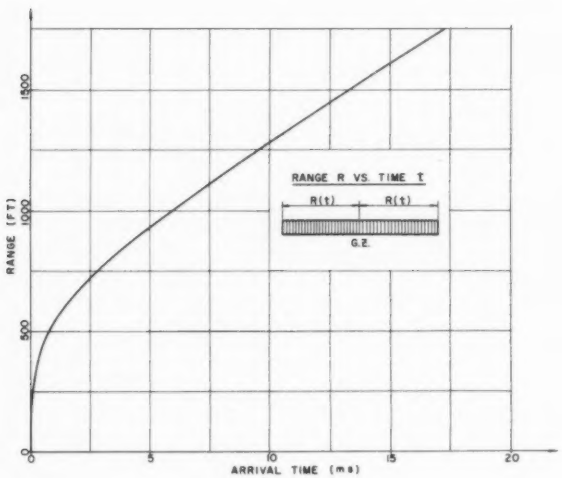
RANGE R VS. TIME t
R(t)
R(t)
G.Z.
RANGE (FT)
ARRIVAL TIME (ms)
0
500
1000
1500
5
10
15
20

FIG. 8

w = specific weight = 167 lb per cu ft

ρ = mass density = 5.186 $\frac{\text{lb sec.}^2}{\text{ft}^4}$

ν = Poisson's ratio = 0.25

c_{Rayleigh} = velocity of Rayleigh waves = $\frac{c_s}{\gamma}$ = 9,174 fps.

Figs. 9 (a), 9 (b), and 9 (c) give typical stress versus time histories at the indicated locations for the Rayleigh stresses σ_{rr}, $\sigma_{\theta\theta}$, σ_{rz} and σ_{zz}. The time t is measured from the instant of the explosion at r = 0 and hence, there is a delay before the first Rayleigh signals arrive at the indicated field points. The results, which are typical at all field points in the medium, indicate that the stresses σ_{rr} are larger than the other stresses so that the importance of the Rayleigh effects can generally be judged by considering σ_{rr}. Fig. 10 shows the computed time history for the stress σ_{rr} at a number of depths at the location r = 2000 ft. The rapid attenuation of the Rayleigh stress with depth is clearly shown.

The peak values of the stresses σ_{rr}, $\sigma_{\theta\theta}$ and σ_{zz} at various depths can be used to obtain peak stress versus depth curves at each location, defined by the coordinate r. Figs. 11 through 13 show the rapid attenuation of the peak stresses σ_{rr}, $\sigma_{\theta\theta}$ and σ_{zz} with depth at the location r = 2000 ft, 3200 ft and 5000 ft respectively. In each case, the peak values of the shear stress σ_{rz} were found to be comparable to the peak values of the direct stress σ_{zz}. Consequently, the stress versus depth curves for σ_{rz} are not shown on these figures. Attention is again drawn to the fact that the formulas developed by Chao, Bleich and Sackman[3] and in this paper cannot be applied for points on the surface, z = 0, because negative powers of z occur in these expressions. Computational difficulties would arise for very small depths in the neighborhood of z = 0, and only results for points at a depth of 25 ft or more were obtained. The trend of these results as a function of the depth is such that rather large stresses, σ_{rr} and $\sigma_{\theta\theta}$, can be expected near the surface (the vertical stress σ_{zz} and the shear stress σ_{rz} on the free surface must vanish). The existence of such high stresses in the elastic analysis makes it inapplicable to actual situations near the surface $z \to 0$ and therefore the additional effort requires to derive an appropriate analysis for shallow depth was not expended.

It is of interest to investigate the effect of a change in the shear wave velocity c_s, that is, a change in the shear modulus μ of the medium, on the Rayleigh stresses σ_{rr}, $\sigma_{\theta\theta}$, and σ_{zz}. Figs. 14 and 15 show the results which are produced by a 20 MT explosion on an elastic medium in which c_s is reduced to 6,000 fps but whose weight, w = 167 lb per cu ft is kept the same as the original medium.

The peak stress versus depth curves at r = 3200 ft, in Figs. 12 and 15 can be compared to show the effect of the decrease of the shear modulus of the medium. The peak stresses σ_{rr}, $\sigma_{\theta\theta}$, and σ_{zz} at each depth are considerably lower for the slower medium (c_s = 6000 fps) than for the original medium (c_s = 10,000 fps). The characteristic rapid attenuation of the peak stresses with depth is shown for both media.

Applicability of the Results to Actual Situations.—The analysis and the results obtained in this paper have been based on the assumption that the medium

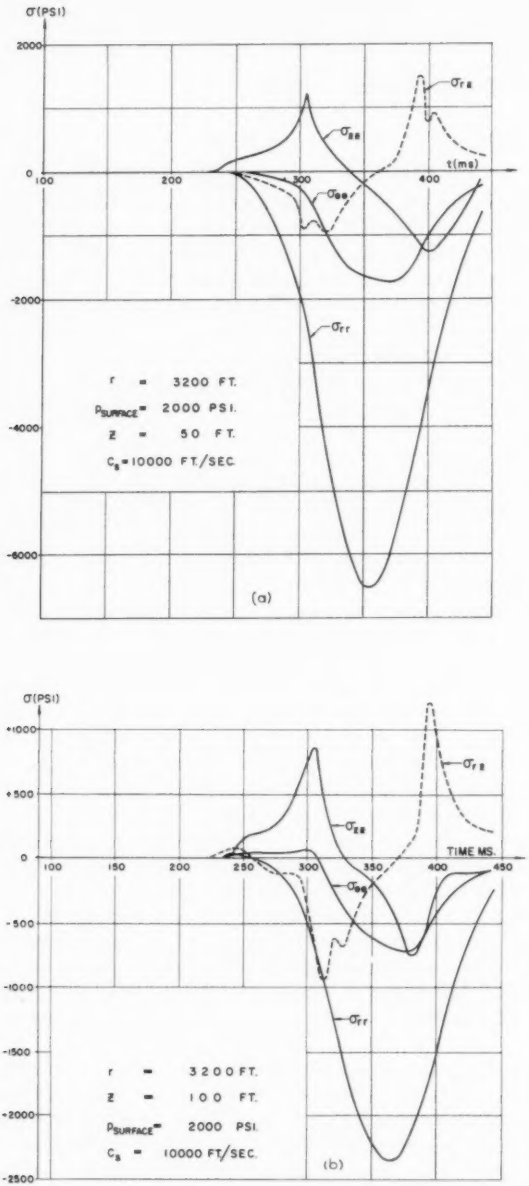

FIG. 9.–STRESSES DUE TO RAYLEIGH WAVES

is and remains linearly elastic under the application of the surface pressures and that the effects from the slamming of the bomb casing into the medium are not considered. The elastic assumptions can be violated in two regions: (1) in the crater region which surrounds Ground Zero, and (2) at those points near the surface of the medium at which the Rayleigh stresses predicted by elastic theory exceed the stresses that the rock materials under consideration are likely to withstand elastically.

In the vicinity of Ground Zero and the surrounding crater region, the elastic theory is not valid because, at the extremely high pressures in this region, the medium acts essentially as a fluid. The existence of Rayleigh waves requires an interaction between direct and shear stresses which does not occur in a fluid and one may conclude that the inception of Rayleigh waves in the crater region will be inhibited. Because a substantial portion of the Rayleigh wave effects from the elastic theory originate from the high intensity pressures ac-

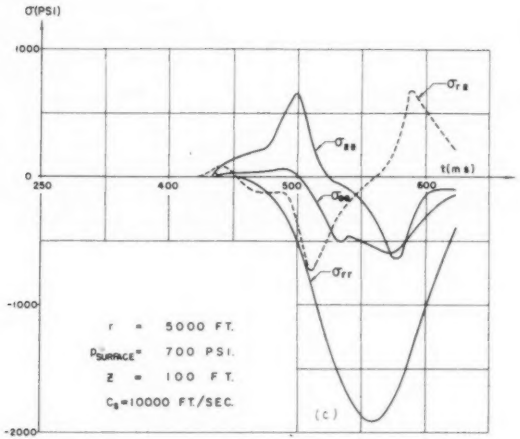

FIG. 9.—*CONTINUED*

ting in the neighborhood of Ground Zero, the results predicted by the elastic theory will be exaggerated and the Rayleigh stresses will therefore be an upper bound to the stresses that are produced in the real medium. The problem of the Rayleigh wave effects, which include the effect of the crater, is currently (1961) under investigation.

The Rayleigh stresses predicted by the present theory near the surface of the elastic half-space will in some regions be larger than the stresses that an actual medium (such as a competent rock which could be considered to act elastically up to certain pressure levels) can withstand. Because the state of stress in surface waves is inherently deviatory (that is, having considerable shear deformation), the medium would act inelastically in such regions with a consequent further reduction in the Rayleigh stresses from the elastic theory.

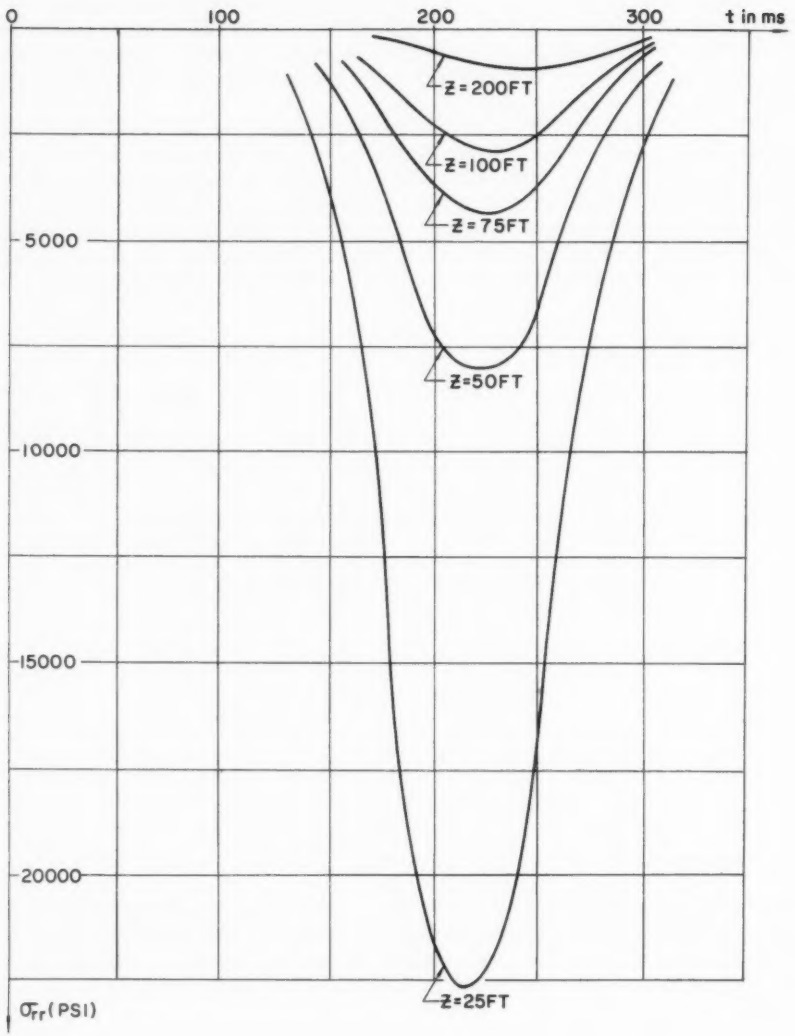

FIG. 10.—RAYLEIGH STRESSES AT r = 2000 FT (C_S = 1000 FPS)

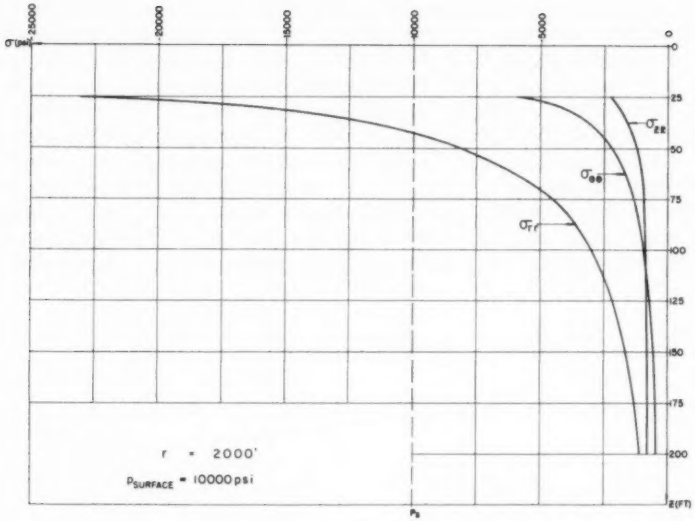

FIG. 11.—STRESSES DUE TO RAYLEIGH WAVES VERSUS DEPTH AT r = 2000 FT AND p surface = 1000 PSI

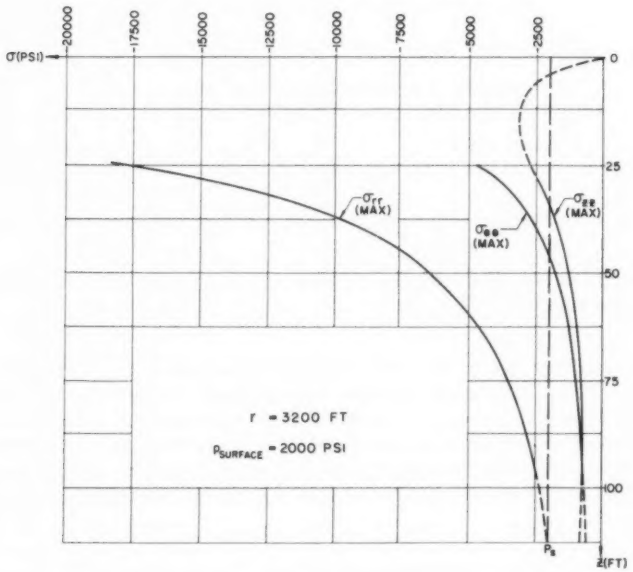

FIG. 12.—STRESSES DUE TO RAYLEIGH WAVES VERSUS DEPTH AT r = 3200 FT AND p surface = 2000 PSI

(Dissipative effects will lead to lower stresses due to surface waves. Such waves in a viscoelastic medium have been considered by J. Lubliner.[9])

Although the Rayleigh stresses predicted by the elastic theory are an upper bound to the true stresses in the medium, they are quite useful for practical design purposes. A major use of the results lies in the application of the stress versus depth curves in Figs. 11 through 13 and Fig. 15 in the design of deep underground facilities. From these curves, it is possible to determine at each location r those depths at which the Rayleigh stresses will be comparable to, or less than, the stresses from the P (dilatational) and S (shear) waves which are also produced by the surface pressures acting on the elastic half-space. It is noted that in each location r = 2000 ft, 3200 ft, and 5000 ft, the depths at which Rayleigh effects become small as compared to P and S wave effects are

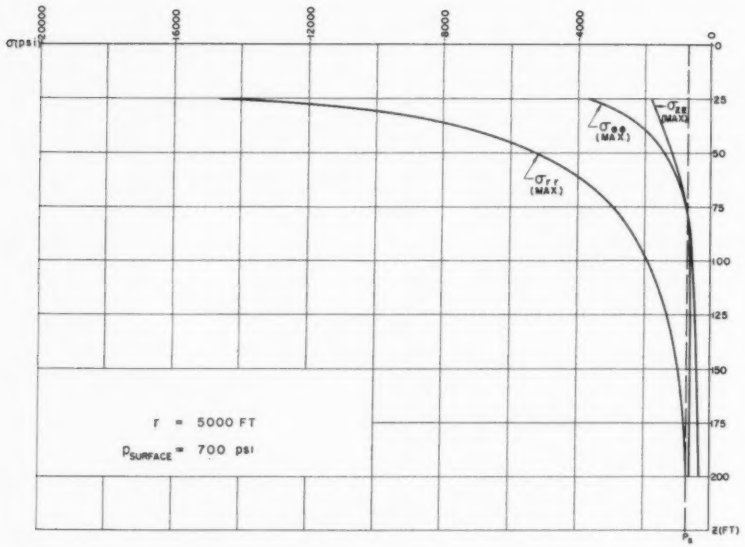

FIG. 13.—STRESSES DUE TO RAYLEIGH WAVES VERSUS DEPTH AT r =5000 FT AND p surface =700 PSI

relatively shallow due to the very rapid attenuation of the Rayleigh stresses with depth. This knowledge enables the designer to use certain simplified analyses[10] to obtain pressure inputs on deep underground structures. In such cases, diffraction information and shock spectra which are established on the basis of these simplified analyses could be safely used for design purposes. A detailed study of these procedures in the design of underground structures is available.[10a]

9 "Surface Waves in a Viscoelastic Half-Space," by J. Lubliner, ONR Report Nr. 064-417, Report No. 9, Columbia Univ., New York, April, 1960.

10 "Theoretical Studies on Ground Shock Phenomena," by M.L. Baron, H.H. Bleich, and P. Weidlinger, Paper No. SR-19, Mitre Corp., October, 1960, (a) Sections 3 through 6.

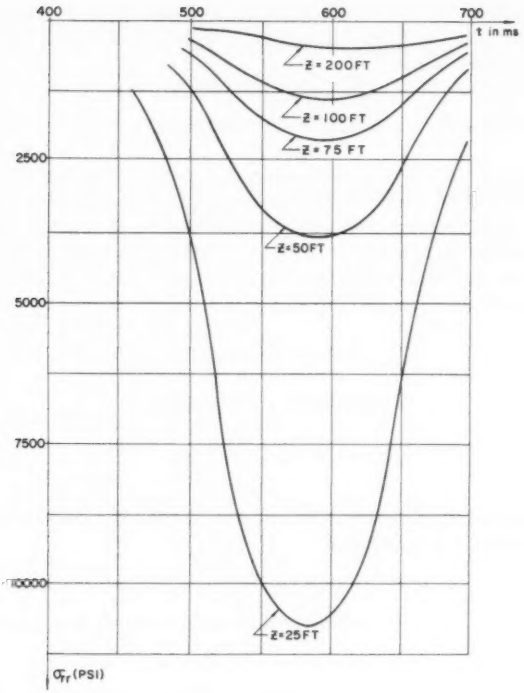

FIG. 14.—RAYLEIGH STRESSES AT r=3200 FT (C_S = 6000 FPS)

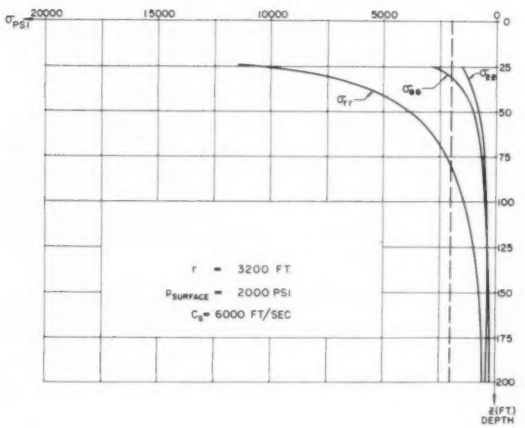

FIG. 15

The displacements produced by Rayleigh waves are also of considerable interest. Computations for these results are being run (as of 1961) and are to be reported at a later time.

ACKNOWLEDGMENTS

This paper is the result of investigations sponsored by the MITRE Corporation under contract with Paul Weidlinger, F. ASCE, Consulting Engineer.

The writers wish to acknowledge the contribution of Jerome Sackman of the University of California, Berkeley, Calif. for his participation in the analytical formulation of the present problem and of Ronald Check of Paul Weidlinger, Consulting Engineer.

APPENDIX.—NOTATION

The symbols used in the paper are presented here for case of reference and for the convenience of discussers:

$c_{Rayleigh}$ = velocity of Rayleigh waves in the elastic medium;

c_s = velocity of shear waves in the elastic medium;

I_1 = integral - See Eq. 20;

$p(t)$ = time varying uniformly distributed pressure over a circle of radius R;

P = concentrated load;

$R(t)$ = range of pressure distribution; see Fig. 1;

r,z = coordinates of a point in the elastic half-space; see Fig. 1;

r', θ = coordinates; see Fig. 2;

t = time;

u_r, u_z = displacements in the r and z directions, respectively;

$\dot{u}_r^*$, $\dot{u}_z^*$ = influence coefficients for the displacements; see Eqs. 17 and 18;

w = specific weight of elastic medium;

$Z_1(r,z,y,\tau)$, $Z_2(r,z,y,\tau)$ = functions; see Eqs. 21a and 21b;

$\gamma = \dfrac{c_s}{c_{Rayleigh}}$ = ratio of velocities;

$\nu = \dfrac{1}{4}$ = Poisson's ratio;

μ = shear modulus of elastic medium;

ρ = mass density of elastic medium;

$\sigma_{ij}(r,z,t)$ = stresses produced by Rayleigh waves;

$\dot{\sigma}_{ij}^{*}$ = influence coefficients for Rayleigh stresses; see Eqs. 8 through 12; and

σ_{rr}, $\sigma_{\theta\theta}$, σ_{zz}, σ_{rz} = direct and shear stresses produced by Rayleigh waves.

Journal of the
ENGINEERING MECHANICS DIVISION
Proceedings of the American Society of Civil Engineers

INTERFACIAL MIXING IN STRATIFIED FLOW

By Enzo Oscar Macagno,[1] Aff. ASCE, and Hunter Rouse,[2] F. ASCE

SYNOPSIS

In order to effect a state of stratified flow in which the source of interfacial turbulence would be the instability of the interface itself, apparatus was devised which would permit the counterflow of two superposed streams of different densities to be maintained for a considerable period of time over an appreciable length of uniform passage. By means of chronophotography of injected droplets and analysis of point samples of fluid, measurements were made of velocity and density distributions across the interface for various flow regimes. In accordance with indications of dimensional and stability analyses, results were presented in the form of dimensionless ratios of interfacial shear and of mass transport as functions of the Froude and Reynolds numbers.

INTRODUCTION

Density stratification occurs in such natural fluid systems as the oceans and the atmosphere as well as in those that are man-made, and this can have an important influence upon the flows that take place. In many instances two or more layers of fluid of different densities flow in such a way that they preserve their identity even when the fluids are miscible and appreciable diffusion

Note.—Discussion open until March 1, 1962. To extend the closing date one month, a written request must be filed with the Executive Secretary, ASCE. This paper is part of the copyrighted Journal of the Engineering Mechanics Division, Proceedings of the American Society of Civil Engineers, Vol. 87, No. EM 5, October, 1961.

[1] Asst. Prof. of Fluid Mechanics, State Univ. of Iowa, and Research Engr., Iowa Inst. of Hydr. Research, Iowa City, Iowa.

[2] Prof. of Fluid Mechanics, State Univ. of Iowa, and Dir., Iowa Inst. of Hydr. Research, Iowa City, Iowa.

occurs across the transition zones between them. As a first approximation such layers can be considered to be separated by an interface, rather than by an interlayer of finite thickness, along which shear occurs and across which mass transfer takes place.

The analysis of the flow of strata of different densities requires a knowledge of conditions at solid boundaries as well as along the internal boundaries between the individual layers. The conditions at solid boundaries are fairly well known, although the problem of boundary roughness is far from solved. The conditions at inner boundaries, on the contrary, have been only scantily explored. To be sure, it is possible to state them in the case of laminar flow, and some laminar-flow problems have been solved mathematically. However, as soon as the flow becomes unstable and the interface is deformed by waves, it is no longer possible to evaluate even the mean shear stresses. When turbulence develops, still another unknown is introduced: the rate of mixing of the neighboring fluids and the resulting change in the density distribution.

As in many other problems, when mathematical analysis is not yet feasible, one can resort to studies at model scale. However, no model study can make ultimate sense without knowledge of fundamental relationships on which to build either exact or approximate criteria of similitude. In the present instance, approximate criteria for the general case of stratified flow must be based upon the parameters derived for the case of discrete strata separated by interlayers of negligible thickness.

The goal of this investigation was an experimental study of interfacial instability and subsequent mixing - due, however, to conditions prevailing directly at the interface as contrasted to previous studies involving rather arbitrary or specialized boundary conditions. Only to mention among those studies the ones that were the most useful during the present research, reference is made to the articles by G. I. Taylor[3] on the stability of superposed streams of different densities, by G. H. Keulegan[4] on interfacial mixing and instability, by A. T. Ippen, F. ASCE, and D. R. F. Harleman,[5] M. ASCE, on subsurface flow, and by J. P. Raynaud[6] on underflow of silt-laden water. All involved the flow of one layer under or over another that was stagnant except for the motion induced by shear.

Following the previously cited investigations, various papers have been published in the 1950's presenting new findings either in the theoretical or in the experimental field. The series on the hydrodynamical discussion of stability was culminated by the contributions of S. Feldman[7] and W. P. Graebel.[8] Both papers contain solutions of the Orr-Sommerfeld equation for two-layered stratified flows, taking into account the effect of surface tension in addition to that of

---

3 "An Experiment on the Stability of Superposed Streams of Fluid," by G. I. Taylor, Proceedings, Cambridge Phil. Soc., Vol. 23, 1927, pp. 730-731.

4 "Interfacial Instability and Mixing in Stratified Flow," by G. H. Keulegan, Journal of Research of NBS, Vol. 43, 1949, pp. 487-500.

5 "Steady-State Characteristics of Subsurface Flow," by A. T. Ippen and D. R. F. Harleman, Proceedings, Semicentennial Symposium on Gravity Waves, NBS Circular 521, 1952, pp. 79-93.

6 "Etudes des Courants d' Eau Boueuse dans les Retenues," by J. P. Raynaud, 4th Congress of Large Dams, New Delhi, Question 14, 1951, pp. 137-161.

7 "On the Hydrodynamic Stability of Two Viscous Incompressible Fluids in Parallel Uniform Shearing Motion," by S. Feldman, Journal of Fluid Mechanics, Vol. 2, Part 4, 1957, pp. 343-370.

8 "The Stability of a Stratified Flow," by W. P. Graebel, Journal of Fluid Mechanics, Vol. 8, Part 3, 1960, pp. 321-336.

density and of viscosity. The case of flow considered by Graebel corresponds to the one in the present experiments, but his solution was confined to essentially vertical flow, while that considered herein is nearly horizontal. Graebel's results indicate that rather low critical Reynolds numbers can be expected. On the experimental side, the decade has seen frequent contributions by Keulegan and his associates. Particular reference is made to the paper by K. Lofquist,[9] which presents results similar to those for shear stress contained herein, although for a dissimilar case of flow.

A different and also somewhat abstract approach to the problem of interfacial mixing was followed by H. Rouse, F. ASCE, and J. Dodu[10] in an experimental study of the turbulent diffusion between miscible fluids of different densities induced by oscillation of a grid in one of the layers. The present investigation, in contradistinction, was intended to cover a process of diffusion across an interface due to self-generated turbulence rather than turbulence imposed by external means. Knowledge existing at the time the present investigation was started, in 1957, indicated both the feasibility and the desirability of this approach. The idea of making the interface the plane of maximum shear had already been under investigation at the Iowa Institute of Hydraulic Research by Rouse and C. S. Yih. A considerable amount of work was still necessary to reach the stage of successfully controlling the flow, and to develop a technique of observation which would reveal the mechanism of interfacial mixing and allow the researcher to obtain quantitatively useful data. That the investigation was to be carried on at a small scale was justified partly by economical reasons but mainly by previous experience showing that important relationships can often best be revealed at a small scale in which much more effective control of the phenomena can be exercised. A subsequent investigation should then continue the exploration of the interfacial behavior at a much larger scale, either through controlled experiments in the laboratory or through the analysis of field data obtained under natural conditions.

Notation.—The letter symbols adopted for use in this paper are defined where they first appear, in the illustrations or in the text, and are arranged alphabetically, for convenience of reference, in the Appendix.

STABLE LAMINAR STRATIFIED FLOW

The following analysis of two-layered laminar stratified flow has the purpose of defining the conditions under which a nearly antisymmetrical flow is possible. In the case of the uniform two-dimensional motion indicated in Fig. 1, the Navier-Stokes equations for the upper layer reduce to

$$0 = \rho_1 g \sin\theta - \frac{\partial p_1}{\partial x} + \mu_1 \frac{\partial^2 u_1}{\partial y^2} \quad \ldots\ldots\ldots\ldots \quad (1)$$

$$0 = -\rho_1 g \cos\theta - \frac{\partial p_1}{\partial y} \quad \ldots\ldots\ldots\ldots\ldots \quad (2)$$

---

9 "Flow and Stress Near an Interface Between Stratified Liquids," by K. Lofquist, The Physics of Fluids, Vol. 3, No. 2, 1960, pp. 158–175.

10 "Diffusion Turbulente à Travers une Discontinuité de Densité," by H. Rouse and J. Dodu, La Houille Blanche, Vol. 10, No. 4, 1955, pp. 522–532.

and for the lower layer to

$$0 = \rho_2 g \sin \theta - \frac{\partial p_2}{\partial x} + \mu_2 \frac{\partial^2 u_2}{\partial y^2} \quad \ldots\ldots\ldots \quad (3)$$

$$0 = - \rho_2 g \cos \theta - \frac{\partial p_2}{\partial y} \quad \ldots\ldots\ldots\ldots \quad (4)$$

The boundary conditions at the top are

$$u_1 = 0 \text{ for } y = h_1 \quad \ldots\ldots\ldots\ldots \quad (5)$$

and at the bottom

$$u_2 = 0 \text{ for } y = - h_2 \quad \ldots\ldots\ldots\ldots \quad (6)$$

while at the interface

$$u_1 = u_2 \text{ for } y = 0 \quad \ldots\ldots\ldots\ldots \quad (7)$$

$$\mu_1 \frac{\partial u_1}{\partial y} = \mu_2 \frac{\partial u_2}{\partial y} \text{ for } y = 0 \quad \ldots\ldots\ldots\ldots \quad (8)$$

and

$$p_1 = p_2 \text{ for } y = 0 \quad \ldots\ldots\ldots\ldots \quad (9)$$

As u_1 and u_2 are functions only of y, Eqs. 1 to 4 together with Conditions 9 give

$$p_1 = - \rho_1 g y \cos \theta + K x + C \quad \ldots\ldots\ldots\ldots \quad (10)$$

$$p_2 = - \rho_2 g y \cos \theta + K x + C \quad \ldots\ldots\ldots\ldots \quad (11)$$

Upon integration of Eqs. 1 and 3 and use of the conditions at the interface, there results

$$u_1 = \frac{K_1}{2 \mu_1} y^2 + \frac{A}{\mu_1} y + B \quad \ldots\ldots\ldots\ldots \quad (12)$$

and

$$u_2 = \frac{K_2}{2 \mu_2} y^2 + \frac{A}{\mu_2} y + B \quad \ldots\ldots\ldots\ldots \quad (13)$$

where

$$K_1 = K - \rho_1 g \sin \theta \quad \ldots\ldots\ldots\ldots \quad (14)$$

$$K_2 = K - \rho_2 g \sin \theta \quad \ldots\ldots\ldots\ldots \quad (15)$$

The coefficients A and B are constants that can be determined through the use

of Conditions 5 and 6:

$$A = \frac{\mu_1 K_2 h_2^2 - \mu_2 K_1 h_1^2}{2(\mu_1 h_2 + \mu_2 h_1)} \quad \ldots\ldots\ldots\ldots (16)$$

and

$$B = \frac{K_1 h_1^2 h_2 + K_2 h_2^2 h_1}{2(\mu_1 h_2 + \mu_2 h_1)} \quad \ldots\ldots\ldots\ldots (17)$$

Upon substitution of A and B in Eqs. 10 and 11, it follows that

$$u_1 = \frac{K_1}{2\mu_1} y^2 + \frac{\left(K_2 h_2^2 - K_1 h_1^2 \frac{\mu_2}{\mu_1}\right) y - \left(K_1 h_1^2 h_2 + K_2 h_2^2 h_1\right)}{2(\mu_2 h_1 + \mu_1 h_2)} \quad \ldots\ldots (18)$$

$$u_2 = \frac{K_2}{2\mu_2} y^2 + \frac{\left(K_2 h_2^2 \frac{\mu_1}{\mu_2} - K_1 h_1^2\right) y - \left(K_1 h_1^2 h_2 + K_2 h_2^2 h_1\right)}{2(\mu_2 h_1 + \mu_1 h_2)} \quad \ldots\ldots (19)$$

If the zero-velocity line and the interface coincide, $u_1 = u_2 = 0$ at $y = 0$, which results in

$$K_1 h_1 = - K_2 h_2 = M \quad \ldots\ldots\ldots\ldots (20)$$

and it then follows that

$$u_1 = \frac{M y^2}{2\mu_1 h_1} - \frac{M y}{2\mu_1} = \frac{M}{2\mu_1}\left(\frac{y^2}{h_1} - y\right) \quad \ldots\ldots\ldots (21)$$

and

$$u_2 = - \frac{M}{2\mu_2}\left(\frac{y^2}{h_2} + y\right) \quad \ldots\ldots\ldots\ldots (22)$$

If the rates of flow of the two fluids are made equal,

$$\int_0^{h_1} u_1 \, dy = \frac{M}{2\mu_1} \frac{h_1^2}{3} - \frac{M h_1^2}{4\mu_1} = - \frac{M}{12\mu_1} h_1^2 \quad \ldots\ldots\ldots (23)$$

and

$$\int_{-h_2}^{0} u_2 \, dy = - \frac{M}{2\mu_2} \frac{h_2^2}{3} + \frac{M h_2^2}{4\mu_2} = \frac{M}{12\mu_2} h_2^2 \quad \ldots\ldots\ldots (24)$$

which yields, finally,

$$\frac{h_1}{h_2} = \sqrt{\frac{\mu_1}{\mu_2}} \quad \ldots\ldots\ldots\ldots\ldots (25)$$

Evidently, if the ratio μ_1/μ_2 is kept nearly equal to unity, the ratio h_1/h_2 will deviate still less from unity, and for all practical purposes the stratified flow can then be considered to consist of two layers of equal depth separated by an interface coincident with the plane of zero velocity.

Once it is possible to produce the laminar flow of two layers with a velocity distribution which is like a sine curve, the stability of the motion can be studied. With the inflection point at the interface, it is there that disturbances can be expected to grow rather than at any other level. It is in this sense that antisymmetrical flow is considered to have inherent conditions of instability, as opposed to other cases in which disturbances develop elsewhere and are propagated to the interfacial region.

DISCUSSION OF INSTABILITY

In 1945, Rouse[11] concluded that, other things being equal, the relative stability of a given flow should depend upon the velocity gradient, the wall distance,

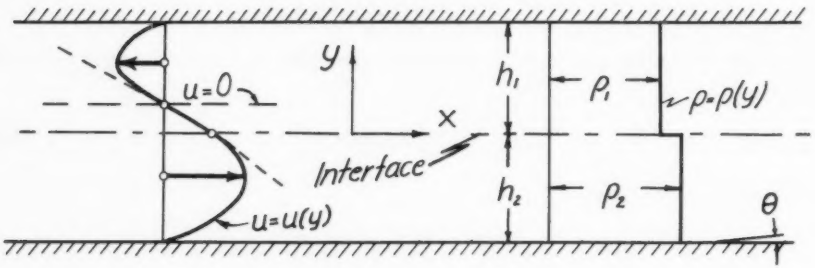

FIG. 1.—DEFINITION SKETCH FOR STRATIFIED FLOW WITHOUT MIXING

and the kinematic viscosity, three variables which combine to yield the nondimensional parameter

$$\chi = \frac{y^2 \frac{du}{dy}}{\nu} \qquad \text{..... (26)}$$

Evaluation of this parameter for various points in laminar flow near a boundary, as shown in Fig. 2, results in a curve with a definite maximum, the location of which should correspond to the zone of minimum stability. Accordingly, comparison of maximum values for different flows - other things again being equal - should permit their relative stability to be assessed. Rouse also found that for conditions corresponding to the lower critical Reynolds number for pipes (that at which turbulence will no longer persist) the maximum value of

11 "A General Stability Index for Flow near Plane Boundaries," by H. Rouse, Journal of the Aeronautical Sciences, Vol. 12, No. 4, 1945, pp. 329-332.

χ was about 500 - not only for pipes and wide channels but also for boundary layers and plane Couette flows.

Evaluation of the same parameter for the antisymmetric condition diagrammed in Fig. 3 indicates that two maxima exist: one in the wall vicinity, as before, but another and much larger one at the center line, where $\chi = 6\, u\, h/\nu$. The latter, according to this criterion, is by far the more susceptible to disturbances of a comparable nature. If, moreover, the value of 500 is assumed to represent the critical limit, this would be found to correspond to a Reynolds number of only $u\, h/\nu = 83$, which is evidently a full order below that for either a wide channel or the boundary region of the antisymmetric case, for which $u\, h/\nu = 2{,}250$. Apart from the stabilizing effect of gravity, which vanishes as the density ratio approaches unity, the zone of interfacial shear in a stratified fluid appears to be relatively susceptible to instability of the Reynolds type.

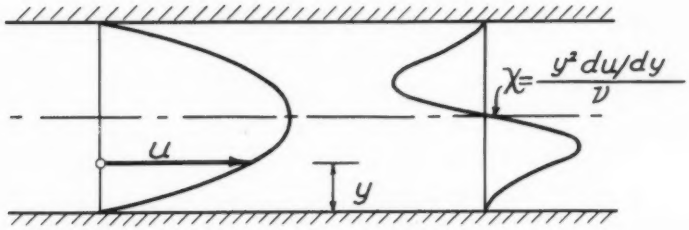

FIG. 2.—VARIATION OF χ IN PLANE POISEUILLE FLOW

To introduce the effect of gravity on stability, the behavior of small disturbances can be examined through a one-dimensional analysis[12] of interfacial waves. For each layer of the stratified flow the following equations apply:[13]

$$\frac{\partial u}{\partial x} + \frac{\partial v}{\partial y} = 0 \quad \ldots\ldots\ldots\ldots\ldots\ldots \quad (27)$$

$$\frac{Du}{Dt} = \rho\, g \sin\theta - \frac{\partial p}{\partial x} + \frac{\partial \sigma_x'}{\partial x} + \frac{\partial \tau}{\partial y} \quad \ldots\ldots\ldots \quad (28)$$

and

$$\frac{Dv}{Dt} = -\rho\, g \cos\theta - \frac{\partial p}{\partial y} + \frac{\partial \sigma_y'}{\partial y} + \frac{\partial \tau}{\partial x} \quad \ldots\ldots\ldots \quad (29)$$

The two-dimensional case is considered, because it has been shown that there is no need to take three-dimensional disturbances into account for the reason that they lead less rapidly to instability (H. B. Squire,[14] Yih[15]). For long

12 "Effect of Turbulence and Channel Slope on Translation Waves," by G. H. Keulegan and G. W. Patterson, Journal of Research of NBS, 1953, pp. 461-512.

13 "Advanced Mechanics of Fluids," by H. Rouse, John Wiley and Sons, Inc., New York, 1959, p. 59.

14 "On the Stability of Three-Dimensional Disturbances of Viscous Flow between Parallel Walls," by H. B. Squire, Proceedings, Royal Soc., A. Vol. 142, 1933, pp. 621-628.

15 "Stability of Two-Dimensional Parallel Flows for Three-Dimensional Disturbances," by C. S. Yih, Quarterly of Applied Mathematics, Vol. 12, No. 4, 1955, pp. 434-435.

waves the acceleration terms in the y-direction can be neglected. Additional assumptions will involve the neglect of $\partial \sigma_x'/\partial x$, $\partial \sigma_y'/\partial y$, and $\partial \tau/\partial x$, and the hypothesis of similar velocity profiles. After integration over y across the strata, for each layer a pair of equations similar to the following is obtained:

$$h \frac{\partial U}{\partial x} + U \frac{\partial h}{\partial x} + \frac{\partial h}{\partial t} = 0 \quad \ldots\ldots\ldots\ldots \quad (30)$$

and

$$\rho\left[\frac{\partial U}{\partial t} + (1-\alpha)\frac{U}{h}\frac{\partial h}{\partial t} + \alpha U \frac{\partial U}{\partial x}\right] = \rho g \sin\theta - \frac{\partial p_i}{\partial x} - \rho \frac{\partial h}{\partial t} g \cos\theta - \frac{\rho f U^2}{8h} \quad \ldots (31)$$

Herein τ has been expressed in terms of the resistance coefficient, α is the ratio $\int_0^h u^2\, dy/U^2 h$, and p_i is the pressure at the interface. If the linearization of the equation is performed and p_i is eliminated, one obtains the differential equation

$$\left(1 + \frac{\rho_2}{\rho_1}\right)\frac{1}{U_1^2}\frac{\partial^2 h'}{\partial t^2} + 2\left(\alpha_1 + \frac{\rho_2}{\rho_1}\frac{U_2}{U_1}\alpha_2\right)\frac{1}{U_1}\frac{\partial^2 h'}{\partial x\, \partial t} + \frac{h_1 \Delta\gamma}{\rho_1 U_1^2}\left(1 - \frac{\rho_2}{\rho_1}\frac{h_2}{h_1}\right)\frac{\partial^2 h'}{\partial x^2}$$

$$+ \left[\alpha_1 + \alpha_2 \frac{\rho_2}{\rho_1}\left(\frac{U_2}{U_1}\right)^2 \frac{\partial^2 h'}{\partial x^2} + R' \frac{\partial h'}{\partial t} + R'' \frac{\partial h'}{\partial x}\right] = 0 \quad \ldots \quad (32)$$

where the subscripts 1 and 2 correspond to the upper and lower layer, respectively, and R' and R'' indicate terms containing the resistance coefficients f_1 and f_2:

$$R' = \frac{\rho_2}{\rho_1}\left(\frac{U_2^2}{8 U_1^2 h_2}\frac{\partial f_2}{\partial U_2} + \frac{f_2 U_2}{4 h_2 U_1^2}\right) - \frac{1}{8 h_1}\frac{\partial f_1}{\partial U_1} + \frac{f_1}{4 U_1 h_1} \quad \ldots \quad (33)$$

and

$$R'' = \frac{\rho_2}{\rho_1}\left(\frac{U_2^3}{8 U_1^2 h_2}\frac{\partial f_2}{\partial U_2} - \frac{U_2^2}{8 U_1^2}\frac{\partial f_2}{\partial h_2} + \frac{3 f_2 U_2^2}{8 h_2 U_1^2}\right)$$

$$- \left(\frac{U_1}{8 h_1}\frac{\partial f_1}{\partial U_1} - \frac{1}{8}\frac{\partial f_1}{\partial h_1} + \frac{3 f_1}{8 h_1}\right) \quad \ldots\ldots\ldots\ldots \quad (34)$$

Eq. 32 is a linearized form of an approximate equation for the interfacial waves. However, all the essential factors have been preserved in it, so that the pertinent dimensionless parameters involved can be recognized: ρ_2/ρ_1, the ratio of densities; h_2/h_1, the ratio of depths of the two layers; $U_1/\sqrt{h_1 \Delta\gamma/\rho}$, the Froude number; R_1, R_2, the Reynolds numbers of each layer, included in the corresponding resistance coefficients; α_1, α_2, the velocity distribution coefficients. It should be noted that two Reynolds numbers are equivalent to one

Reynolds number and the viscosity ratio. The ratio of mean velocities U_1/U_2 is not listed among the dimensionless parameters, because of the imposed requirement that $h_1 U_1 = h_2 U_2$. Eq. 32 can be written completely in nondimensional form, but no new nondimensional variables will be added.

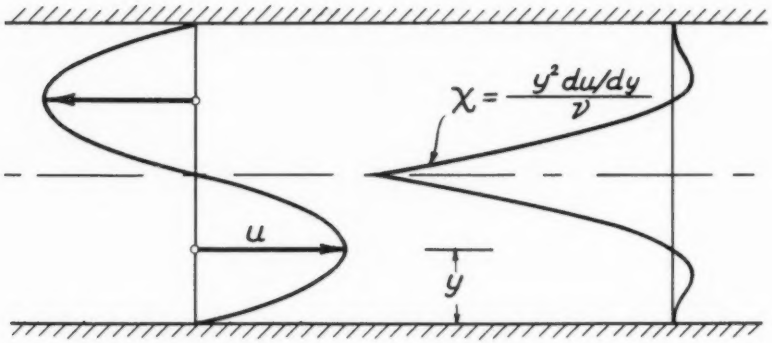

FIG. 3.—VARIATION OF χ IN ANTISYMMETRIC FLOW

When the two layers are made of equal thickness, the equation for the disturbance h' becomes simpler, and under the assumption of equal resistance in both layers with practically the same viscosity it follows that

$$\frac{\partial^2 h'}{\partial t^2} + 2\,\alpha\,U\,\frac{\partial^2 h'}{\partial x\,\partial t} + \frac{1}{2}\,\frac{h\,\Delta\gamma}{\rho\,U^2}\cos\theta\,\frac{\partial^2 h'}{\partial x^2}$$

$$+ \alpha\,U^2\,\frac{\partial^2 h'}{\partial x^2} + r'\,\frac{\partial h'}{\partial t} + r''\,\frac{\partial h'}{\partial x} = 0 \quad \ldots\ldots\ldots \quad (35)$$

in which r' and r'' are simpler expressions of the terms R' and R''. The relationship

$$h' = C\,e^{i(\xi t + \eta x)} \quad \ldots\ldots\ldots\ldots\ldots \quad (36)$$

which satisfies this equation, represents a disturbance which can be made as small as desired by assigning convenient values to C. After substitution of h' into Eq. 35 an equation for ξ is obtained, from which the condition that will make $\xi = 0$ can be derived - that is, the condition for neutral disturbances which neither grow nor decay. Because in this approximation the terms involving resistance cancel, there results, for laminar flow and for small differences in density, the rather simple condition

$$F^2 = \frac{\cos\theta}{3\sqrt{2}} \quad \ldots\ldots\ldots\ldots\ldots \quad (37)$$

Because the Froude and Reynolds numbers are related in the case of laminar flow by the equation

$$F^2 = \frac{1}{12} R \sin\theta \quad \ldots\ldots\ldots\ldots\ldots\ldots \quad (38)$$

it follows that the equation for the neutral curve in the F - R plane is simply

$$F = \left(18 + \frac{144}{R^2}\right)^{-1/4} \quad \ldots\ldots\ldots\ldots \quad (39)$$

The question of instability cannot, of course, be answered quantitatively by two such partial approaches, even if they are superposed in some way. How-

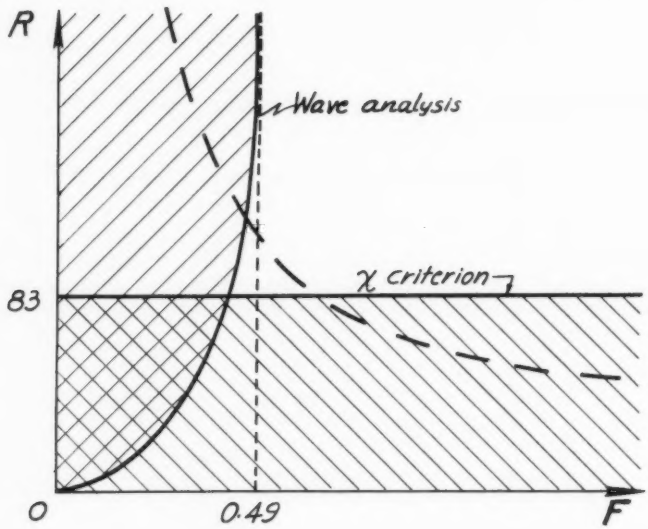

FIG. 4.—SCHEMATIC REPRESENTATION OF THE STABILITY FUNCTION

ever, one can expect to acquire at least a qualitative indication from such a combination. If the lines represented by the two analyses are plotted, a zone in the Froude-Reynolds plane is determined (doubly hatched in the Fig. 4) which must certainly belong to the stable region. At least a portion of the neighboring zones in the singly hatched regions should also belong to the stable portion of the plane. In all probability the boundary between the two zones is of the form indicated schematically by the dashed curve. It is the experimental determination of the indicated function that is the goal of this investigation.

EXPERIMENTAL APPROACH

There is a simple and interesting experiment attributed to Helmholtz in which two fluids of different density are made to flow one over the other by

carefully tilting the tube that contains them. The interface is first seen to be very smooth, then to become regularly wavy, and finally to disrupt with the onset of turbulent motion. The experiment can be repeated indefinitely if the two fluids are not miscible; it can also be performed very well with miscible fluids, although each repetition becomes more difficult.

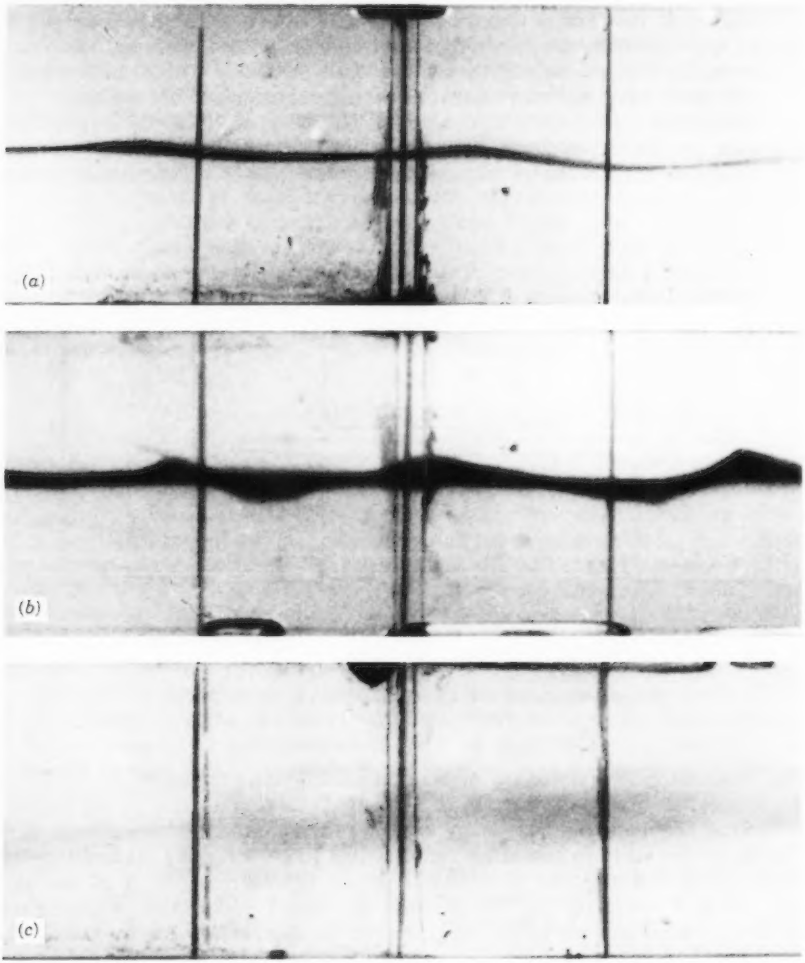

FIG. 5.—SUCCESSIVE STAGES OF INTERFACIAL DISTURBANCE

For the experiment with miscible fluids, care has to be exercised to have an initially neat interface. To make this region clearly visible, dye can be injected between the two fluids. The process of mixing is very well defined if two chemical indicators (such as phenolphthalein and sodium hydroxide) are used in

such a way that color will appear where mixing takes place. Figs. 5(a), (b), and (c) show interfacial conditions with regular waves, with waves on the verge of breaking, and with turbulent mixing, respectively. The experiments were performed with fresh and salt water. Dye was used in the first two, and chemical indicators were introduced in the third.

In the Helmholtz experiment, which has been studied in some of its aspects by G. H. Mittendorf,[16] A. M. ASCE, when the difference in densities is small the symmetry of the flow is almost perfect and external disturbances can be minimized; the phenomenon has a transient character, however, and lasts only for a minute or two unless a rather large scale is used. Yet even if a large scale were to be adopted, every aspect of the phenomenon would still vary with time. Therefore, to keep both layers in motion and to stabilize the occurrence at different stages, an apparatus was devised that would bring two streams flowing in opposite directions into contact for a reach of considerable length.

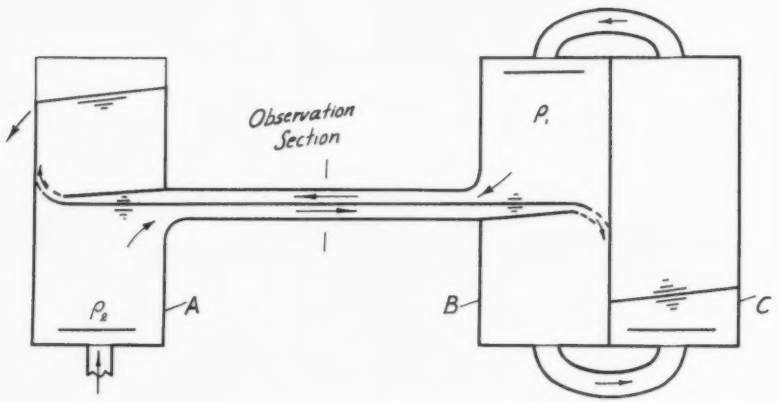

FIG. 6.—SKETCH OF EXPERIMENTAL APPARATUS

In Fig. 6 a sketch is given of the apparatus used, which consisted mainly of two tanks connected by a 36-in. conduit of 2-in. by 6-in. rectangular cross section. A third tank provided the necessary capacity for running the experiment during the time required to establish the flow and to perform the measurements. The apparatus was mounted on a tiltable frame in order to give it an adequate slope. Tank B had a lid so that it could be closed during the experiments. Tank A was open, and one of its sides served as an overflow for the fresh water leaving the apparatus.

To perform an experiment, the unit was first completely filled with fresh water and then an inflow of salt water was started very slowly at the bottom of tank A. There, salt water was diverted radially and parallel to the bottom by

16 "The Instability of Stratified Flow," by G. H. Mittendorf, thesis presented to the State Univ. of Iowa, at Iowa City, Iowa, in 1961, in partial fulfilment of the requirements for the degree of Master of Science.

a plate and thence upward through wire screens. In this way a neat interface would be formed, and the inflow could be gradually increased as the interface became more remote. When the interface reached the inlet of the rectangular duct, the salt water would start to flow down the slope toward tank B and then to tank C. As the salt water entered tank C, it displaced fresh water, which moved through the apparatus in the opposite direction and wasted over the weir of tank A. The duration of the experiments depended on the rate of inflow of the salt water and the capacity of tank C.

During the experiment the discharge and the slope were varied in such a way that two layers of equal thickness would form. To aid in this operation the two tailplates indicated in Fig. 6 had to be adjusted somewhat. One of the main experimental difficulties was to do this in a short time and in such a way that no appreciable disturbances could originate where the fresh and the salt water entered the working section and thus affect the flow within. A very persistant disturbance of another type was the intrusion of the fluid of intermediate density resulting from mixing of the two fluids; this, instead of flowing away, would accumulate in the end tanks, and sometimes had to be bled off in order to keep the interface clean. The great change in the thickness ratio of the two strata in the tailplate sections tended to stabilize the interface in the approach section even while considerable turbulence was developing in the zone under study.

TECHNIQUES OF OBSERVATION AND MEASUREMENT

In addition to measurement of the discharge, slope, temperature, and geometrical dimensions involved, the velocity and density distributions at the center line of the central section of the rectangular duct were subjected to careful and detailed investigation. The choice of this one section for the distribution studies was determined for reasons not only of convenience but of achieving a state of symmetry in the two strata. It was further assumed that the wall effects were of small magnitude, so that the central portion of the flow could be treated as two-dimensional. Preliminary measurements as well as calculations were made to verify this assumption.

The velocity measurement was based on the technique of photographing the motion of small particles suspended in the fluid, because the velocities were in the low range and disturbances of the flow were to be avoided. The well-known procedure of chronophotography was adapted to the case by using as timer a Strobolume activated by an electrical clock combined with a photocell. After considering and experimenting with several different tracers, the choice was made in favor of a mixture of two different fluids in the proper proportion to yield the desired density. For each experiment three mixtures of n-butyl phthalate and xylene with a bit of white paint were prepared to match the densities of fresh water, salt water, and the intermediate mixture. The mixture was injected by means of hypodermic needles in such a way as to produce small clusters of droplets essentially instantaneously but with practically no disturbance, as was verified under conditions of laminar flow. To take pictures of the droplets, a narrow strip was illuminated with both continuous and intermittent light. The channel was made of black plastic, so that the droplets moved against a dark background and left continuous traces on the film with bright dots corresponding to the flashes emitted by the Strobolume. Usually some 30 to 50 pictures were taken in each run in order to ensure a good average, es-

pecially in the case of turbulent motion. The traces left on the film generally appeared to have a head and a tail of unequal length, and this helped to determine the direction of the motion. No effort was made to synchronize the camera shutter and the flashing light in such a way as to make different heads and tails, because it was found that mere chance was enough to obtain the desired result in most of the pictures.

The frequency of the flashing light was controlled first by means of a mechanical contactor and then by a combination of an electric clock operating a notched aluminum disk and an electric circuit with a photocell. A beam of light passing through the notches excited the photocell, which in turn operated

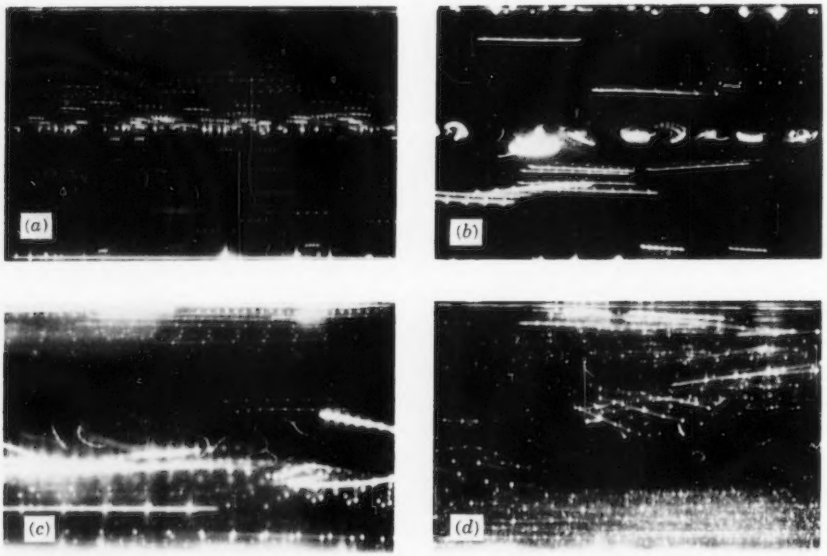

FIG. 7.—CHRONOPHOTOGRAPHS OF ONSET OF MIXING

the Strobolume. Both timers were built at the Iowa Institute using standard equipment and instruments.

To determine the density distribution, samples were taken at different levels in sufficiently small amounts to minimize disturbance of the flow and to withdraw fluid only from the desired elevation. The samples were diluted afterward to a larger volume and their electrical conductivity was measured to determine the salinity and therefrom the density. Sampling at and near the lateral walls was carried on in a few experiments to explore the conditions of mixing in that region. It was found that the density distribution there was somewhat distorted with respect to that of the center and the results much less consistent. This vindicated an earlier rejection of optical methods based on transverse beams of light for determining the density distribution, because

they would include wall effects. It was concluded that the use of very fine hypodermic needles would yield a truer profile even if they slightly disturbed the flow.

DIRECTLY OBSERVED INTERFACIAL CONDITIONS

Qualitative as well as quantitative observations can be of great value in the study of a phenomenon which has modes of occurrence yet to be disclosed. To the naked eye and to the photographic camera interesting features of the stratified flow under consideration were made observable by refraction due to the density stratification or through the addition of dyes or the injection of particles. The accompanying photographs (Fig. 7) illustrate the principal features thus observed.

In Fig. 7(a) the motion is laminar with straight streamlines; the interface coincides with the line of zero velocity, which is indicated by droplets of intermediate density appearing as dots at the center line. Fig. 7(b) corresponds to an interface with regular waves, and Fig. 7(c) to an interface with waves which break and start to show irregularity and randomness. Fig. 7(d) depicts the motion after turbulence has developed and active mixing occurs across the interface.

Based on the qualitative conditions observed both visually and photographically, each experiment was labeled with the symbol L, W, I, or T, corresponding, respectively, to uniform laminar motion, laminar motion with regular waves, irregular motion with breaking waves and incipient turbulence, and, finally, pronounced turbulence in the interfacial region. These symbols were then plotted as points in the **F - R** plane. As can be seen in Fig. 8, the four corresponding regions are clearly distinguishable. To express the correlation in quantitative form, however, some measurable quantity had to be considered. The resistance coefficient, the shear stress at the interface, and the rate of mixing across it were therefore evaluated as described in the following sections.

THE RESISTANCE COEFFICIENT

The stratified flow under investigation consists of two streams flowing in opposite directions and separated by a plane of zero velocity. Considering the forces acting on two fluid prisms of length Δx, as indicated in Fig. 9, one can write

$$m_1 g \sin\theta + (\tau_1)_m P \Delta x - A \Delta p = 0 \quad \ldots\ldots\ldots \quad (40)$$

and

$$m_2 g \sin\theta - (\tau_2)_m P \Delta x - A \Delta p = 0 \quad \ldots\ldots\ldots \quad (41)$$

where P is the wetted perimeter, A is the cross-sectional area of each stream, and $(\tau 1)_m$ and $(\tau 2)_m$ represent the corresponding mean shear stresses over floor, walls, and interface. From the two preceding equations, after elimination of Δp one obtains

$$\tau_m = \frac{(\tau 1)_m + (\tau 2)_m}{2} = \frac{1}{2} \frac{m_2 - m_1}{P \Delta x} g \sin\theta \quad \ldots\ldots\ldots \quad (42)$$

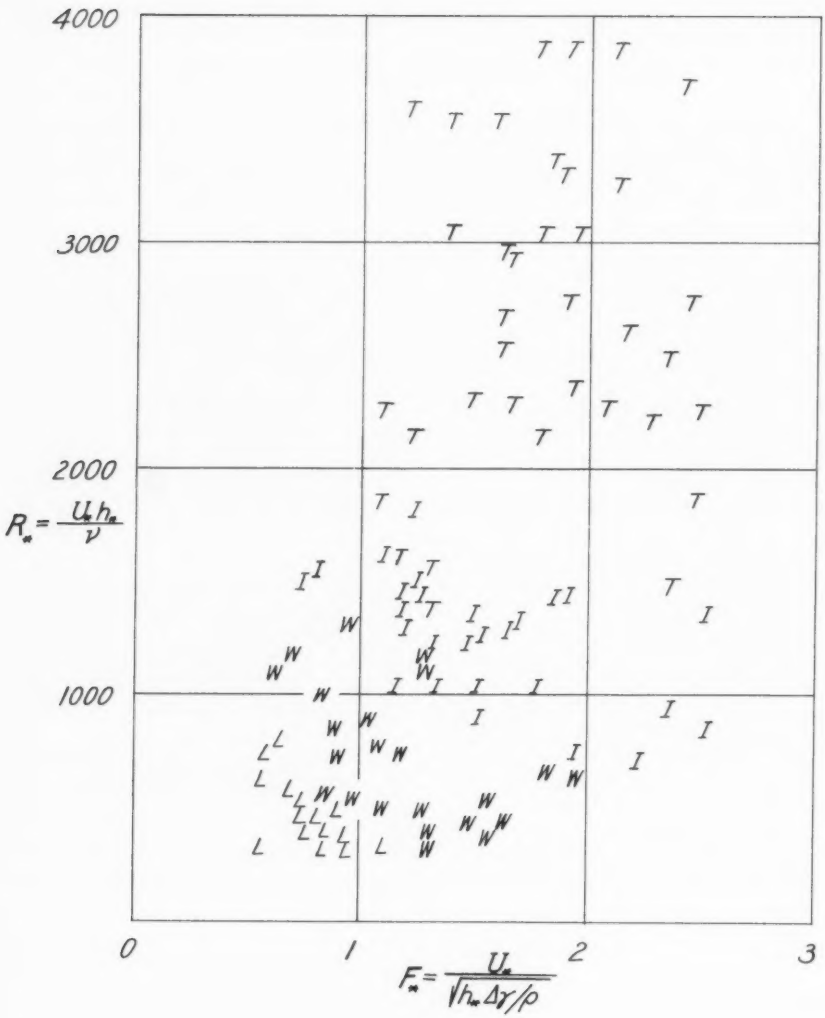

FIG. 8.—OBSERVED ZONES OF LAMINAR FLOW, WAVES, INSTABILITY, AND TURBULENCE IN FROUDE-REYNOLDS PLANE

The masses m_2 and m_1 depend on the density distribution and are to be calculated through integrals of $\rho(y)$ over the corresponding volumes. Approximate values of m_1 and m_2 can be obtained if a linear distribution of density is as-

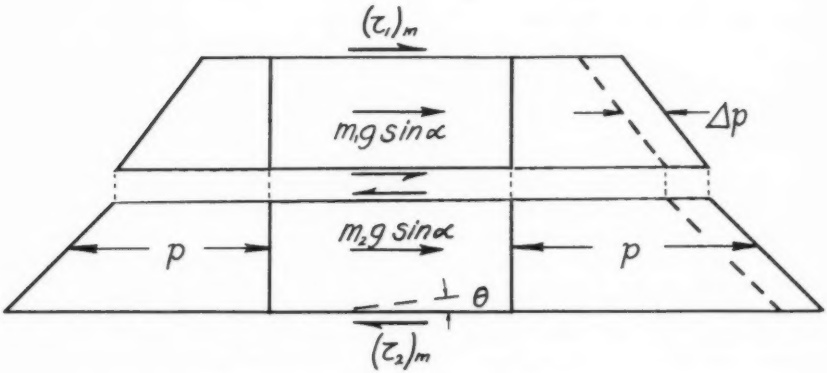

FIG. 9.—FREE-BODY DIAGRAM OF FLUID ELEMENTS

sumed over the region where it changes from ρ_1 in the upper layer to ρ_2 in the lower layer. In this way it is seen that

$$m_1 \approx \rho\left(h - \frac{\delta}{2}\right) \Delta x + \int_0^{\delta/2} \left[\rho_1 + \left(\frac{1}{2} - \frac{y}{\delta}\right)\Delta\rho\right] \Delta x \, dy = \rho_1 \, h \, \Delta x + \frac{\Delta\rho}{8} \, \delta \, \Delta x \quad ..(43)$$

and, similarly, that

$$m_2 \approx \rho_2 \, h \, \Delta x - \frac{\Delta\rho}{8} \, \delta \, \Delta x \quad \ldots\ldots\ldots\ldots \quad (44)$$

Substituting m_1 and m_2 in the expression for τ_m yields

$$\tau_m \approx \frac{1}{2} \, \Delta\rho \left(R - \frac{b\,\delta}{4\,P}\right) g \sin\theta \quad \ldots\ldots\ldots\ldots \quad (45)$$

where $R = A/P$ is the hydraulic radius. The resistance coefficient is then given by

$$f \approx \frac{4 \, g \, \Delta\rho \left(R - \frac{b\,\delta}{4\,P}\right)}{\rho \, U^2} \sin\theta \quad \ldots\ldots\ldots\ldots \quad (46)$$

Since J. Boussinesq[17] has treated the general problem, the solution for laminar flow in a rectangular pipe can be evaluated therefrom. The corre-

17 "Mémoire sur l' Influence des Frottements dans les Mouvements Réguliers des Fluides," Journal de Mathématiques Pures et Appliquées, 2nd Series, Vol. 13, 1868, pp. 377-424.

sponding resistance coefficient is given by

$$f_L = \frac{\phi(b/h)}{R} \quad \ldots\ldots\ldots\ldots\ldots\ldots \quad (47)$$

Hence the ratio f/f_L becomes

$$\frac{f}{f_L} \approx \frac{4\left(\frac{R}{h} - \frac{b\,\delta}{4\,P\,h}\right)}{\phi\,(b/h)} \frac{R}{F^2} \sin\theta \quad \ldots\ldots\ldots\ldots \quad (48)$$

This expression, although an approximate one, shows that the correlation of f/f_L with the Reynolds and Froude numbers will be essentially in terms of the relative thickness of the mixing zone.

The experimental determination of the resistance coefficient f required the measurement of the discharge, the density distribution, the slope, and the dimensions of the cross section of the conduit. The corresponding values of f/f_L are given in Fig. 10, which shows how they correlate with the Reynolds and Froude numbers of each stream. There is a region in the F - R plane where f/f_L approaches unity, though in the mean it remains somewhat greater. Where the flow is established and completely stable, the value should be exactly unity; this leads to the conclusion that the lack of establishment and the presence of initial disturbances are responsible for f/f_L being slightly greater than unity even in the zone where stable laminar flow is to be expected. That the magnitude of the ratio otherwise steadily increases with F and R, as anticipated, is quite evident from the diagram.

DIMENSIONAL ANALYSIS FOR SHEAR STRESS AND RATE OF MIXING

To study the interfacial shear stress and the rate of transfer of mass across the interface, these were next correlated with the independent variables of the problem. The quantities U_* and h_* (Fig. 11) were selected to represent the geometric and kinematic variables of the interfacial layer, in order to divorce the analysis so far as possible from the dimensions of the test section itself. Because the variations in density and viscosity were small, the mean values ρ and μ were considered accurate enough for the expression of inertial and viscous forces. On the other hand, gravitational effects being essentially dependent on the difference between the two specific weights rather than upon their absolute values, $\Delta\gamma$ was introduced as the corresponding independent variable. The dimensionless variables found through the approximate analysis of an earlier section are thus reduced to a Froude number and a Reynolds number, the others being eliminated by the conditions h_1/h_2, $\rho_1 \approx \rho_2$, and $\mu_1 \approx \mu_2$.

Instead of considering directly the interfacial shear stress τ_i, its ratio to the viscous stress $(du/dy)_0$, which also depends on the above-listed variables, will be analyzed. For turbulent flow the shear stress has been represented by the sum of two terms $\mu(du/dy) - \rho\,\overline{u'\,v'}$. In the present case values of the shear stress greater than $\mu(du/dy)$ can be expected as soon as the flow ceases to correspond to the steady-state solution of the parallel laminar flow, though the initial increase is not due to turbulent transfer of momentum so much as to a difference in regime. If desired, the ratio can be considered as a "total"

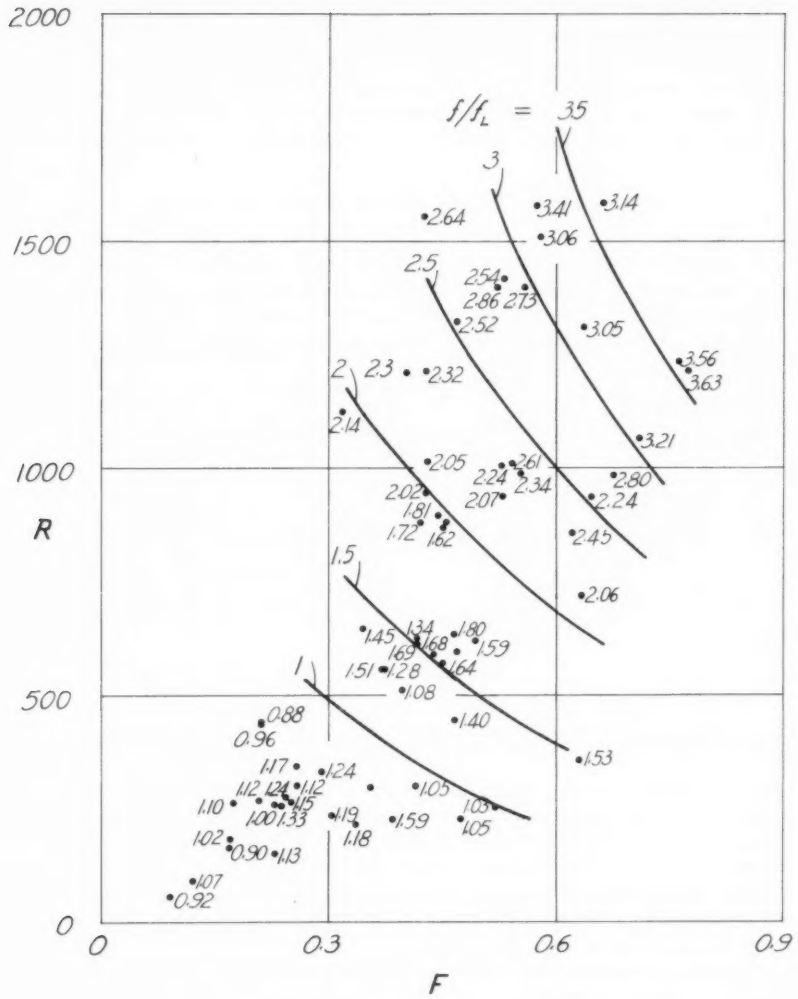

FIG. 10.—VARIATION OF THE MEAN RESISTANCE COEFFICIENT WITH **F** AND **R**

viscosity coefficient. If, then

$$\tau_i = f(U_*, h_*, \rho, \mu, \Delta\gamma) \quad \ldots\ldots\ldots\ldots \quad (49)$$

dimensional analysis will immediately yield

$$S = \frac{\tau_i}{\mu(du/dy)_0} = f(F_*, R_*) \quad \ldots\ldots\ldots\ldots \quad (50)$$

For the rate of transfer of mass as represented by the mean velocity V of transverse motion across the interface,

$$V = f(U_*, h_*, \rho, \mu, \Delta\gamma) \quad \ldots\ldots\ldots\ldots \quad (51)$$

for which it again follows by dimensional analysis that

$$T = \frac{V}{U_*} = f(F_*, R_*) \quad \ldots\ldots\ldots\ldots\ldots \quad (52)$$

Note should be taken of the assumptions made relative to two different aspects of the analysis. One is implicit in the usual method of selecting variables of primary influence and disregarding those of secondary influence. The other involves the arbitrary separation of regions of flow which are supposed to have

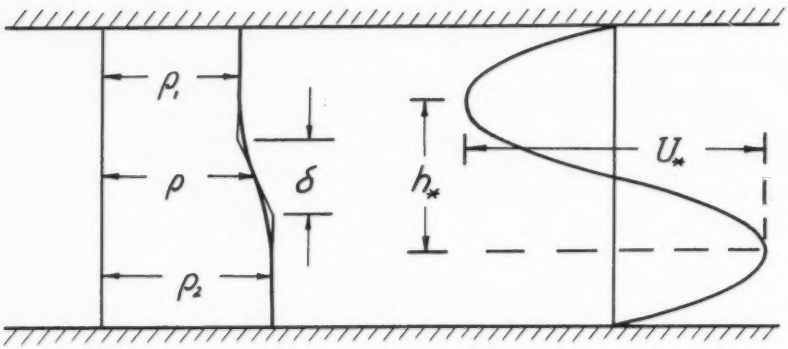

FIG. 11.—INTERLAYER NOMENCLATURE

their own mechanical inner laws at least to a first degree of approximation. This is certainly a questionable step which should be carefully checked under different conditions. In the present experiments it was subjected to verification by changing the variable h_* in the ratio of 1 to 2, with satisfactory results.

SHEAR STRESS AT THE INTERFACE

The resistance coefficient f gives only an indirect measure of the interfacial conditions, because it averages effects over the whole perimeter of each stream, including the walls. It is thus a variable which corresponds to a given rectangular section, whereas in order to obtain from these experiments a picture that is focused on the interface itself, it is desirable to interpret them in a manner that minimizes boundary effects.

The calculation of the shear stress at the interface for two-dimensional conditions is similar to that of the resistance coefficient except that it requires consideration of the local value of the shear stress at the top and bottom bound-

aries of the conduit. This would involve considerable difficulty were it not that the rather low values of the Reynolds number ensured the existence of laminar motion at those boundaries (as could be seen from the photographic records) even when turbulence occurred at the interface. If the equations for two elementary prisms in each layer are written and any change of momentum is neglected, it is found that

$$\tau_1 \Delta x + \tau_i \Delta x + \left(\rho_1 h \Delta x + \frac{\Delta\rho}{8} \delta \Delta x\right) g \sin\theta - h \Delta p = 0 \quad \ldots \quad (53)$$

$$- \tau_2 \Delta x - \tau_i \Delta x \quad \left(\rho_2 h \Delta x - \frac{\Delta\rho}{8} \delta \Delta x\right) g \sin\theta + h \Delta p = 0 \quad \ldots \quad (54)$$

where τ_i is the shear stress at the interface. A linear variation of the density has been assumed over the thickness δ of the mixing zone. After elimination of Δp the expression for τ_i becomes

$$\tau_i = \frac{1}{2} \Delta\rho \left(h - \frac{\delta}{4}\right) \sin\theta - \frac{1}{2} (\tau_1 + \tau_2) \quad \ldots \quad (55)$$

The flow in the wall boundary layers being laminar, it follows that

$$\tau_1 + \tau_2 = \mu_1 \left(\frac{du}{dy}\right)_{y=h} + \mu_2 \left(\frac{du}{dy}\right)_{y=-h} \quad \ldots \quad (56)$$

and hence

$$\tau_i = \frac{1}{2} \Delta\rho \left(h - \frac{\delta}{4}\right) g \sin\theta - \frac{1}{2} \left[\mu_1 \left(\frac{du}{dy}\right)_n + \mu_2 \left(\frac{du}{dy}\right)_{-h}\right] \quad \ldots \quad (57)$$

In accordance with the foregoing section, the ratio $\mathbf{S} = \tau_i/(du/dy)_0$ has been chosen to represent the interfacial shear in a dimensionless form. Like the ratio f/f_L, $\mathbf{S}$ must be unity for parallel laminar flow and should become greater than unity as soon as the flow becomes either nonuniform or unsteady. In order to correlate the ratio $\mathbf{S}$ with the Froude and Reynolds numbers, the latter parameters were so evaluated that only the region of flow in the vicinity of interface need be considered. The representative length chosen was h_*, the distance between the two maxima of the velocity distribution curve, and the representative velocity was selected to be U_*, the maximum relative velocity between the two layers. (This amounts, it should be remarked, to treating the interfacial region as a layer with its own inner laws, an approach which must be tested further to verify to what extent it may hold with different velocity distributions in the rest of the fluid.)

The correlation of $\mathbf{S}$ with the variables

$$\mathbf{R}_* = \frac{U_* h_*}{\nu} \quad \ldots \quad (58)$$

and

$$\mathbf{F}_* = \frac{U_*}{\sqrt{h_* \Delta\gamma/\rho}} \quad \ldots \quad (59)$$

is shown in Fig. 12. The scattering is in this case greater than in the case of the resistance coefficient, which is probably due to the difficulties involved in determining exact values of du/dy and δ. Nevertheless, there is certainly a definite trend, and tentative curves have been fitted which show the approximate dependence of the shear-stress ratio upon the special Froude and Reynolds numbers. These results are rather similar to those reported by Lofquist for another case of flow.[9]

TRANSFER OF MASS

The onset of instability brings about a more active interfacial diffusion, which up to that point was due only to molecular motion. The more turbulent the motion becomes, the more intense must be the transfer of mass from the denser to the less dense fluid. The mean value of the velocity of mass transfer was calculated in the following manner: On the basis of symmetry it was assumed that, whereas across such an interface the volumetric flux must be zero, the mass flux per unit width is given by $\rho_2 \, V \, L - \rho_1 \, V \, L$, where V represents the mean velocity of transfer. The longitudinal flux of mass at the entrance section of each layer is given simply by the product of the rate of flow and the corresponding density. This flux is increased with longitudinal distance for the fresh-water stream and decreased for the salt-water stream by diffusion across the interface. The amounts of increase and decrease can be evaluated with respect to the mass flux at the central section through integrals of the form $\int \rho(y) \, u(y) \, dy$ over the corresponding section. An approximate expression of these integrals is obtained by assuming that for the mixing zone

$$\rho = \frac{1}{2} (\rho_1 + \rho_2) - \alpha \, y = \rho - \alpha \, y \quad \ldots\ldots\ldots\ldots \quad (60)$$

where

$$u = \beta \, y \quad \ldots\ldots\ldots\ldots\ldots\ldots \quad (61)$$

which consists in substituting for the density and velocity curves the tangents at their inflection points. It then follows that

$$V \, \Delta\rho \, \frac{L}{2} = \int_0^h \rho(y) \, u(y) \, dy - \rho_1 \, q \quad \ldots\ldots\ldots\ldots \quad (62)$$

$$V \, \Delta\rho \, \frac{L}{2} = \rho_2 \, q - \int_{-h}^0 \rho(y) \, u(y) \, dy \quad \ldots\ldots\ldots\ldots \quad (63)$$

or

$$V \, \Delta\rho \, \frac{L}{2} = \int_0^{\delta/2} (\rho - \alpha \, y) \, \beta \, y \, dy + \rho_1 \int_{\delta/2}^h u \, dy - \rho_1 \, q \quad \ldots\ldots \quad (64)$$

$$V \, \Delta\rho \, \frac{L}{2} = \rho_2 \, q - \int_0^{\delta/2} (\rho + \alpha \, y) \, \beta \, y \, dy - \rho_2 \int_{\delta/2}^h u \, dy \quad \ldots\ldots \quad (65)$$

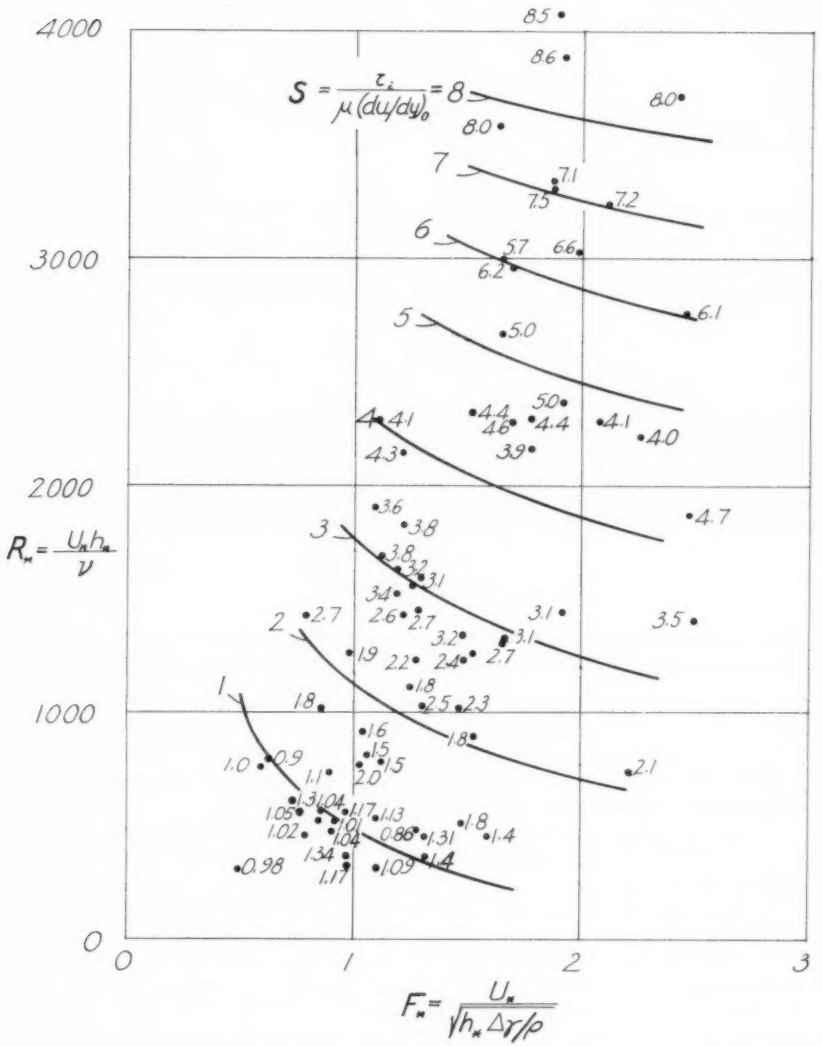

FIG. 12.—VARIATION OF INTERFACIAL SHEAR WITH F_* AND R_*

Combination of these two expressions yields

$$V \Delta\rho L = -2 \alpha \beta \int_0^{\delta/2} y^2 \, dy - \Delta\rho \int_{\delta/2}^{h} u \, dy + q \Delta\rho$$

$$= -\alpha \beta \frac{\delta^3}{12} + \Delta\rho \int_0^{\delta/2} u \, dy = \beta \frac{\delta^2}{8} \Delta\rho - \alpha \beta \frac{\delta^3}{12} \quad \ldots\ldots (66)$$

and finally,

$$V \approx \frac{\beta \delta^2}{8 L} - \frac{\alpha \beta \delta^3}{12 L \Delta\rho} \quad \ldots\ldots\ldots\ldots (67)$$

This velocity was correlated with the same variables as was the shear stress, and through dimensional analysis it was found that

$$\frac{V}{U_*} = f(F_*, R_*) \quad \ldots\ldots\ldots\ldots (68)$$

A plot of V/U_* on the plane $F_* - R_*$ (Fig. 13) shows that the interfacial mixing varies systematically with these variables. Tentative curves fitted to the experimental points show a trend similar to that of the curves for shear stress. This could certainly be expected, since the shear stress depends on diffusion of momentum, while the rate V measures the diffusion of matter.

CONCLUSIONS

This laboratory study has disclosed a number of significant facts regarding interfacial conditions in a stratified flow; these can be summarized as follows:

1. Four successive regimes have been found to exist in the interfacial region:

   a. The initial uniform laminar regime is confined to a rather small zone of the F - R plane, the latter parameters being defined in terms of variables describing a layer in the neighborhood of the interface.

   b. Such uniform laminar motion is first affected by the onset of motion of a non-turbulent type with relatively little secondary flow and a very small amount of mixing.

   c. In a third region of the F - R plane the interfacial conditions are characterized by breaking waves, which produce a more effective mixing.

   d. Finally, the waves become of complex spectrum with random characteristics, and turbulence develops in the neighborhood of the interface.

2. The interfacial shear stress, expressed in terms of the ratio of the actual stress to the viscous stress for the mean flow, shows a definite correlation with the Froude and Reynolds numbers.

3. A similar correlation exists for the rate of mixing across the interface. This was to be anticipated, since - though determined independently - the shear is a measure of momentum transport and the mixing a measure of mass transport.

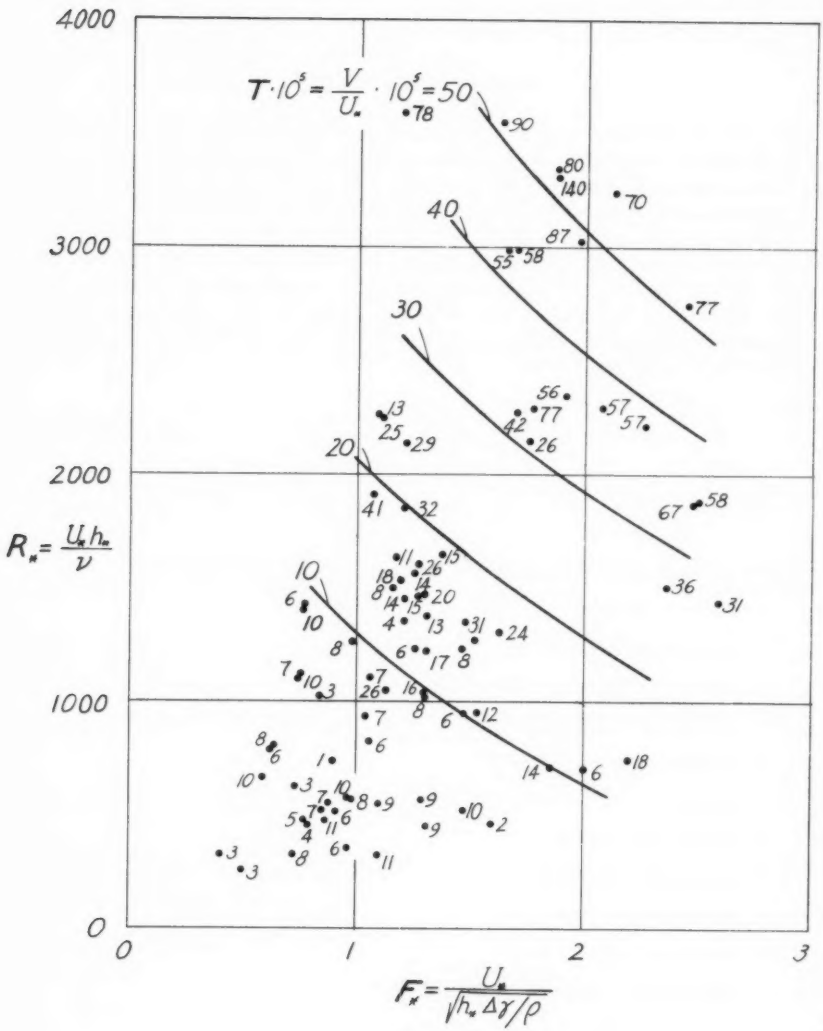

FIG. 13.—VARIATION OF THE MIXING COEFFICIENT WITH F_* AND R_*

4. To be of general significance, these studies must be now extended to large-scale conditions in which the boundaries are remote from the interfacial zone.

ACKNOWLEDGMENTS

All parts of the foregoing investigation were supported by the Office of Ordnance Research under Contract No. DA-11-022-ORD-2523. The experimentation and analysis of results were performed by the first author under the general direction of the second. George H. Mittendorf, as Research Assistant with the Institute, participated in many of the experimental runs. Valuable advice was given by Minerva C. Flores, in regard to the technique of droplet injection, and by James A. Kent, in connection with the photographic recording of the droplet behavior. The paper was first presented at the October, 1960 ASCE Convention in a program arranged by the Committee on Fluid Dynamics of the Engineering Mechanics Division.

APPENDIX.—NOTATION

The following symbols have been adopted for use in this paper:

F = Froude number;

f = resistance coefficient;

g = acceleration of gravity;

h = thickness of fluid stream;

h_* = thickness of interlayer;

m = mass;

P = wetted perimeter;

p = pressure intensity;

R = Reynolds number;

U = mean velocity of flow;

U_* = differential velocity of interlayer;

V = mean velocity of mass transfer;

u, v = velocity components;

x, y = Cartesian coordinates;

α = $\int_0^h u^2\, dy/U^2\, h$;

γ = specific weight;

δ = interlayer thickness;

μ = dynamic viscosity;

ν = kinematic viscosity;

ρ = mass density;

σ = normal stress;

τ = shear stress;

τ_m = mean shear stress along wetted perimeter; and

χ = stability parameter.

Journal of the
ENGINEERING MECHANICS DIVISION
Proceedings of the American Society of Civil Engineers

DISCUSSION

Note.—This paper is a part of the copyrighted Journal of the Engineering Mechanics Division, Proceedings of the American Society of Civil Engineers, Vol. 87, No. EM 5, October, 1961.

DYNAMIC RESPONSE OF BEAMS TRAVERSED BY TWO-AXLE LOADS[a]

Closure by Robert K. Wen

ROBERT K. WEN,[14] A. M. ASCE.—The writer wishes to thank Enno Penno for his discussion. The greater influence of higher frequencies shown in the records of the support reactions of the test bridge is, of course, not unexpected. The shear is proportional to the third derivative of the deflection function while the bending moment is to the second. For the form of the deflection function (Eq. 5), the contribution to the shear and moment response of, say, the nth mode is proportional to $1/n$ and $1/n^2$, respectively. Furthermore, whereas the second mode does not contribute anything to the bending moment at mid-span, it does affect the end reactions.

Penno stated that the magnitude of the total dynamic increment of the reactions could still be predicted by computations within a narrow margin. From this it might be conjectured that the contributions of the higher modes response would be quite small as compared to that of the first mode, although their presence was distinctly noticeable.

When a highway vehicle moves over an uneven bridge deck, it is essentially subjected to an external forcing function. In this case, the importance of damping of the response of the vehicle and that of the bridge would increase with the number of cycles of energy input, assuming that a synchronization or resonant condition is met. If the number depending on, for example, the spacing of the 3/4 in. by 4 in. boards used in the tests is appreciable, it would seem that one should be able to observe a reasonably distinct phenomenon of resonance exhibited by the bridge response.

On the other hand it would seem more difficult to observe in field experiments the theoretically predicted "resonant speeds" due to the timing of the two axle loads applied to a (theoretically) smooth deck. In this case essentially there are only two cycles of energy input. This limits the magnitude of the effects of this type of "resonance." Such limited effects could then be overridden (and become undiscernible in experiment) by the effects of other factors that may have existed in the actual test bridge-vehicle system, such as the nonlinearity of the vehicle springs and the deck unevenness, but have not been accounted for in the theoretical calculations.

---

[a] October, 1960, by Robert K. Wen (Proc. Paper 2624).

[14] Assoc. Prof., Civ. Engrg. Dept., Michigan State Univ., East Lansing, Mich.

BEARING CAPACITY OF FLOATING ICE SHEETS[a]

Discussion by G. Y. Sebastyan and F. Penner

G. Y. SEBASTYAN[22] and F. PENNER.[23]—This paper was interesting because of the similarity of the problem to the load carrying capacity of portland cement concrete pavements.

It is The Canadian Department of Transport's responsibility to design and evaluate the load carrying capacity of airport pavements. For some time it was felt that there is a definite need to re-evaluate the conventional method of design (Westergaard analysis) of portland cement concrete pavements on the basis of field performance for those constructed in accordance with Department of Transport design standards and specifications.

In the summer of 1959 and 1960, a comprehensive load testing program was conducted on a number of airport sites with varying subgrade soil condition, sub-base, base and portland cement concrete slab thickness. In all, more than fifty plate load tests were performed.

One static load test was performed on a free corner of the slab with the corner freed from the adjacent slabs by cutting through the slab with a diamond saw. On completion of the test, the concrete was removed from an area sufficient to class the test as unconfined and a standard static test was performed on the top of the base course. A 12-in. diameter plate was the minimum diameter that was used for the static base tests. One static load test was performed on the diagonally opposite corner of the slab without removing any load transfer devices. An additional static load test was performed on the center of the adjoining slab parallel to the center line of the runway. All of these tests were performed on sound concrete slabs free of cracks. Tested slabs were located a minimum of one panel distance from the edge of the pavement.

The deflection measurements for the corner tests were made by means of five dial micrometers placed in a line along the bisector of the corner, and spaced approximately 20 in. on center. The first dial was placed as close to the corner as possible with all deflections taken from an independent datum.

The deflection measurements for the center tests were made by means of four micrometers placed in a line along the bisector of the opposite corners. Two dial micrometers were placed on the plate, the other two 40 in. from the center of the plate. Absolute deflections were measured.

A load of 2,000 lb was applied for 30 sec to obtain proper seating. The dial micrometers were then zeroed. The first load of 5 kips was applied for 10 min. Dial readings were taken at 1 min, 3 min, 5 min, 9 min, and 10 min on the two

---

[a] October, 1960, by G. G. Meyerhof (Proc. Paper 2627).

[22] Design Engr., Engrg. Design, Const. Branch, Canadian Dept. of Transport, Ottawa, Canada.

[23] Eng., Const. Branch, Canadian Dept. of Transport, Winnipeg, Canada.

dials closest to the plate and at 10 min on the three remaining dials. This procedure was repeated with 5 kip load increments until the pavement failed or the capacity of the load testing equipment was reached.

A note was made of the load when the first crack appeared, and the actual load at sudden loss of bearing during load application.

For free corner tests any possible edge support was removed for the following distance from the corner: 8 ft for up to 7 in. concrete slab thickness

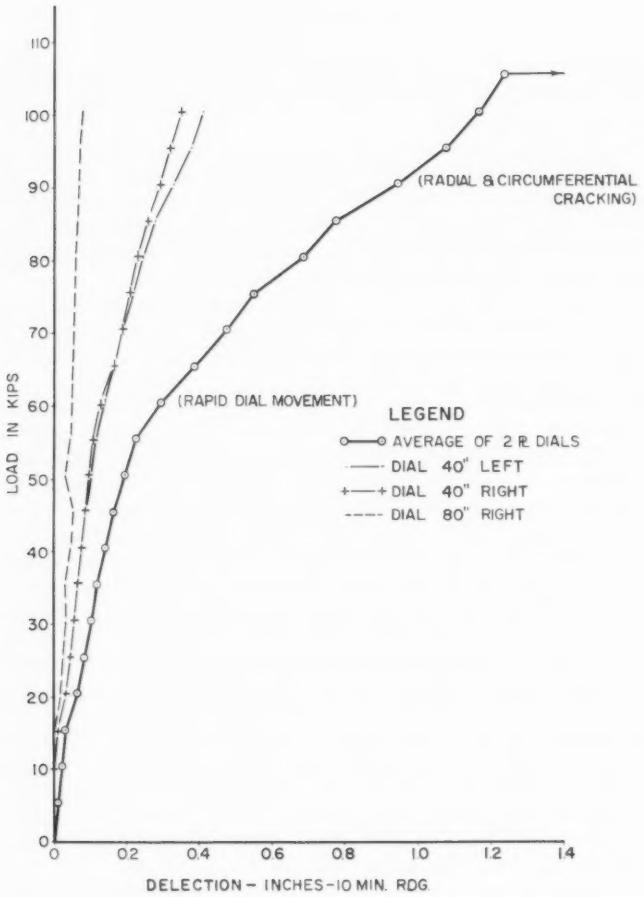

FIG. 13.—SAMPLE LOAD VERSUS DEFLECTION GRAPH

and 10 ft for concrete slabs more than 7 in. thickness. After completion of the free corner test, three beams of 6 in. by 6 in. by 30 in. were sawed out. The flextural strengths (American Society for Testing Materials ASTM C78-59), the Young's modulus of the concrete, and the unit weight was determined together with the compressive strengths (ASTM C-116-59-T).

After the free corner test was completed, all fractured concrete was removed and one static load test was performed on the top of the base course. Loading in the static base test continued until 0.5 in. deflection was obtained or until the capacity of the test unit was mobilized. After completing the static base test, three field California Bearing Ratio (CBR) tests and two field density tests (ASTM D1556-58T) were performed.

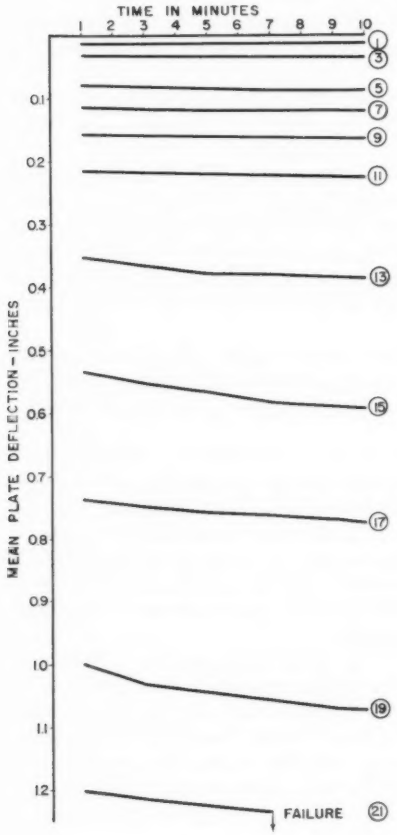

FIG. 14.—SAMPLE TIME VERSUS DEFLECTION CURVES UNDER SUCCESSIVE LOAD INCREMENTS

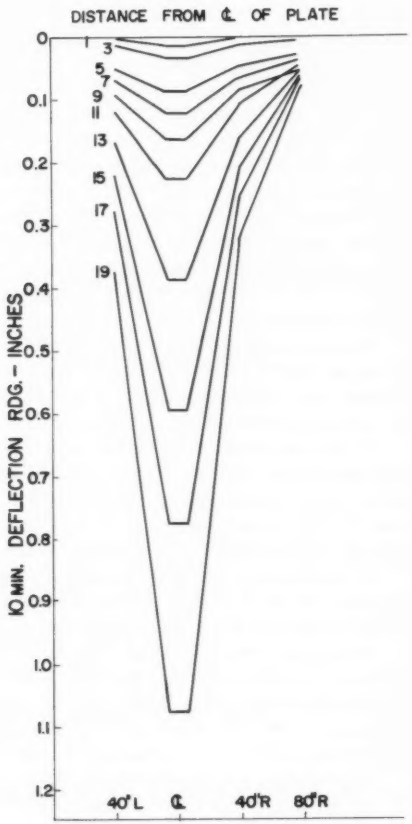

FIG. 15.—SAMPLE DEFLECTED SHAPE OF SLAB UNDER SUCCESSIVE LOAD INCREMENTS

Load testing of rigid pavement slabs was conducted when the corners and edges of the slab were curled downward. Testing commenced between 12 a.m. and 2 p.m. local standard time. Slabs to be tested remained unshaded until the time of the test. Tests were completed by 1 hr after sunset.

A standard auger hole was drilled to a depth of 10 ft from the top of the slab at each free corner test location. Soil samples recovered were classified in accordance with the U. S. Corps of Engineers soil classification system, and the moisture content was determined at 2 ft intervals. Sketches and photographs were made of the crack pattern for the slabs tested to destruction.

Typical examples of the type of data received from the field and the method of presentation are given in Figs. 13, 14, 15, 16, and 17.

The load - deflection and time - deflection relationship, together with the shape of the deflection bowl and the modulus of subgrade reaction were determined at various loadings and deformations. A short summary of the test results is given in Table 3.

The tables give, in addition to the physical data, the comparison between the actual load carried and the load carrying capacity determined on the basis of the Westergaard equations and the Meyerhof analysis.

The measured load carrying capacity was found to be considerably higher in almost every instance under the test conditions used than that predicted by the Westergaard equations. This shows that a limit design method might well be the correct approach. On the other hand, the reason for the lower values obtained using the Westergaard equation might be attributed to the assumption made in evaluating the influence of the subgrade on the load carrying capacity of the system.

Instead of assuming the subgrade to be a heavy liquid, the total subgrade reaction can be determined on the basis of the measured deflection bowl, together with the integration of the effect of the modulus of subgrade reaction at various deflections.

It is considered that these test results are most significant. Together with the evaluation of the effect of traffic and a limit design method of analysis may form a new basis for portland cement concrete pavement evaluation. The object of this presentation is to make available field data which indicates the inherent applicability of Meyerhof's analysis to portland cement concrete slabs.

It is intended that the evaluation of these test results and the possible modification of the Canadian Department of Transport's rigid pavement evaluation method will be the subject of a separate paper.

Notes on Table of Load Test Results.—(The yield load, center loading condition.) In some cases, the yield point could be determined from a break in the load-deflection curve (Fig. 16). In other cases, the load-deflection curve exhibited no definite yield point (Fig. 17). In these latter cases no yield load is reported in the table, although in some cases yielding must have occurred.

Originally, the panels were 50 ft to 100 ft long, but at the time of the test, these were sub-divided by one or more transverse cracks. In no case, was the length of the sound section less than the width.

An assumed "E" value was used. The "E" value is the mean of tests on three beams from this airport. An assumed flexural strength was used for these sites.

The value reported is the mean of 52 breaks from beams cut at various locations in the field in 1955. At that time, the concrete was approximately 11 yr old. While the beams were not cut from the slabs actually tested, they were cut from similar concrete placed under the same conditions. Therefore, the average strength of the beams should represent the average strength of the slabs tested. The value reported has been computed from the strength of 28-day construction control beams cast during the day when the test section was constructed. The

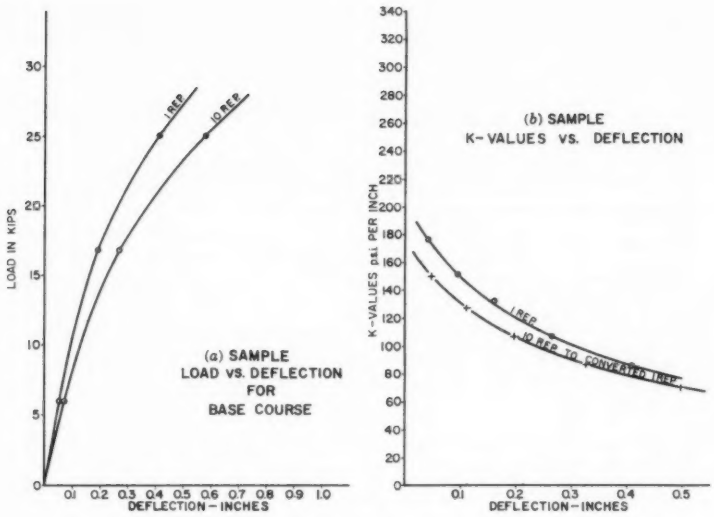

FIG. 16

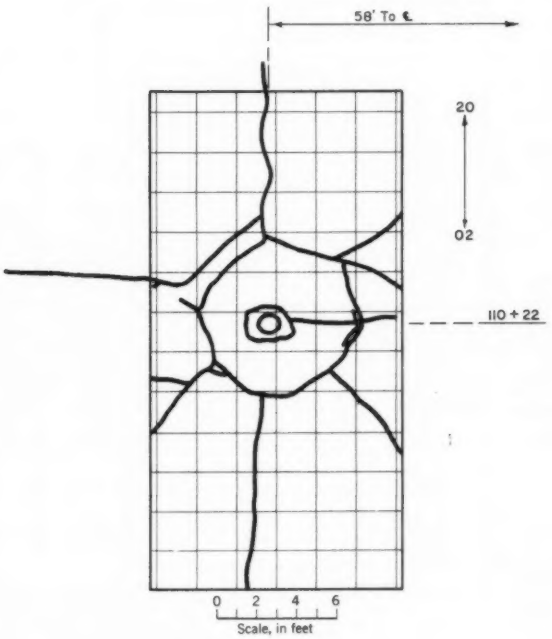

FIG. 17.—SAMPLE SLAB CRACKING DIAGRAM

TABLE 3.—LOAD TEST RESULTS FOR PORTLAND CEMENT CONCRETE

Airport	Test Number	Loading Condition	Plate Diam. Surf. Test	Concrete Slab Size ft x ft x in.	*Young's Modulus for Concrete "E"	Mean Flexural Strength P.S.I.	Base k P.C.I.	Base Test Plate Diam. inch	Base k 30" ϕ P.C.I.	Yielding Load kip	Yielding Defl. kip	Collapse Load kip	Collapse Defl. in.	Punching Load kip	Punching Defl. in.	Reaction Limit Load kip	Reaction Limit Defl. in.	Radial Distance to Crack	Westergaard Load kip	Westergaard Defl. in.	Meyer-hof P kip
1	2	3	4	5	6	7	8	9	10	11	12	13	14	15	16	17	18	19	20	21	22
A	2	C	12	ax20 x6.5	6.38	615	430	12	210							125.3	.16		20.8	.015	62.0
		FC	12									24.8	.12					27.0	16.5	.081	24.3
	3	C	12	ax20 x6	6.35	623	1150	12	560	60.3	.031					130.3	.095		20.8	.011	62.9
		FC	12									35.3	.092					25.5	17.3	.051	23.2
	4	C	12	ax20 x6.75	5.76	589	1700	12	830							140.3	.10		25.4	.009	78.0
		FC	12									40.3	.08					23.3	21.8	.048	29.0
	5	C	12	20x20 x11	5.36	481	920	12	449	75.0	.004					140.3	.053		44.6	.017	138.0
		KC	12							75.0	.05	105.3	.085					28.5	34.3	.058	53.3
		FC	12									70.3	.105					28.0	34.3	.058	53.3
	13	C	8	20x20 x11	5.06	496	1800	12	879							150.2	.114		45.0	.008	150.0
		KC	12							95.2	.07	110.2	.097					15.3	38.2	.046	60.0
		FC	12									75.2	.06					25.5	38.2	.046	60.0
	14	C	8	20x20 x11	5.24	477	590	12	288							150.2	.15		38.9	.012	124.0
		KC	12									110.2	.075					23.0	32.5	.071	51.0
		FC	12									60.2	.092						32.5	.071	51.0
	15	C	12	ax20 x6.75	6.38	635	700	12	342							140.3	.073		24.4	.014	74.6
		FC	12							40.3	.078	50.3	.175					34.0	19.6	.068	27.0
	16	C	12	ax20 x8	5.73	567	840	12	410			150.3	.238					48.0	30.0	.012	92.0
		FC	12									28.8	.12					42.4	23.6	.063	34.5
	17	C	12	ax20 x7	6.03	597	480	12	234							140.3	.186		23.4	.015	69.5
		FC	12									30.3	.091					41.0	21.7	.090	27.2
	19	C	12	ax20 x7.5	4.80	543	420	12	205							150.2	.10		24.1	.016	72.7
		DC	12									35.3	.115					36.3	20.0	.046	44.5
		FC	12									30.2	.14					29.5	19.1	.087	28.0
	20	C	4	ax20 x7.25	6.00	569	1150	12	562					105	.215		(Punching)		85.5		85.5
		C	8							38.0	.03					140.2	.178		20.6	.008	75.2
		DC	12							45.0	.07	55.0	.12					36.5	23.0	.030	46.4

		FC	12										30.2	.08				21.2	21.2	.052	29.4
	21	C	8	ax20	7.5	5.45	563	700	12	342							150.2	.145		23.1	.011	73.2
		DC	12								45.0	.14	55.2	.18					34.0	22.2	.037	47.5
		FC	12										24.7	.065					26.0	20.5	.068	30.6
A	22	C	8	ax20	x8	5.99	615	650	12	317	60.0	.013					145.2	.12		28.0	.013	89.6
		DC	12										35.2	.075					35.5	26.5	.044	58.9
		FC	12										23.9	.085					24.0	25.2	.080	37.4
	23	C	12	ax20	x7½	6.28	599	980	12	478							145.2	.10		28.4	.011	87.9
		DC	12										30.3	.055					25.5	24.4	.032	51.3
		FC	12										34.2	.08					30.8	22.8	.056	32.4
	24	C	8	ax20	x8	5.21	598	870	12	425							150.2	.18		27.4	.011	91.2
		DC	12										40.3	.11					34.7	27.1	.038	58.2
		FC	12										30.2	.08					28.5	25.6	.068	37.0
	33	C	12	ax20	x7	6.29	639	1700	12	830							140.3	.10		28.9	.009	89.8
		FC	12										45.3	.06					25.4	21.5	.062	32.3
	34	C	8	20x20	x11	5.02	515	1500	12	732							145.2	.07		46.1	.009	150.0
		KC	12										130.2	.10					34.0	39.3	.053	60.4
		FC	12										55.2	.07						39.3	.053	60.4
B	2	C	12	25x12.5x11		5.50c	600e			291h							120.0	.20		53.5	.016	140.0
	4	C	12	25x12.5x11		5.50c	600e			342h							120.0	.15		54.2	.015	144.0
	6	C	12	25x12.5x7		5.50c	644f			153j	90.0	.24					125.0	.55		24.1	.019	63.5
	8	C	12	25x12.5x6		5.50c	644f			183j	56.0	.23	90.0	.96	105	1.3			42.0	19.2	.017	50.0
	9	C	12	25x12.5x6		5.50c	644f			160j	45.0	.18	110.0	1.23	120	1.5			30.0	18.8	.018	49.6
	10	C	12	25x12.5x6		5.50c	644f			158j	60.0	.22	90.0	.68	125	1.4			54.0	18.8	.018	49.6
	13	C	12	20x20.0x12		5.50c	696g			291h							100.0	.12		72.7	.019	212.0
	14R	C	12	20x20.0x12		5.50c	624g			291h				(Jack failed)			50.0	.037		64.5	.017	275.0
	14L	C	12	20x20.0x12		5.50c	637g			291h							102.0	.09		66.0	.017	199.0
	15L	C	12	20x20.0x12		5.50c	554g			291h							100.0	.07		57.4	.015	173.0
	15R	C	12	20x20.0x12		5.50c	610g			291h							55.0	.048		63.3	.016	190.1
	16	C	12	20x20.0x12		5.50c	565g			291h							95.0	.106		58.5	.015	177.0
	31	C	12	25x12.5x6		5.50c	644f	160	30	160	55.0	.25	90.0	.77	100	1.00			48.0	18.9	.019	49.7

TABLE 3.—*CONTINUED*

Airport	Test Number	Loading Condition	Plate Diam. Surf. Test	Concrete Slab Size ft x ft x in.	*Young's Modulus for Concrete "E"	Mean Flexural Strength	Base k	Base Test Plate Diam.	Base k 30" ϕ	Yielding		Collapse		Punching		Reaction Limit		Radial Distance to Crack	Westergaard		Meyer-hof
										Load	Defl.	Load	Defl.	Load	Defl.	Load	Defl.		Load	Defl.	P
										kip	in.	kip	in.	kip	in.	kip	in.		kip	in.	kip
1	2	3	4	5	6	7	8	9	10	11	12	13	14	15	16	17	18	19	20	21	22
D	6	C	12	ax20 x6¾	5.48	533	212	12	104			100.0	.16			135.3	.52	48.0	18.2	.019	55.3
		FC	12									35.3	.16					32.0	14.3	.103	21.1
	7	C	12	ax20 x6½	6.05	434	470	12	230			120.0	.17			150.3	.42	44.0	14.4	.008	42.8
		FC	12									25.3	.12					27.0	11.3	.052	16.8
	13	C	12	a20 x8	5.73	492	414	12	202	120.0	.20					130.3	.23		24.0	.013	73.5
		KC	12									45.3	.15					32.0	18.7	.066	28.8
		FC	12									50.3	.11					32.0	18.7	.066	28.8
	14	C	12	ax20 x6½	5.05	550	1100	12	537	90.0	.077	110.3	.15					48.0	21.8	.011	66.4
		FC	12									25.3	.07					27.0	18.4	.058	24.4
	15	C	12	ax20 x6½	5.50	563	550	12	269	100.3	.22	110.0	.38			135.3	.49	36.0	20.2	.014	61.5
		FC	12									30.3	.08					25.0	16.1	.071	22.6
	16	C	12	ax20 x8	5.79	426	460	12	224							135.3	.12		20.9	.011	63.4
		KC	12							81.0	.09	90.3	.12					33.0	16.4	.060	26.4
		FC	12									35.3	.06					34.0	16.4	.060	26.4
	17	C	12	ax20 x8	5.45	564	510	18	348	70.0	.036					140.3	.11		29.2	.013	90.6
		KC	12									70.3	.075					27.0	22.2	.067	34.6
		FC	12									45.3	.08					36.0	22.2	.067	34.6
	18	C	12	ax20 x8	6.29	552	860	18	585							145.2	.10		30.2	.009	95.0
		KC	12							85.0	.095	95.3	.13					38.0	24.0	.049	34.8
		FC	12									40.3	.10					27.0	24.0	.049	34.8
	19	C	12	a20 x7½	6.46	545	1150	12	561	130.0	.08					135.3	.084		26.4	.009	83.7
		FC	12									35.3	.07					27.0	21.2	.047	30.3
	20	C	12	a20 x7¾	5.50c	429	300	12	147							140.3	.073		19.4	.014	79.0
		KC	12									90.3	.10					38.0	15.1	.075	23.6
		FC	12									35.0	.10					32.0	15.1	.075	23.6
	21	C	12	ax20 x7	5.77	578	1400	18	953							145.3	.086		26.6	.008	84.0
		FC	12									40.3	.04					31.0	23.0	.042	30.8

	22	C	12	ax20 x8	6.01	540	380	12	186						145.3	.108		26.0	.015	106.0
		FC	12									30.3	.13				30.0	20.2	.080	30.5
		KC	12									55.3	.15				29.0	20.2	.080	30.5
	23	C	12	ax20 x6½	5.12	543	210	18	143	115.0	.21	140.3	.34		150.3	.38	36.0	18.1	.017	54.8
		FC	12									30.3	.13				34.0	14.3	.093	21.0
E	1	F.C.	12	ax12.5x7	4.47d	730			164l			18.9	.09				37.0	22.4	.13	32.8
	2	F.C.	12	ax12.5x7	4.47d	645			164l			12.7	.07				37.0	19.9	.12	29.0
	5	F.C.	4¾	ax10.0x7	4.47d	570			164l			16.4	.07				20.0	12.6	.087	22.3
	8	F.C.	12	ax10.0x6.5	4.47d	490			164l			22.9	.20				31.0	13.5	.087	19.7
	9	F.C.	12	ax10.0x7	4.47d	655			164l			14.9	.26				33.0	20.2	.12	29.4
	11	F.C.	12	ax12.5x7	4.47d	500			164l			14.9	.17				37.0	15.4	.09	22.5
C	9	C	12	20x20 x12	5.50c	525g			300k						100.0	.085		54.5	.014	164.0
		KC	12	20x20 x12	5.50c										100.0	.14		41.4	.077	65.5
	10	C	12	20x20 x12	5.50c	615g			300k						100.0	.13		64.0	.016	192.0
		KC	12	20x20 x12	5.50c										110.0	.115		48.5	.091	76.7
	11	C	12	20x20 x12	5.50c	582g			300k						95.0	.07		60.5	.015	181.5
		KC	12	20x20 x12	5.50c										110.0	.075		45.9	.086	72.5
	12	C	12	20x20 x12	5.50c	558g			300k						110.0	.11		58.0	.015	174.0
		KC	12	20x20 x12	5.50c										110.0	.075		44.0	.082	69.7
	13	C	12	20x20 x12	5.50c	650g			300k						110.0	.11		67.5	.017	203.0
		KC	12	20x20 x12	5.50c										105.0	.06		51.2	.096	81.1
	14	C	12	20x20 x12	5.50c	594g			300k						105.0	.10		61.6	.016	185.5
		KC	12	20x20 x12	5.50c										110.0	.065		46.8	.088	74.1

Legend

C. . . . Center of Slab K.C. . . . . Keyed Corner
F.C. . . . Free Corner D.C. . . . . Dowelled Corner

*Column #6—x 10.6 P.S.I.

28-day strength was increased according to Portland Cement Association (PCA) specifications.[24] The value reported was computed from the mean result of repetitive plate bearing tests on the subgrade, according to the Department of Transport Procedures.

Procedures.—The value reported was computed from a repetitive plate bearing test at each location, according to the Department of Transport Procedures. The value reported was computed from the mean result of four repetitive plate bearing tests on the base at this Airport, according to the Department of Transport Procedures. The value reported was determined from one test at this airport.

Keyed corners were considered as free corners for the purposes of these computations. It is realized that this is a conservative assumption. A theoretical investigation of the dowelled/dowelled corners revealed there was some justification for assuming a semi-infinite plate condition and this was done in six cases at airport A. This is not a conservative assumption, but it was felt that it was more realistic than disregarding altogether the effect of the dowell.

The factor M_o for use in Fig. 4 (a) was taken as $\frac{f_b h^2}{6}$ for each loading condition, in which f_b is the measured "modulus of rupture." For corner loading (90° Wedge) an equivalent a was determined as the radius of a quadrant whose area equaled the area of the plate used for the test. For edge loading (semi-infinite plate), an equivalent a was determined, as the radius of a semi-circle whose area equaled the area of the plate used in the test. For each loading condition the equivalent a was further modified by the addition of a depth factor $\left(+ h/2\right)$ since in all test locations $a < 2h$.

24 "Design of Concrete Airport Pavements," Portland Cement Assn.

ELASTO-PLASTIC ANALYSIS BY NUMERICAL PROCEDURES[a]

Closure by Annabel L. Tong

ANNABEL L. TONG,[15] M. ASCE.—The writer wishes to mention the possibility of programming the computation steps of this numerical procedure to high speed digital computers. In spite of the simplifications used by this method, the computation work involved, if done manually, is still time-consuming especially for the bending or buckling of framed structures. The majority of the work in this analysis can be programmed to a small or medium sized computer with controlled degree of accuracy. For example, in the case of column buckling, Eqs. 18, 19, 20, and 21 are first derived for a column of specific material and cross-sectional shape. Corresponding values in Figs. 11, 12, and Table I can be computed by the computer and stored in its memory units or directly printed out in table formats for future uses. The steps for constructing Figs. 13, 14, and 15 can be programmed and results can be arranged in groups under given loadings. For example, the various L_1 values and the corresponding $\epsilon 1$ or δ_0-d_1 could be stored in pairs under given P/A and pre-selected deflection δ_0. The next step is to regroup these data by storing L_1 and the corresponding δ_0 in pairs for given P/A and ϵ_1. By logical decision, the computer will then choose the maximum number among a group of numbers represented L_1 under each pair of P/A and ϵ_1. This step is equivalent to the step for determination of maximum point Q_1 of a curve as shown in Fig. 15. The chosen maximum length will furnish one point on the buckling curves plotted in Fig. 6. The program for this problem may be written in many separate steps. The results from each step would be printed out and checked before the next step is accomplished. Once such a program is available, it could be used repeatedly for columns of other cross-sectional shapes and materials with slight modification.

A generalized column curve would be possible for members of various sections and end conditions if shape factors and effective length factors are introduced to this analysis. As basis for design, a member of rectangular section may be assumed to have a shape factor k = 1, and columns of hinged ends have an effective length factor K = 1. Then the factor k for member of section other than rectangle should be applied to the eccentricity ratio ($e\ c/R^2$) and the factor K for restrained columns should be applied to the slenderness ratio (L/R). The column curves then are plotted in scales of P/A versus K L/R for various kec/R^2. The effective lengths of restrained columns are determined by methods commonly used in the elastic analysis. The determination of the shape factor is by crude approximation. References for the k values for various cross-sectional shapes are available (7).

---

[a] December, 1960, by Annabel Tong (Proc. Paper 2690).

[15] Struct. and Hydr. Engr., Stearns and Wheeler, Cons. Engrs., Cazenovia, N. Y.

RESPONSE OF MULTI-STORY STRUCTURES TO EARTHQUAKE[a]

Discussion by Richard G. Troy

RICHARD G. TROY,[14] M. ASCE.—Berg's stimulating paper prompted the writer to make some calculations for the four-story frame. These consisted of estimating the first mode period of the bare steel frame, ascertaining the approximate effect of the usual solid concrete fireproofing of columns and girders on the value of the first mode period and comparing the seismic coefficients tabulated by the author in Table 1 with those obtained by applying the provisions of the latest edition of the Los Angeles City Building Code.

In estimating the period, the bare steel frame was loaded at the floor levels with the loads shown in Fig. 1 of the paper and the column and girder moments were obtained by the portal method. The story deflections were then computed and the total top story deflection was obtained. This value was substituted in the formula

$$T = 0.29\sqrt{D_T} \quad \ldots\ldots\ldots\ldots\ldots\ldots \quad (4)$$

in which D_T is the total top story deflection in inches and the coefficient 0.29 is the average of the coefficients in the formulas for the free period of a weighted cantilever and a uniformly loaded cantilever, the coefficients being 0.32 and 0.26, respectively. A value of T = 1.92 sec was obtained that compares with 2.01 sec obtained by the author.

The effect of solid fireproofing was found by calculating the increase in stiffness of the columns and girders. A lightweight concrete with n = 16 was assumed and the moments of inertia of the cracked and uncracked sections were found assuming a rectangular concrete section with 2 in. minimum cover over the steel sections. The uncracked fireproofing in some cases increased the stiffness by more than 100%. The increase, considering the fireproofing cracked, was less, as was to be expected. If it is assumed that the solid fireproofing increases the stiffness of columns and girders by 75%, then the total top story deflection will be 57% of that of the bare steel frame and the free period will be reduced by 25%. This would give a period for the fireproof frame of 1.92 x 0.75 = 1.44 sec, that would be equivalent to the undamped structure with shear walls of Berg's paper. The use of a stone concrete with a smaller n value would increase the stiffness of the frame even more than light-weight concrete with a resulting reduction in free period. No account was taken of the contribution of the floor to the stiffness of the girders with a portion thereof acting as an enlarged top flange. This would further stiffen the frame and reduce the period.

---

[a] April 1961, by Glen V. Berg (Proc. Paper 2790).

[14] Structural Engr., Stacy & Skinner, Los Angeles, Calif.

Any yielding or slip in the girder to column connections, on the other hand, would tend to counteract this increase in stiffness.

The comparison of seismic coefficients revealed some interesting differences. In 1960 the Los Angeles City Building Code was revised and a more elaborate set of procedures was designed to calculate seismic loads. Previous to this, the seismic coefficients for buildings thirteen stories or less were determined from the formula $\frac{60}{N + 4.5}$ where N was the number of stories above the one under consideration. The new code defines base shear as

$$V = K C W \quad \ldots\ldots\ldots\ldots\ldots\ldots \quad (5)$$

in which K is a factor dependent on the type of building construction, C is a factor

$$C = \frac{0.05}{\sqrt[3]{T}} \quad \ldots\ldots\ldots\ldots\ldots\ldots \quad (6)$$

dependent on the period T

$$T = \frac{0.05}{\sqrt{D}} \quad \ldots\ldots\ldots\ldots\ldots\ldots \quad (7)$$

of the structure and W is the total dead load of the structure with a qualification added for storage buildings. A formula is given for the period T based on the height and width in the direction of motion of the building. It is further stated that T = 0.10 x number of stories for all buildings with a moment resisting frame carrying 100% of the seismic loads, and that T need not be taken at less than 0.10 sec.

For the four-story frame the code would give T = 0.4 sec, a value which is 20% of the value given by the author. Nevertheless, the use of this value for T will result in seismic coefficients that are in line with those given in Table 1(a) of the paper. The following is a tabulation of the seismic coefficients according to the 1960 Los Angeles City Code for the values of T as listed:

T = 2.01 sec (Bare steel frame)	T = 1.44 sec (Fireproofed frame)	T = 0.4 sec. (Los Angeles Code values)
$C_4 = 0.044$	$C_4 = 0.048$	$C_4 = 0.077$
$C_3 = 0.038$	$C_3 = 0.041$	$C_3 = 0.066$
$C_2 = 0.032$	$C_2 = 0.035$	$C_2 = 0.056$
$C_1 = 0.027$	$C_1 = 0.029$	$C_1 = 0.047$

From this it appears that one is ill-advised in substituting the actual free period of a flexible low building into the Los Angeles Code formula. It is also indicated that the procedures in the code are a device for obtaining seismic loadings that reflect past damage experience rather than being precise methods for finding the dynamic characteristics of structures.

The seismic coefficients for the eight-story frame were also determined to see if they were in line with Berg's values. The results are as follows:

T = 0.8 sec
(Los Angeles
Code value)

$C_8 = 0.065$

$C_7 = 0.061$

$C_6 = 0.056$

$C_5 = 0.052$

$C_4 = 0.048$

$C_3 = 0.044$

$C_2 = 0.040$

$C_1 = 0.036$

It is evident that the new Los Angeles Code has reduced the seismic loadings appreciably over those of the old code especially in the upper stories. A consideration of Berg's data for the viscous damped frames would seem to justify this except for the El Centro, Calif. ground motion as it affects the four-story frame. It would appear from his data also that higher seismic loadings than the code would prescribe should be used for structures where little damping will be present, even though their construction would justify the lower coefficients as stated in the code.

With regard to damping provided by non-structural elements, the writer feels that too much emphasis has been placed on their furnishing such damping. The modern multi-story building does not often have tile or masonry partitions. The usual practice is to use movable partitions that extend up to the ceiling line. Where plaster partitions are used, the plaster is stopped at the ceiling line unless a fire rated wall is required, in which case the partition is plastered up to the underside of the floor above. This is the case around elevator shafts, stair wells and duct shafts. Where the plaster is stopped at the ceiling line the light gage metal studs extend beyond and are fastened at the underside of the floor above. These studs bending about their weak axis will furnish only a small amount of resistance to motion. The fire rated walls therefore furnish the lion's share of non-structural damping together with the curtain wall, which, in keeping with modern practice, is lightweight and in many cases largely glass. As a result, the fire rated partitions will be damaged in an earthquake if they are expected to furnish damping. There then arises the question whether such damage should be tolerated or some sort of fire rated joint should be devised at the tops of such partitions to allow the floor above to move without dragging the partitions with it. The initial cost of the fire rated partitions in a typical multi-story office building will amount to a considerable sum of money. Needless to say the cost of repairing or replacing them if they are badly cracked might well equal or exceed their initial cost. Therefore, the decision to count on non-structural items for damping should be reached after consideration is given to the economics involved.

With regard to damping provided by inelastic deformation, the writer feels that Housner's thesis might win acceptance for certain types of structures such

as water towers and certain industrial structures. It is doubtful if many practicing structural engineers or building officials would accept it for the design of multi-story apartment or office buildings.

The author has made a valuable contribution to the literature on seismic analysis. It is to be hoped that other studies can be made of actual buildings designed for seismic forces and that field measurements of their dynamic characteristics during various stages of construction be available for use in such studies.

COMMENTARY ON PLASTIC DESIGN IN STEEL[a]

Closure by Committee

CLOSURE BY JOINT WRC-ASCE COMMITTEE ON PLASTICITY RELATED TO DESIGN.—This closure applies to the seven progress reports which comprise the Commentary on Plastic Design in Steel. The Joint Committee is pleased to note the several constructive discussions that were submitted. They serve to indicate possible refinements to the plastic method of design and to state areas where misconceptions may exist.

The Joint Committee considers that Su has misinterpreted the contents and purpose of the Commentary.

The discussion of Art. 6.2 (Local Buckling) of the Commentary by M. N. Fialkow, F. ASCE, is primarily concerned with the fact that Eq. 6.16 (which gives the maximum allowable beam-depth to web-thickness ratio for members subjected to axial force and bending moment) is based on a maximum strain of four times the yield strain. Fialkow shows with two examples that theoretically much larger strains can exist in a hinge at the time the failure mechanism has formed.

Fialkow's critical review of the fundamental limitations of Eq. 6.16 is appreciated. However, the members of the Joint Committee responsible for the publication of the Commentary feel that the local buckling guides set forth in Art. 6.2 are satisfactory. It is not stated in this article that the strain must be limited to 4 ϵ_y. Eq. 6.16 is suggested as a guide for checking the critical d/w ratio of beam-columns in plastically designed structures. The formula is based on a recommendation in Ref. 6.27, (In ASCE Manual 41, This is Ref. 6.25). which states that "except in cases requiring large rotations, the curve $\epsilon = 4\ \epsilon_y$ can be used." The limitations of Eq. 6.16 are also clearly stated in Art. 6.2, and the guide is recommended for structures for which ordinarily no deflection and rotation analysis would be performed. Furthermore, the curves in Fig. 6.11 enable the designer to determine the maximum allowable value of d/w when larger strains are encountered, such as in more complicated structures; also, such relationships should be helpful in providing bounds in cases involving dynamic loading.

The Joint Committee feels that Eq. 6.16 is appropriate for plastic design for the following reasons:

1. The development of Fig. 6.11 on which Eq. 6.16 is based contains a number of conservative assumptions (Ref. 6.27). Local buckling of the web is assumed to take place as soon as the yield stress is reached, at the start of the strain-hardening range. Thus, the material is not assumed to strain-harden,

[a] Published in seven Progress Reports as follows: Report No. 1 and 2, Chapters 1 to 5, July 1959; Report No. 3 and 4, Chapters 6, October 1959; Report No. 5, Chapters 7, Jan. 1960; Report No. 6 and 7, Chapters 8 and 9, April 1960.

however, strain-hardening actually does occur, especially when the moment is not uniform.

2. The theory on which the curves in Fig. 6.11 are based does not consider the large post-buckling strength which is available even for thin webs.[1]

3. It is shown in Art. 9.8 of the Commentary that for more complex structures a major part of the rotation of the first hinge takes place after almost all the strength of the structure has been realized (Fig. 9.9). Thus, even if large strains are present at the formation of the mechanism, the strains at 95% of the maximum load may be considerably less. Therefore, an undue concern about the exact magnitude of the strains is not warranted. Also it is impossible to obtain a reliable estimate of the strains at failure from the hinge angles, if these are determined under the assumption that the hinges form at a point. A more exact strain calculation involves a complicated elastic-plastic analysis; only for the simplest of structures are such analyses expedient.

4. A considerable quantity of experimental evidence has shown that the local buckling rules of Art. 6.2 are satisfactory. Much of this evidence is given in Ref. 6.27 in which experiments were made to substantiate the local buckling theory. Further evidence can be seen in Figs. 5.10 and 5.11 of the Commentary where the full-scale frame test results are tabulated. It may be observed that the predicted ultimate load was attained even by frames fabricated from members which had high d/w ratios (for example d/w = 42 for the 10B17 members which were part of several of these frames). About forty experiments on beam-columns have shown that the primary cause of failure is always lateral-torsional buckling or general column instability. (The results of several of these tests are given in Figs. 7.19, 7.20, and 7.21 of the "Commentary on Plastic Design in Steel.") Several of these experiments were performed on laterally braced 8B13 columns (d/w = 35). Even for $P = 0.6\ P_y$ failure was due to general column instability.

The Plastic Design Commentary is a running account of conducted research, and as such it cannot be expected to have the "last say" about many of the problems studied in it. The problem of inelastic instability is certainly a complicated one, and it is hoped that future research will contribute to a better understanding of the problem. In particular, as the Commentary implies, future research should provide experimental data that can be used for comparison with the theory on which Eq. 6.16 was based.

Hashim H. Hamzawi, A. M. ASCE, correctly stated that a "critical" section might occur at some intermediate point in a tapered haunch if the adequacy of the haunch is checked only at its two ends. However, Hamzawi did not say that the magnitude of the inadequacy is small indeed. For the linear moment diagram given in Hamzawi's example it can be shown that the deficiency in resisting plastic moment at the critical section is only from 1% to 5% of the total at that section. (8.7)

Using Hamzawi's symbols, the following reduction in moment occurs at $x = L/2$ when $M_A = M_{pA}$ and $M_B = M_{pB}$

$$M = \frac{1}{4}\sigma_{yp}\, w n^2 L^2 \quad \ldots\ldots\ldots\ldots\ldots \quad (8)$$

---

[1] "New Aspects Concerning Inelastic Instability of Steel Structures," by B. Thürlimann, Proceedings, ASCE, Vol. 86, No. ST1, January, 1960, p. 99.

For all practical purposes this amount can be neglected in a design using an adequate load factor as recommended in Art. 4.8 of the Commentary.

Garden has presented an interesting refinement for including the effect of spread of plasticity in the calculation of deflections by the slope-deflection method. The refinement seems more adapted to orderly computation than the other precise methods in the report.

It would be interesting to obtain values of the commuted curvature and center of gravity of commuted curvature for average wide-flange and I shapes. This would be relatively simple triangular moment diagrams of the type shown in the discussion. In the case of members with a constant applied moment equal to M_p along a finite length and members with a plastic hinge forming in a region of uniform load, additional limitations would have to be introduced. Possibly consideration of these limitations might involve introducing the effect of strain-hardening into the calculations.

The Joint Committee is pleased to note the rapid strides made in the field of structural design in steel from 1940-1960. In large measure, these advances have resulted from an understanding of the relation between ductility and the performance of steel structures. The Commentary suggests how the property of ductility may be used in structural design and reviews the necessary secondary design considerations which insure that ductility is fully and safely utilized. The resulting design method, known as Plastic Design in Steel, has been used in many structures built in the United States and abroad.

The seven progress reports which constitute the Commentary have been assembled in one volume and published in June of 1961 as ASCE Manual of Engineering Practice No. 41. In addition to the topics covered in the progress reports, this Manual contains an extensive list of references plus author and subject indexes.

The Joint Committee is well aware that continuing research on the inelastic behavior of steel structures is necessary. Some of this work is currently (1961) underway. Its completion will make it possible to utilize more fully the potential of plastic design in such structures as multi-story frames and stiffened plate assemblies, a potential that experience has shown will combine effectively the dual objectives of safety and economy in steel structures.

PROCEEDINGS PAPERS

The technical papers published in the past year are identified by number below. Technical division sponsorship is indicated by an abbreviation at the end of each Paper Number: the symbols referring to Air Transport (AT), City Planning (CP), Construction (CO), Engineering Mechanics (EM), Highway (HW), Hydraulics (HY), Irrigation and Drainage (IR), Pipeline (PL), Power (PO), Sanitary Engineering (SA), Soil Mechanics and Foundations (SM), Structural (ST), Surveying and Mapping (SU) and Waterways and Harbors (WW), divisions. Papers sponsored by the Department of Conditions of Practice are identified by the symbols (PP). For dates and order coupons, refer to the appropriate issue of "Civil Engineering." Beginning with Volume 32 (January 1956) papers were published in journals of the various Technical Divisions. To locate papers in the Journals, the symbols after the paper number are followed by a numeral designating the issue of a particular Journal in which the paper appeared. For example, Paper 2760 is identified as 2760(ST1) which indicates that the paper is contained in the first issue of the Journal of the Structural Division during 1956.

VOLUME 82 (1956)

OCTOBER: 2815(SU3), 2816(EM5), 2817(ST11), 2818(SU3), 2819(HY9), 2820(EM5), 2821(ST10), 2822(EM5), 2823(EM5), 2824(SA5), 2825(SM5), 2826(EM5), 2827(EM5), 2828(SU3), 2829(ST10), 2830(ST10), 2831(PO)[P], 2832(EM5)[P], 2833(ST10), 2834(ST10), 2835(SA5)[P], 2836(SM5)[P].

NOVEMBER: 2837(ST11), 2838(ST11), 2839(CO3), 2840(ST11), 2841(SA5), 2842(WW4), 2843(ST11), 2844(HY9), 2845(ST11), 2846(HY9), 2847(WW5), 2848(WW4), 2849(SM4), 2850(ST11), 2851(CO3), 2852(HY9), 2853(HY9), 2854(ST11), 2855(HY9), 2856(HY9), 2857(SA5), 2858(WW4), 2859(WW4)[P], 2860(SA5), 2861(CO3), 2862(CO3), 2863(SA5), 2864(CO3)[P], 2865(HY9)[P], 2866(SA5)[P], 2867(ST11)[P].

DECEMBER: 2868(ST12), 2869(SM5), 2870(SM5), 2871(IR3), 2872(SM4), 2873(SM4), 2874(ST12), 2875(SM5), 2876(SM4), 2877(WW4), 2878(ST12), 2879(SM5), 2880(ST12), 2881(SA6), 2882(SM5), 2883(SM5), 2884(SM5), 2885(SM5), 2886(EM6), 2887(EM6), 2888(SM5), 2889(SM5), 2890(EM6), 2891(SM5)[P], 2892(ST12), 2893(ST12), 2894(HW4)[P], 2895(SM5)[P], 2896(SM5)[P], 2897(ST12)[P].

VOLUME 83 (1957)

JANUARY: 2898(PP1), 2899(PP1), 2900(HY1), 2901(SA1), 2902(SM1), 2903(ST1), 2904(ST1), 2905(SU1), 2906(HY1), 2907(HY1), 2908(PO1), 2909(HY1), 2910(HY1), 2911(HY1), 2912(ST1), 2913(HY1), 2914(PO1), 2915(ST1), 2916(HY1), 2917(SA1), 2918(SA1), 2919(SU1)[P], 2920(SA1)[P], 2921(ST1), 2922(PP1)[P], 2923(PO1)[P], 2924(ST1)[P], 2925(ST1)[P].

FEBRUARY: 2926(WW1), 2927(EM1), 2928(EM1), 2929(WW1), 2930(WW1), 2931(EM1), 2932(SM1), 2933(WW1), 2934(SM1), 2935(EM1), 2936(SM1), 2937(PL1), 2938(PL1), 2939(PL1), 2940(PL1), 2941(EM1), 2942(ST2), 2943(EM1), 2944(WW1), 2945(WW1), 2946(SM1), 2947(WW1), 2948(SM1), 2949(WW1), 2950(WW1)[P], 2951(EM1)[P], 2952(PL1)[P], 2953(ST2)[P], 2954(PL1)[P].

MARCH: 2955(ST2), 2956(HY2), 2957(AT1), 2958(CO1), 2959(HY2), 2960(HY1), 2961(SM2), 2962(HY2), 2963(HY2), 2964(HW1), 2965(SA2), 2966(CO1), 2967(HY2), 2968(HY2), 2969(SA2), 2970(ST2), 2971(CO1), 2972(AT1), 2973(HY2), 2974(AT1), 2975(HY1), 2976(HY2), 2977(HY2), 2978(SA2), 2979(ST2), 2980(HY2), 2981(HY2)[P], 2982(HW1)[P], 2983(SA2)[P], 2984(CO1)[P], 2985(CO1)[P], 2986(HY1)[P], 2987(ST2)[P], 2988(AT1)[P], 2989(HW1)[P].

APRIL: 2990(SM2), 2991(SM2), 2992(SM2), 2993(SM2), 2994(SM2), 2995(SM2), 2996(SM2), 2997(SM2), 2998(SM2), 2999(SM2), 3000(SM2), 3001(SM2), 3002(ST4), 3003(SM2)[P], 3004(SM2)[P], 3005(ST4)[P].

MAY: 3006(AA), 3007(WW2), 3008(HY3), 3009(WW2), 3010(HY3), 3011(CO2), 3012(WW2), 3013(HY3), 3014(HW2), 3015(HW2), 3016(HY3), 3017(HY3), 3018(SA3), 3019(WW2), 3020(SA3), 3021(WW2), 3022(WW2)[P], 3023(HY3), 3024(SA3), 3025(HY3), 3026(SA3)[P], 3027(HY3)[P].

JUNE: 3028(SA3), 3029(EM3), 3030(EM3), 3031(HY3), 3032(EM3), 3033(HW2), 3034(HY3), 3035(EM3), 3036(HY3), 3037(PO2), 3038(SA4), 3039(CO3), 3040(EM3), 3041(HW2)[P], 3042(EM3)[P], 3043(ST5), 3044(ST5), 3045(ST5), 3046(ST5)[P].

JULY: 3047(PO3), 3048(SU2), 3049(HY4), 3050(PO3), 3051(HY4), 3052(PO2), 3053(SU2), 3054(HY4), 3055(CO3), 3056(PO3), 3057(PO3), 3058(SA4), 3059(CO3), 3060(PO3), 3061(SA4), 3062(HY4), 3063(HY4), 3064(ST6), 3065(HY4), 3066(HY4), 3067(HY4), 3068(PO3)[P], 3069(SU2)[P], 3070(SU2)[P], 3071(HY4), 3072(HY4)[P], 3073(SU2), 3074(SA4)[P].

AUGUST: 3075(WW3), 3076(WW3), 3077(WW3), 3078(SM3), 3079(ST6), 3080(EM4), 3081(SM3), 3082(EM4), 3083(WW3), 3084(SM4), 3085(SM3), 3086(EM4), 3087(EM4), 3088(WW3), 3089(SM3), 3090(AT2), 3091(AT2), 3092(AT2), 3093(AT2), 3094(AT2), 3095(AT2), 3096(AT2), 3097(AT2), 3098(AT2), 3099(AT2), 3100(AT2), 3101(AT2), 3102(AT2), 3103(SM4), 3104(ST6), 3105(HW4), 3106(ST6), 3107(HW4), 3108(ST6), 3109(HW4), 3110(ST6), 3111(EM4), 3112(SM4), 3113(CO3), 3114(WW3)[P], 3115(ST6)[P], 3116(EM4)[P], 3117(SM4)[P].

SEPTEMBER: 3118(SA5)[P], 3119(HW3)[P], 3120(HY5)[P], 3121(SA5), 3122(PL4), 3123(IR3), 3124(HY5), 3125(HY5), 3126(HY5), 3127(HY5), 3128(HY5), 3129(HY5), 3130(HY5), 3131(CP1), 3132(HY5), 3133(HY5), 3134(HY5), 3135(HY5), 3136(HY5), 3137(HY5), 3138(CO3), 3139(PL4), 3140(SA5), 3141(SA5), 3142(SA5), 3143(SA5), 3144(PL4)[P], 3145(EM5)[P], 3146(EM5), 3147(SM5), 3148(SM5)[P], 3149(SM5)[P].

OCTOBER: 3150(PP2), 3151(PP2), 3152(PP2), 3153(SM5), 3154(SM5), 3155(ST7), 3156(ST7), 3157(ST7), 3158(ST7), 3159(ST7), 3160(SM5), 3161(EM6), 3162(ST7), 3163(ST7), 3164(ST7), 3165(ST7), 3166(EM6), 3167(SM5), 3168(SM5), 3169(ST7), 3170(ST7), 3171(EM6), 3172(EM6), 3173(SM5)[P], 3174(ST7)[P].

Table of contents of several papers, grouped by divisions.

AMERICAN SOCIETY OF CIVIL ENGINEERS

OFFICERS FOR 1941

PRESIDENT

GLENN W. HOLCOMB

VICE-PRESIDENTS

Term expires October, 1941:
GEORGE E. MEAD
LAWRENCE A. ELSENER

Term expires October, 1942:
DONALD H. SAWYER
WILLIAM J. WILGUS

DIRECTORS

Term expires October, 1941:
THOMAS J. FRATAR
FARE FOWLER
DANIEL B. LUDLOW
CHARLES W. STILLMAN
ANGEL G. ORTEGA
JOHN H. RHEINS, JR.
R. E. TRAICH

Term expires October, 1942:
ELMER C. JETHRO
SAMUEL A. GARTER
THOMAS H. SHARP
BRENT R. DAVIS
WOODROW W. BAUM
BERNHARD HOFFMANN

Term expires October, 1943:
ROGER D. SHERMAN
HENRY W. SUTE
PAUL F. GRIGGS
HERBERT BRUCE
JOHN D. WATSON
GARNER E. DAVIS

PAST PRESIDENTS

Members of the Board

FRANCIS S. FRIEL

FRANK A. MARSTON

EXECUTIVE SECRETARY
WILLIAM H. WILEY

TREASURER
LAWRENCE CHENEY

ASSISTANT SECRETARY
DEAN B. MAYNARD

ASSISTANT TREASURER
CHARLES A. HOWARD

PROCEEDINGS OF THE SOCIETY

HAROLD T. LARSEN
Manager of Technical Publications

PAUL A. PARISI
Editor of Technical Publications

BENJAMIN SCHREITER
Assistant Editor of Technical Publications

PHILIP LASCHWARTZ
Assistant Editor of Technical Publications

COMMITTEE ON PUBLICATIONS

HENRY H. SIBLEY, *Chairman*

WILLIAM G. BAKER, JR., *Vice-Chairman*

BERNHARD HOFFMANN

ROBERT W. CRUM

ROGER D. SHERMAN

HENRY W. SUTE

GARNER E. DAVIS